HYPOTONIC DELIVERY OF DRUGS AND DRUG-LOADED NANOPARTICLES TO THE GASTROINTESTINAL TRACT

By

Katharina Maisel

A dissertation submitted to Johns Hopkins University in conformity with the requirements for the degree of Doctor of Philosophy

Baltimore, Maryland

December, 2014

ABSTRACT

Innovative gastrointestinal (GI) drug delivery vehicles such as mucus penetrating nanoparticles (MPP) and fluid-absorption inducing (hypotonic) delivery vehicles have potential to improve therapeutic outcomes over conventional methods such as mucoadhesive particles (MAP) for GI diseases, including ulcerative colitis (UC) and HIV pre-exposure prophylaxis (PrEP). More than 80% of all drugs are absorbed via the GI tract for either systemic or local treatment. MAP delivered to the GI tract are thought to improve oral absorption or local targeting of difficult-to-deliver drug classes. Mucus is a continuously secreted barrier that effectively traps foreign particulates to protect the underlying epithelium. Rapid clearance of the most superficial luminal mucus layers in the GI tract may limit the effectiveness of MAP. Here, I test the current dogma of mucoadhesion by comparing MAP and MPP GI drug delivery via the oral and rectal routes. In addition I investigate the development of several vehicles including rectal enemas and gels for more effective delivery of nanocarriers or free drugs.

First, I illustrate that MPP uniformly coat all surfaces of the GI epithelium, while MAP aggregated in mucus in the center of the lumen, far away from the absorptive epithelium, both in healthy mice and mice with UC. In the mouse colorectum, MPP penetrated into mucus in the deeply in-folded surfaces to evenly coat the entire epithelial surface. Moreover, in UC mice, MPP were transported preferentially into the disrupted, ulcerated tissue. Next, I sought to design an effective enema vehicle for delivering MPP and non-mucoadhesive drugs locally to the colorectum. I found that MPP and free drug are only rapidly transported to the epithelial surface in sodium-based enemas, while potassium-based or isotonic and hypertonic (secretion-inducing) enemas cause

heterogeneous surface coverage. Strongly hypertonic and hypotonic enemas cause rapid systemic drug absorption, while moderately hypotonic enemas improve local drug retention in tissue. Finally, I designed a microbicide-loaded MPP for PrEP, to be delivered in a novel osmotic thermogel. The MPP formulation evenly coated both the vaginal and colorectal epithelium and the hypotonically delivered thermogel effectively traps HIV, and significantly enhances drug and nanoparticle retention in the cervicovaginal tract.

Advisor: Justin Hanes, PhD

Thesis Committee: Justin Hanes, PhD; Richard Cone, PhD; Craig Hendrix, MD; Rangaramanujam Kannan, PhD; Youseph Yazdi, PhD; Laura Ensign, PhD

ACKNOWLEDGMENTS

I have had the opportunity to work with and be guided by many incredibly intelligent and wonderful people throughout graduate school. First, I would like to thank my advisor Dr. Justin Hanes for giving me the opportunity to work in his lab, allowing me the freedom to explore new research directions while making sure I kept the big picture in mind, always being open to giving advice personally or professionally, and teaching me about translating research to the clinic. I would like to thank my unofficial "co-advisor", Dr. Richard Cone, for his always giving me his undivided attention, and guiding and supporting me professionally and personally in my research, professional development, and career decisions. I also need to thank my other collaborators and committee members: Dr. Craig Hendrix for giving me invaluable insights into the process of designing products that are translatable into humans; Dr. Rangaramanujam Kannan for supporting me in exploring new endeavors in the dendrimer realm in addition to always providing me with his wisdom on research and career decisions; Dr. Youseph Yazdi for sitting through many hours of research discussions and providing his insights on product development and big picture applications; and finally, Dr. Laura Ensign for teaching me everything I needed to know when I first joined the laboratory, for supporting me in venturing into new research directions (and convincing me not to get upset when things did not work out the way I intended), for welcoming me into her family and making Baltimore a place I could call home, and for being an inspiration in continuing onto a career in academia.

I also need to thank many members of the Hanes Lab and Center for Nanomedicine. I'd like to especially thank those who came before me, who have taught

me so much, and were always willing to give up some of their valuable time: Drs. Craig Schneider, Elizabeth Nance, Jung Soo Suk, Ben Schuster, Anthony Kim, Qingguo Xu, Tao Yu, Himat Patel, Manoj Mishra, Wojciech Lesniak, and Jie Fu. Next I'd like to thank those who have been in the lab with me throughout all these years, my classmates Jane Chisholm and Clark Zhang, who have been wonderful to bounce ideas off of, get encouragement and boost my confidence in next steps, and who have been all around fantastic friends. I look forward to seeing you both graduate soon! Next, I'd like to thank Shu Chattopadhyay for supporting me in my endeavors first as an undergraduate student, then as a master's student, and now as a young PhD student. He has been invaluable to completing my work and I am so proud to see him grow into his new responsibilities as a doctoral candidate. I need to thank all the other current and former members of the Hanes and Cone lab "vag team" Terence Tse, Kunal Parikh, Thuy Hoang, Taarika Babu, Kevin DeLong, Derek Cerchione, Mihika Reddy, Megan Lamberti, Emily Toler, Stephen Chen, Veda Prasad, and Ashil Koranne. Joseph Vargas and Nicole Turner deserve special thanks for keeping everything running behind the scenes. I'd also like to thank Dr. Thomas Moench for his input on many of my research questions and struggles. Finally I'd like to thank all other members of the Center for their support, helpful attitude, and making the lab an all-around friendly, family-like environment.

Most importantly I would like to thank my friends and family for their support and inspiration. Thanks to all my friends in and out of graduate school, in particular my best friend and former lab member Dr. Ben Tang for helping me through many crises, reading endless drafts of papers/letters/emails/abstracts, and always making me laugh even when I felt down. I'd like to thank my brother Simon and his wife Tanya for their

constant support and always welcoming me into their home in Boston. Ben, Simon, and Tanya formed my Boston support group that allowed me to escape into another city on numerous occasions throughout my PhD. Last but not least I'd like to thank my wonderful parents for everything they have done to get me here: taking the leap to move to the USA and deciding to stay here, supporting me emotionally, physically, intellectually, financially, and in every other possible way, and giving me the strength to follow my dreams. Without their inspiration, love, and guidance I would not have made it this far. Tausend Dank!

TABLE OF CONTENTS

LIST OF TABLES

LIST OF FIGURES

1. INTRODUCTION AND SIGNIFICANCE

More than 80% of all drugs are delivered to the gastrointestinal (GI) tract for either systemic or local treatment or prevention of diseases [1-3]. To achieve optimal drug absorption, medications need to reach as much of the epithelial tissue as possible [4-7]. However, the high tortuosity of the GI epithelium and the sticky mucus barrier coating the GI epithelium make this difficult, especially for drugs with poor water solubility [4, 8-10]. Mucus is the first line of defense at mucosal surfaces, effectively trapping most pathogens and particulates by hydrophobic and electrostatic interactions [8, 9].

Hydrophobic drugs will interact with the mucus barrier and can become trapped in it [11-14]. The incorporation of these drugs into nanotechnology has significantly improved their solubility and thus their drug absorption; however, most GI nanocarriers have been designed to adhere to mucus. Mucoadhesion can limit nanocarrier distribution on the epithelial surface and likely leads to their clearance along with the mucus layer [5-7, 15]. Nanoparticles designed to slip through the mucus barrier may be able to reach the more slowly cleared adherent mucus layers and thus may enhance GI drug distribution and retention. Optimizing nanoparticle size and surface characteristics that makes them mucus penetrating is thus of particular importance. Hydrophilic drug molecules, unlike hydrophobic drugs, have little interaction with mucus, are able to diffuse through the mucus barrier and take advantage of fluid flow toward the epithelium, or advection (directional fluid flow), that leads them to effectively reach the underlying epithelium [11, 16, 17]. Fluid flow toward the epithelium naturally occurs in the small intestine, as outlined in Chapter 2, but many vehicles for local delivery to the colorectum are not designed with

fluid flow absorption in mind. To optimize colorectal drug delivery of hydrophilic drugs or non-mucoadhesive nanoparticles, the design of an optimal delivery vehicle is essential.

In chapter 2 of this thesis I introduce the mucus barrier, fluid absorption throughout the GI tract, the development of mucus penetrating nanoparticles (MPP) for GI applications, the treatment of inflammatory bowel disease (IBD) and prevention of sexually transmitted infections (STIs) that could benefit from the use of MPP and drug delivery vehicles designed with fluid absorption in mind. In Chapter 3, I show the surface characteristics and sizes necessary to make nanoparticles MPP in the different parts of the GI tract, their distribution on GI tissue, and the effects of fluid absorption on their distribution in healthy and inflamed tissue. In Chapter 4, I discuss the effects of ion composition of an enema formulation on the distribution of MPP and free drug, local toxicity, and drug pharmacokinetics. Chapter 5 outlines the development of a mucus penetrating nanocrystal formulation and an osmotic thermogel for improved distribution and retention of anti-HIV drugs in the colorectum and cervicovaginal tract. In addition, in Appendix I, I address the paradox that only low molecular weight (MW) poly(ethylene glycol) (PEG) would result in non-mucoadhesive coatings while the use of high MW PEG would cause mucoadhesion, by illustrating that sufficiently dense high MW PEG coatings indeed result in particles that are non-mucodhesive. In Appendix II, I discuss the use of another class of nanocarriers, dendrimers, for application in the GI tract and other mucosal surfaces including the respiratory and cervicovaginal tracts.

2. BACKGROUND – CONSIDERATIONS FOR GASTROINTESTINAL DRUG DELIVERY

2.1 Mucus

Our gastrointestinal (GI) tract has many quite remarkable functions. For example, it uses strong acids in the stomach to disinfect and break up peptides, all without breaking down its own cell membranes. It is also the home to 90% of our non-eukaryotic inhabitants: ~10^{14} bacteria and viruses; however, most of the time we do not get infected [18]. The dead and keratinized 'horny' cell layers of our skin protects most of our exposed outer surfaces, but it is mucus that protects all our moist most mucosal surfaces. Most of us usually experience mucus as the slimy, yucky substance we produce when we have a stuffy nose or a chest cold, but mucus is the reason enormous moist mucosal surfaces of our gut, lungs, mouth, eyes, and reproductive tracts, usually do not get infected. How does mucus protect these surfaces? First, it is an excellent lubricant that protects against mechanical damage. Second it is remarkable 'filter' that traps pollutants, irritants, dust, and pathogens and is then rapidly cleared from the body or sent to the stomach to be sterilized by acid [8].

Mucus forms a porous hydrogel that traps pathogens and particulates via size exclusion as well as electrostatic and hydrophobic interactions, and also by the selective trapping actions of secreted antibodies [9, 19, 20]. The gel properties of mucus are produced by mucin fibers. Mucins are peptidoglycans 0.3-2 MDa in size [8, 9]: they have a long peptide backbone that is highly glycosylated. The outermost tips of the sugars (glycans) on mucins are negatively charged, giving an overall negative charge to mucin fibers [8, 9]. This effectively traps many pathogens or particulates that have a positive charge. In

addition to the glycosylated regions, the mucin peptides also contain hydrophobic regions that bundle mucin fibers into cables, and effectively trap hydrophobic particulates [8, 9]. Mucin fibers are extraordinarily long, and are linked together to form fibers several microns long. Antibodies secreted into mucus greatly enhance the ability to trapping pathogens and toxins in mucus gel. Most antibodies synthesized by the immune system are secreted into mucus. They diffuse rapidly through the gel, retarded only slightly by transient, low affinity bonds with the mucus gel [21]. However, when they accumulate on the surface of a pathogen they form enough multivalent adhesive interactions with the gel to trap the pathogen [22, 23]. Once particles, pathogens, or cells are trapped in mucus, they are cleared along with it: mucus is constantly secreted and cleared to further prevent pathogens and harmful particulates from reaching the surfaces of our mucosal epithelia. The types of components, their ratios, the mucin type, the mucus turnover rate, and the mucus thickness vary at the different parts of the body and throughout the GI tract, as illustrated in Table 2-1.

The lubricant characteristic of mucin gels arises from their shear-thinning viscoelasticity. This lubricating action is of particular importance in the GI tract, where undigested, fibrous and often jagged surfaces of chyme are transported by peristalsis along the entire 7-8 m of the small and large intestine. Shear thinning occurs when two surfaces move by each other and a slippage plane forms midway between the surfaces [9]. Thus each surface retains and unstirred layer of mucus coats and adheres to the bolus of chyme (food) and another layer adheres to the epithelial surface. Despite peristalsis occurring all along the intestine, the unstirred mucus layers remain essentially intact and

nutrients and particulates must diffuse through these adherent layers to reach the absorptive epithelium [8, 9].

2.1.1 Stomach

Mucus in the stomach has two layers: the firmly adherent inner layer and the loosely adherent outer layer. The inner mucus layer is anchored to the epithelial cells and mainly made of MUC5AC, which serves as a barrier to the stomach acid, hydrogen chloride (HCl) [24]. HCl produced by the parietal cells can penetrate through this layer via temporary canals [4, 24-26]. The epithelial cells excrete bicarbonate locally that leads to a gradient of pH that goes from near-neutral close to the epithelial cells and highly acidic in the lumen of the stomach. The outer mucus layer consists mainly of MUC6 and is thought to have an additional hydrophobic barrier composed of zwitterionic phospholipids that prevents the stomach acid from leaking back to the epithelial layer once it is secreted [27-29]. Mucus has also recently been found to be resistant to changes in pH, making it a formidable protective barrier for the gastric epithelium against the highly acidic stomach contents [30]. When this barrier is compromised, the epithelial tissue can be damaged, making it easier for infections to occur and ulcers to form [4, 31].

2.1.2 Small Intestine

The small intestine has a loosely adherent outer mucus layer and is thought to also have a very thin inner mucus layer though this has not been confirmed in humans [31]. The outer layer consists mainly of MUC2 mucin that mainly lubricates the food boluses coming through the small intestine for digestions [31]. The mucus layer of the small intestine is relatively thin compared to the stomach and colon, largely due to the difference in function of the small intestine. The small intestine serves mainly to digest

and absorb nutrients and is kept quite sterile; after most bacteria and viruses are eliminated in the stomach, additional bacteriocidal peptides and proteins that are secreted by Paneth cells and enterocytes [32-34]. In fact, one could argue that mucus also ought to be digested by all the enzymes present in the small intestine, but mucins are actually only slowly degraded, suggesting that they must have co-evolved with digestive enzymes to resist degradation. Rapid mucus secretion from the crypts also prevents digestive enzymes as well as bacteria from reaching the epithelial layer in the small intestine [31, 33]. Disruption of the mucus barrier can thus lead to infections, epithelial injury by digestive enzymes, and chronic inflammatory diseases such as inflammatory bowel disease.

2.1.3 Colon

The large intestine, or colon, has a thick inner and outer mucus layer both composed of mainly MUC2 mucin produced by goblet cells. In the inner mucus layer, MUC2 expands >1000 fold after secretion and forms lamellar sheets that effectively prevent bacterial penetration [33, 35, 36]. Once these sheets reach the threshold to the outer mucus layer, they are further cleaved to allow a 3-4 fold expansion that results in a more loosely adherent layer [37]. The outer mucus layer allows bacterial penetration and forms the home of the most of our gastrointestinal microbiome. The relationship with these bacteria is mutually beneficial, as the mucus they live in provides part of their food source, while the bacteria produce short chain fatty acids, acetate, and other nutrients for our colonic epithelium [38]. However, these bacteria commensal can be harmful when they reach and infect our epithelial cells. For this reason, the colonic mucus layers are several hundred microns thick in humans and are constantly secreted and cleared upon defecation. When the mucus barrier is compromised, as it is in certain chronic

inflammatory diseases like ulcerative colitis, bacteria are able to reach and infect the epithelium.

2.2 Food absorption and the mucus filter barrier

To effectively absorb nutrients via the GI tract, nutrients must get through the constantly secreted and sloughed mucus barrier. Digestive enzymes make hydrolytic cleavages that fragment ingested food into small pieces and molecules in our gastrointestinal lumen and must get to the epithelium to be absorbed. With mucus secretion occurring at a velocity of about 0.2-2 μm/s, diffusion alone would not be sufficient to bring food particulates and molecules close enough to the epithelium for absorption. The body has developed a clever way to overcome this barrier: fluid flow. Nine liters of fluid enter our GI tract per day, of which >95% is reabsorbed [8, 39]. This creates fluid flux from the lumen to the epithelium at a velocity of 1-10 μm/s, and this fluid flow can drag along (advectively transport) food particulates and small molecules, provided they can penetrate the mucus barrier. This rapid advective transport delivers nutrients to the base of the villi for absorption in a matter of minutes. Fluid secretion and re-absorption is brought about by ion transport, the details of which are discussed in the next section. In fact, the body uses ion transport to drive both water secretion and water absorption, since transporting ions is much more efficient than directly transporting molecules of water: Water has a molarity of 55M (based on the density, 1000g/L, and molecular weight, 18g/mol, of water), the molarity of serum solutes is about 1/3M (~300mM), and therefore for every one solute molecule there are ~180 water molecules [40]. Each single solute molecule transported will thus cause ~180 water molecules to follow by osmosis. Pumping ions is even more efficient, since for every actively pumped cation an anion will follow, to maintain electric

charge balance, so for every ion that is actively pumped, one counterion and ~360 water molecules follow!

2.3 Fluid flow in the gastrointestinal tract

2.3.1 Ion movement

Most nutrient absorption occurs in the small intestine. Enzymes and other digestive molecules break up carbohydrates and proteins, and emulsify lipids in the mouth and stomach prior to entering the duodenum. In the duodenum, proteases, amylases and lipases further break down these nutrients until they are small enough to diffuse to the brush-border epithelial cells [41]. Then, brush-border hydrolysis breaks the arriving molecules into absorbable pieces; e.g. sucrose (table sugar) is broken into fructose and glucose and then absorbed by glucose transporters. Many of the nutrient transporter proteins require co-transport of ions to allow absorption [42]. The ion transport, mainly sodium transport, also drives water movement across the epithelial surface, and the water in turn drags along nutrients and small molecule drugs toward the cells for brush-border hydrolysis and absorption. This continuous cycle is mainly driven by ion gradients established by the highly elaborate ion channel and transport systems of the small intestinal enterocytes.

The large intestine also takes advantage of ion-transport driven water absorption: its main job is to re-absorb fluid from and nutrients produced by bacteria that are further digesting the chyme exiting the small intestine. The colorectum is inhabited by a vast number and types of bacteria that break down indigestible food molecules to use as fuel for themselves and produce short chain fatty acids such as propionate, acetate, and butyrate, of which butyrate in particular serves as nutrient for colonocytes [31]. These

nutrients must penetrate the thick colonic mucus layer to reach the epithelium, but would fail to do so if the osmotic gradient resulting from digestive processes were not counteracted by an osmotic gradient created by active ion absorption [42]. The body again employs an elaborate ion channel and transport system in the large intestinal enterocytes to maintain a continuous ion, and hence water absorption by the colorectal epithelium.

2.3.1.1 Small intestine

When acidic chyme is transported by peristalsis from the stomach to the small intestine, bicarbonate is secreted primarily by the pancreas neutralize it, but also by local secretion in the duodenum [31, 39, 42]. This occurs via chloride-bicarbonate exchangers or anion selective channels in the apical membrane. When a meal is consumed, the expression of ion-dependent and ion-independent solute carriers is upregulated. In fact many important nutrients such as glucose, fructose, and galactose are transported via sodium-dependent transporters, leading to a net uptake of sodium [39, 42]. To ensure sodium will travel down a concentration gradient, the newly absorbed sodium ions travel across the cell and are shuttled out via basolateral sodium-potassium pump into the interstitial spaces [42]. Anions like chloride follow passively creating electroneutral transport. In the starved state, ion absorption does not stop and now occurs via solute-independent exchangers. In the proximal bowel, chloride ion transport is passive and simply follows sodium transport to make total ion transport electroneutral. If luminal chloride levels need to be increased, cells located closer to the base of the villi will secrete chloride by absorbing from the basolateral side [39, 42]. A sodium-potassium pump then transports sodium back out of the cell and potassium exits the at the basolateral side via potassium channels. Chloride will exit the cell via chloride channels.

2.3.1.2 Large Intestine

In the colon, just like the small intestine, the primary ions shuttled for fluid absorption are sodium, bicarbonate, chloride, and hydrogen. Ion movement into cells in the large intestine mainly occurs via ion exchangers in the apical membrane that pump sodium and chloride into the cells while bicarbonate and hydrogen are secreted [42]. Sodium and chloride transport are not necessarily dependent on each other; for example, the apical membranes of the colonic epithelium also contain epithelial sodium channels that allow sodium diffusion into the cell along its osmotic gradient [39, 42]. Low intracellular sodium concentrations are maintained via sodium-potassium pumps in the basolateral membrane. In the colon, unlike in the small intestine, potassium is then secreted via potassium channels in the apical membrane [42]. Potassium secretion and sodium absorption are both stimulated by chyme reaching the large intestine.

2.3.2 Water movement

The constant sodium flux across the epithelial cells causes water movement across the epithelial layer as well. Based on osmotic pressure differences, every single sodium ion that crosses the epithelial membrane will cause ~360 water molecules to follow (as explained earlier). It has long been thought that water transport mainly occurs via paracellular routes, or through the tight junctions, as water will simply follow the ions. Indeed, the lower electrical resistance of cells in the small intestine [43-45] seems to indicate that they are "leaky" and allow rapid water movement. This is also supported by the low osmotic permeability of membrane vesicles derived from small intestinal cells [46, 47]. However, it has recently been shown that water transport via the paracellular route is limited and cannot account for all water absorption occurring in the small intestine [48-52].

Further research has indicated that aquaporins shuttle water across the cell membrane in an osmosis-driven process [53]. In addition, ion and solute channels can also carry a significant number of water molecules along with the solute [48, 54, 55]. The low permeability of the colonic epithelium makes it highly likely that transcellular movement via aquaporins and ion channels is actually the main route of water movement in the colorectum [48, 54].

2.3.2.1 Role of aquaporins in water movement

Aquaporins have received more attention as vehicles for water movement in recent years. In the small intestine aquaporin expression suggests that aquaporins help mediate water absorption rather than secretion [48]. In both the large and small intestine, aquaporins have been identified in the basolateral and apical enterocyte membranes indicating that water can indeed travel *through* the epithelial cells via aquaporin channels [48]. This occurs via an osmosis-based process, where aquaporins allow water movement from less to more concentrated solutions. However, as food is digested, the process of cleaving proteins, carbohydrates, and other nutrients into smaller and smaller fragments, increases osmolality in the GI lumen to be > 200 mOsm higher than in the blood. If water was only moving passively down its concentration gradient, this would result in water being drawn rapidly into the lumen. It is known, though, that the GI tract *absorbs* water very effectively despite the opposing osmotic gradient, and that active ion transport causes the net absorption of water in both the small and large intestines [54]. It is thus newly stipulated that water is not only absorbed via osmotically driven aquaporin channels, but is also transported in solute transporters.

2.3.2.2 Role of solute transporters in water movement

Researchers over the past twenty years have found more and more indications that aquaporins are not the only water-transporting proteins. In fact many solute and ion transporters also cotransport water; this has been illustrated for a variety of transporters present in the GI tract [54]. Each transporter carries a specific number of water molecules in each turnover cycle ranging from 40 water molecules per glucose molecule in GLUT2 [56] to 590 water molecules per Na+/K+/2Cl- ions in NKCC1 [57]. These transporters are able to actively pump ions and solutes, and thus water, opposing osmotic gradients like those established in the GI tract during digestion. In addition, the number of water molecules transported is not altered when surrounding electrical gradients, concentration or osmotic gradients are changed – the ratio is strictly stoichiometric [54].

2.3.3 Implications for drug delivery

Nutrients are not the only solutes associated with transport across the GI epithelium: medications that mimic nutrients also often take advantage of solute transporters that will co-transport them along with water from the lumen into the cells. Similar to food particulates and molecules requiring a driving force, i.e. water flow, to get past the constantly secreted mucus barrier, drug molecules also take advantage of fluid flowing toward the epithelium [11, 16, 58]. Hydrophilic small molecules in particular, such as drugs mimicking amino acids or nucleotides, can rapidly diffuse through mucus barrier and are rapidly dragged toward the epithelium by the water flux [11, 16, 17]. However, mucus, as described in Section 2.1, consists of mucins with highly negatively charged glycosylated regions. Positively charged drug molecules and polyvalent ions can transiently or permanently bind to these negatively charged glycans, leading to slower diffusion or

entrapment in mucus [8, 11, 16]. Similarly, lipophilic drug molecules are known to bind to non-specifically to proteins like mucins [11, 16]. Indeed, the affinity between lipophilic drugs and mucus has been studied extensively. Researchers have shown that the absorption rate of lipophilic progesterone is dependent on the mucus layer, while less lipophilic hydrocortisone absorption is controlled by the epithelial membrane [59]. In addition, testosterone along with several other lipophilic drug molecules were found to bind to and diffuse more slowly through pig intestinal mucus than hydrophilic molecules [12-14]. Although the movement of these individual molecules is significantly slowed in mucus, the transience of their interactions with mucus allow for their absorption, which is further improved by water absorption driving the individual molecules to the epithelium [9].

While water can drag individual lipophilic drug molecules through mucus and to the epithelium, these drugs do not readily dissolve in the gastrointestinal secretions [11]. Therefore only a small, dissolved fraction will actually reach the epithelium, while the rest of the molecules are suspended in bile salt-coated lipid droplets. These droplets, or micelles, range from 23-35 nm, making them large enough so that diffusion to the epithelial surface would take not suffice to bring them to the absorptive epithelium [58, 60]. Recent advances have shown that bile salts prevent particulates from adhering to mucus [60] and we have shown in this work and previously in the cervicovaginal tract that only non-mucoadhesive particulates can take advantage of fluid flow to get to the epithelial surface [61]. Intestinal mixed micelles, which are coated with bile salts, can thus be dragged toward the epithelial surface by the naturally occurring water absorption and be absorbed there.

Protein-based therapies are a newer class of drugs. Because peptides denature and are broken down easily, they need to be protected against the low pH of stomach acid and the digestive enzymes in the stomach and small intestine. Researchers have found that bioavailability of peptide drugs is significantly enhanced by their encapsulation into nanocarriers [3, 62, 63]. Similar to the bile-salt coated micelles, nanocarriers also need to be able to traverse the mucus barrier to reach the underlying epithelium for absorption. Most nanocarriers exceed the size of bile-salt coated lipids and thus pure diffusion does not suffice for them to reach the GI epithelium. Here water absorption again aids in dragging nanocarriers through mucus and to the epithelium; however, many nanocarriers are composed of hydrophobic polymers that would likely stick to the mucus barrier. Our laboratory has previously developed stealth-nanoparticles that are able to penetrate through human and mouse mucus at a variety of mucosal surfaces [7, 15, 64-68]. The next section discusses what properties can make nanoparticles non-mucoadhesive, how these nanoparticles can be used as biophysical tool to characterize mucus, and how they can be used to determine whether or not fluid absorption is occurring.

2.4 The mucus barrier, fluid absorption, and drug delivery using nanoparticles

Nanocarriers delivered to the GI tract can be effectively trapped in mucus by size exclusion or hydrophobic and electrostatic interactions. GI drug delivery research has mainly focused on developing nanoparticles that strongly adhere to mucus, assuming that this will increase nanoparticle residence time, which would lead to improved drug absorption [69]. However, since these nanoparticles stick to the rapidly cleared sloppy mucus layer, they will likely also be rapidly cleared [4, 5, 7, 70]. To overcome the mucus barrier, our group, inspired by the mucoinert nature of some viruses, has developed

nanoparticles that rapidly diffuse through mucus. We have shown that these mucus penetrating nanoparticles (MPP) can penetrate through the loosely adherent and into more slowly cleared mucus layers, leading to improved drug and gene delivery at mucosal surfaces [5, 7]. In addition, Ying-Ying Wang in [5] has shown that mucoadhesive nanoparticles are unable to take advantage of fluid flow. I have already described how fluid flow in the GI tract can aid in the absorption of nutrients by transporting them through mucus and to the epithelial surface. Mucoadhesive particles are unable to be dragged along with water flow in the GI tract; MPP, however, are able to utilize both inherent and induced fluid absorption to further improve their distribution and retention.

2.4.1 Surface characteristics that yield MPP

We have recently demonstrated that nanoparticles densely coated with polyethylene glycol (PEG) are able to effectively diffuse through human mucus. Previous research indicated that PEG polymers are able to interact with mucins by hydrogen bonding and interpenetration into the mucus network, leading to mucoadhesion [71-74]. Our group further investigated the effects of PEG coatings on nanoparticle interaction with mucus. We demonstrated that nanoparticles coated densely enough with low molecular weight (MW), <10 kDa, PEG could indeed avoid interaction with the mucus barrier [15, 75]. When more than 60% of the surface of hydrophobic, mucoadhesive nanoparticles (MAP) was coated with 2 kDa PEG, their transport rates increased >700-fold compared to those with approximately 40% less PEG on their surface [75]. The particles coated with low-density PEG had transport properties equivalent to uncoated nanoparticles.

PEG coverage of nanoparticles can also be correlated to their surface charge, namely their ζ-potential. Based on the existing literature and our work, we determined

that a near-neutral ζ-potential is necessary to indicate that a nanoparticle is mucus penetrating. The threshold for this lies between -7 mV and -10 mV and nanoparticles with a ζ-potential ≤ -10mV will be mucoadhesive [75]. In the same studies we found that coating nanoparticles with 10 kDa PEG at a similar density as 2 kDa PEG (67% for 2 kDa PEG vs 64% for 10 kDa PEG) caused them to be mucoadhesive [75]. We postulated that this was due to the previously mentioned interpenetration and hydrogen bonding of PEG molecules with the mucus mesh. New data presented in Appendix I indicates that MPP can be obtained by coating nanoparticles with PEG MW ≤ 40 kDa.

2.4.2 MPP for mucosal drug delivery

Nanoparticles provide significant advantages for drug delivery compared to free drug vehicles by providing sustained release, surfaces for attaching targeting moieties, and protection against stomach acid and digestive enzymes. Biodegradable nanoparticles are preferred for drug delivery. Our group has thus focused on creating drug-loaded, biodegradable MPP formulations. We have accomplished this both by chemically conjugating PEG to hydrophobic polymers, such as poly(lactic-co-glycolic acid) (PLGA), to ensure sufficient PEG coating on the surface as well as by using all Generally Regarded as Safe, or GRAS, materials such as PLGA coated with Pluronic ® [76, 77]. We determined that not all Pluronic ® types sufficiently coat nanoparticles with PEG: Pluronics ® are triblock copolymers that contain two PEG chains attached to a poly(propylene oxide) (PPO) and only pluronics ® with a PPO chain > 3 kDa and PEG chain of 2 kDa or 5 kDa in size actually make nanoparticles penetrate mucus [77]. Nanoparticles made with polymers containing covalently bound PEG often require the addition of the original polymer to obtain sufficient drug loading (unpublished data and [6,

[78]). However, if nanoparticles are made with insufficient PEG-polymer, this will lead to insufficient PEG coverage, similar to what we illustrated with non-biodegradable MPP [6, 75, 78]. We also recently showed that nanoparticles made via the emulsion method require the addition of low molecular weight surfactants to make MPP. When high molecular weight surfactants were used, nanoparticles were immobilized in mucus, likely due to disruption of the integrity of the PEG architecture on the particle surface [78].

For a long time, mucosal drug delivery focused on making nanoparticles mucoadhesive in order to improve their retention time. We hypothesized that MPP, due to their ability to diffuse in mucus, would be able to penetrate into more slowly cleared mucus layers thus improving their distribution and retention over MAP that will stick to mucus as soon as they encounter it. Indeed, we have demonstrated that MPP significantly improve nanoparticle distribution and retention in the cervicovaginal and respiratory tracts over MAP [5-7, 15, 79]. In the cervicovaginal tract, we found that MPP can reach all portions of the highly folded vaginal epithelial surface and provide >80% tissue coverage after 24h, while free drug loaded gels coat <45% of the epithelial surface [5]. In addition, more than 60% of MPP but only 10% MAP are retained vaginally after a 6 h period [5]. In addition, drug- loaded MPP provided better protection than a 10-fold higher dose of free drug against herpes simplex virus (HSV) when administered 30 min prior to viral challenge [5].

In the respiratory tract, we found that MPP evenly coat the tracheal and bronchial epithelium, and smaller MPP were found in close proximity to the epithelial cells [6]. In contrast, MAP aggregated in clumps away from the epithelial surface. MPP were also retained to a much greater degree: after only 2 h, <45% of MAP but >85% of MPP

remained in the lungs [6]. Similarly, only 25% of biodegradable MAP but >85% biodegradable MPP were retained in the lungs after 2 h, a pattern that continued up to 6 h post administration [6]. In addition to improving retention and distribution, MPP seem to induce little to no toxicity, while MAP seem to cause immune cell infiltration in both the lungs and CV tract [5, 6]. The differences between MPP and MAP have not been elucidated for GI drug delivery and thus are explored in Chapter [insert chapter number for MPP vs MAP] of this thesis.

2.4.3 MPP as tool to understand mucosal physiology

Research has shown that nanoparticles are a useful tool to analyzing biological substances, like mucus. In particular, mucus-penetrating nanoparticles have been utilized to determine the rheological properties of mucus. These properties are the viscosity, represented by the loss (or viscous) modulus G", and elasticity, represented by the storage (or elastic) modulus G'. Bulk rheology of mucus describes it as a viscoelastic material, indicating that it can both flow and deform. Mucus is also described as shear-thinning, such that when high shear rates are applied to it, the resistance to deformation is very low, and mucus behaves like a lower viscosity fluid [8]. Low shear rates cause high resistance to deformation, and mucus behaves more like a solid. While these properties very accurately describe the behavior of mucus at the macro scale, it does not provide sufficient conclusions about the viscosity and elasticity experienced by a small nanocarrier. Indeed, we have shown that nanoparticles that stick to mucus or are larger than the mesh spacing experience mucus as having higher viscosity [15, 30, 80]. This is largely due to the microrheological properties of mucus.

The microrheology of mucus can be studied by following the mean squared displacements (MSD) of nanoparticles in mucus. The Laplace transform of MSD can be related to the viscoelastic modulus by G (s) = $\frac{k_b T}{\pi \cdot a \cdot s \cdot MSD(s)}$ where s is the Laplace frequency, and when G(s) is projected into Fourier space, this results in the complex modulus G*(ω), where the real part is the elastic modulus, G', and the imaginary part is the viscous modulus, G" [80, 81]. Viscoelastic materials like mucus can then be categorized into viscoelastic solids when G'>G" or viscoelastic liquids when G">G'. The relationship between G" and G' can also be described using the phase angle, or δ=tan($\frac{G''}{G'}$) such that a viscoelastic solid has δ<45° and a viscoelastic liquid has δ>45° [82, 83]. Depending on the nanoparticle size and interaction with mucus, it can experience mucus as a viscoelastic liquid or viscoelastic solid. For example, MPP<500nm in size experienced mucus as a viscoelastic liquid, with δ>60°, while MPP 1 μm in size experienced mucus as a viscoelastic solid with δ≈30° [83]. Similarly, we found that mucoadhesive nanoparticles 200 nm in size experienced mucus as a viscoelastic solid, with a microviscosity 7-15 fold lower than the bulk viscosity, due to their mucoadhesive interaction with mucus [80]. Mucoadhesive nanoparticles thus are not effective tools for determining microrheology, as the rheology will likely mainly illustrate the contributions from adhesive interactions instead of local G" and G'. In stark contrast, we have found that microviscosity experienced by 200 nm MPP is 300-1500 times lower than bulk viscosity, and thus MPP experience mucus as a viscoelastic liquid and can serve as tool to determine the viscoelastic properties of the interstitial spaces in mucus [80, 83].

2.4.4 MPP and fluid absorption

More recently we have also utilized MPP to determine the capability of a drug delivery formulation to induce fluid absorption [61]. While the distribution of MAP on the vaginal epithelium is unaffected by fluid flow from the lumen to the epithelium, MPP distribution is significantly different when they are administered in absorption-inducing fluids compared to non-absorption-inducing fluids. Fluid flow, or advection, caused by an absorption inducing (or hypotonic) vehicle rapidly transports MPP through the mucus layer to the epithelial surface, leading nanoparticles to penetrate into the folds of the vagina, or rugae, and uniformly coat the entire vaginal epithelium [5, 61]. In contrast, MPP administered in a vehicle that does not induce advection (or an isotonic vehicle) remain in the lumen. We found that fluids that are moderately hypo-osmolar to blood can still cause fluid absorption to occur within 5 minutes of administration [61]. It is unfortunately difficult to use this rapid nanoparticle movement to estimate the actual time needed for and amount of fluid absorption occurring. Thus MPP can only serve as tool to determine if a vehicle causes fluid absorption or not. In this thesis, I have taken advantage of MPP as such a tool in Chapter (insert enema chapter number) to design a hypotonic enema formulation for rectal drug delivery with particular focus on the delivery of antiretroviral drugs for HIV prevention.

2.5 Gastrointestinal diseases

The GI tract, along with our skin, is one of the surfaces on the body with the most contact to the external elements. While stomach acid removes many pathogens, the GI tract still faces thousands of potential infectious agents – including many viruses and bacteria – on a daily basis. If we consider that uncontrolled growth of our commensal bacteria can also

turn into disease states, the GI tract is a prime target for infection. Local infections by bacteria such as salmonella and viruses such as those causing viral gastroenteritis, can lead to many symptoms including diarrhea, vomiting, and nausea. However, our immune system or currently available medications can often battle these infections. Chronic diseases face unique challenges in that they require long-term drug treatments and often causes are not known. One such diseases is inflammatory bowel disease (IBD), where patients can experience sever pain, diarrhea, and have ulcers located either to the colon (in ulcerative colitis, or UC) or throughout the entire intestine (in Crohn's disease, or CD) [84, 85]. Other chronic conditions include GI cancers and inflammatory bowel syndrome. In addition to chronic diseases of the local epithelium, the GI tract, the colorectum and oral cavity in particular, is a major target for infectious agents that can lead to chronic systemic illness, such as HIV. Here we summarize current treatment methods for IBD and prevention methods for HIV in the GI tract.

2.5.1 IBD

Inflammatory bowel disease is quite common in developed nations, affecting about 1.4 million patients in the US and 2.2 million in Europe [86, 87]. Patients experience symptoms ranging from GI discomforts such as bloody diarrhea, abdominal pain, and vomiting to systemic effects such as weight loss and fever. The disease is believed to be caused by both environmental and genetic factors, as factors like the use of oral contraceptives and smoking can affect the condition [86, 88-92]. IBD presents either as ulcerative colitis (UC), which mainly affects the transverse colon, descending colon, and rectum, or Crohn's disease (CD), which can affect the entire GI tract [85, 93]. Unfortunately, the exact cause of

IBD is still unknown and thus a cure has not been developed; instead, patients receive life-long treatment to alleviate symptoms and improve their quality of life.

Medication for IBD is usually administered via the oral or rectal routes. The rectal route has been shown to have significant benefits for UC treatment because it avoids first-pass metabolism and high local concentrations of active drugs [94]. Rectal formulations include enemas, foams, and suppositories containing a variety of anti-inflammatory drugs such as 5-aminosalicylates (5-ASA) or corticosteroids [95-97]. Out of these, foams and enemas are most promising, as these can deliver drug throughout the entire rectum, sigmoid, and descending colon, unlike suppositories that mainly release drug in the rectum itself [98]. Colon targeting strategies have also been employed in oral delivery of 5-ASA for UC treatments. Many of these release drug on a pH basis, with release occurring between pH 4.5 – 7 [99], since local inflammation can lead to lower pH values than those found in the healthy regions of the GI tract. Several of these have demonstrated significant therapeutic success, though differences between individual formulations have yet to be demonstrated in large-scale studies [100, 101].

Another common method to target drugs to the colorectum and improve bioavailability is the use of prodrugs. Prodrugs are pharmacologically inactive compounds that are converted to their active form by enzymes specifically found in the colorectum such as azoreductase, glycosidase, galactosidase, and others [102-106]. Some 5-ASA prodrugs have been found to have significant improvements over the original 5-ASA compound: patients treated with balsalazide, a sulfa prodrug containing a diazo linkage between 5-ASA and 4-aminobenzoyl-β-alanine, had shorter remission times (64% vs 43% after only 2 weeks and up to 88% vs 57% after 12 weeks) and more

asymptomatic days (10 vs 25 days) compared to the active compound, 5-ASA [107](ref). In addition, 60-80% of patients with mild to moderate UC that were treated with osalazine, a sulfa prodrug of two 5-ASA molecules, had fewer clinical symptoms and signs [108]. The use of prodrugs can thus significantly improve outcomes in UC and make safer, more efficacious, and more tolerable treatment options.

Nanotechnology has more recently received significant attention for use in IBD. Nanoparticles provide sustained release and offer an easy platform for developing targeting strategies that may be implemented to target inflamed tissues [95, 98]. Polymeric nanoparticles are most commonly made of poly(lactic-co-glycolic acid), a FDA approved biodegradable polymer. Investigations using PLGA nanoparticles in murine models of IBD have shown that nanoparticle deposition is size dependent, with amount of deposition increasing as size decreases: 10 μm < 1000 nm < 100 nm [109]. Similarly, nanoparticles seemed to preferentially adhere to inflamed tissues, as was shown by both oral and rectal administration of drug-loaded nanoparticles that led to 3-fold higher drug penetration into ulcerated regions [109-112]. Most conventional nanoparticle systems, however, firmly adhere to the mucus layer coating the gastrointestinal tract (as described earlier) and it is unclear whether or not mucoadhesive or non-mucoadhesive nanocarriers would be most beneficial for IBD treatments. Chapter [MPP vs MAP] of this thesis discusses the differences in distribution of mucoadhesive and non-mucoadhesive nanocarriers in the healthy GI tract. In addition, physiological changes in UC, including mucus hypersecretion and increased epithelial permeability, may alter the characteristics that are necessary to make MPP for UC [113-116]. Recent reports have shown that the mucus barrier, in particular the normally impenetrable adherent layer, is broken down and allows

both bacteria and PEG-coated nanoparticles as large as 2 μm to penetrate into affected regions [109-111, 115]. Chapter [insert MPP vs MAP chapter number] also addresses whether or not these changes in the mucus barrier can alter whether mucoadhesive or non-mucoadhesive nanoparticles are preferable for IBD treatments.

2.5.2 Microbicides for HIV Prevention

Infection with human immunodeficiency virus (HIV) has long been identified as an epidemic and affects more than 35 million people worldwide [117]. Eradication of this virus once an individual is infected has proven extremely difficult. Many recent efforts have therefore focused on developing pre-exposure prophylaxis (PrEP) methods to prevent the ~2 million new HIV infections occurring every year [117]. A significant portion of these infections occur due to unprotected receptive anal intercourse (RAI), which can be in part led back to the 20-fold increased risk of rectal compared to vaginal HIV transmission [118]. In addition, while HIV incidence rates have fallen in many populations, the rate of new infections seems to be stable or increasing for men who have sex with men (MSM) [119, 120]. There is thus a significant need for the development of rectal microbicides.

Rectal microbicides currently in development include oral and rectal formulations. The US Food and Drug Association (FDA) has recently approved Truvada ®, an oral tablet of tenofovir disoproxil fumarate (TDF) and emtricitabine (FTC), both reverse transcriptase inhibitors, as PrEP for high risk populations in the USA [121]. Phase III clinical trials have shown that a daily oral dose of Truvada ® decreases HIV incidence by 44% [122]. When evaluating participants with detectable drug-levels, compared to those of undetectable levels, the chance of HIV transmission was further decreased to a relative 92% reduction of transmission [122]. However, researchers have voiced concerns with oral

PrEP: systemic exposure may lead to antiretroviral resistance and increased availability of oral PrEP may lead to decreased rates of condom use [123, 124]. These concerns are less evident when considering rectal microbicide delivery.

Currently, rectal gels are considered the most promising method for rectal PrEP. Gels or lubricants are widely used for RAI with separate studies showing use by >89% of participants [125, 126]. Several gels have been developed as PrEP. One of these is a gel containing UC781, a non-nucleoside reverse transcriptase inhibitor, which was studied in RMP-01 [126]. In this Phase I trial gels containing 0.1% or 0.25% UC781 were assessed for safety and acceptability. The gels showed mild adverse events (AE) but no changes in mucosal safety markers were observed. Tissue biopsies from participants receiving 0.25% UC781 gel showed marked reduction in tissue of HIV p-24 ex vivo and plasma drug levels were undetectable [126, 127]. While these results were promising for advancing this gel to Phase II development, the US FDA sponsor discontinued clinical development of UC781 as a microbicides in 2010 [121].

Perhaps the most commonly studied microbicide gel is a 1% tenofovir (TFV) gel formulation. Originally intended as a dual-compartment gel, this formulation was tested in the RMP-02/MTN-006 study that showed that rectal gels led to 112-fold higher tissue C_{max} of tenofovir-diphosphate (the active intracellular product of TFV) than oral formulations 30 min after exposure [127]. The study reported no serious AE; however, repeated dosing of TFV gel was associated with increased AE, in particular GI AE. The original formulation was thus deemed unsafe for rectal use, and was later found to be associated with epithelial fracture and sloughing [128]. The epithelial damage was attributed to its high osmolality due to the 20% glycerol content; the drug was then a reformulation

into a reduced-glycerol (5%) rectal formulation (RG 1% TFV gel). The RG formulation has been investigated for safety in the MTN-007 trial. In this study, three different gels, HEC placebo, RG 1% TFV, or 2% nonoxynol 9 (N9, a known spermicide that causes epithelial irritation [129]), were administered daily for 7 days and safety was assessed via histology, fecal calprotectin, epithelial sloughing, cytokine expression (mRNA and protein), microarrays, flow cytometry of mucosal T cell phenotype, and rectal microflora [130]. Fecal calprotectin, rectal microflora, and epithelial sloughing showed no difference between treatment arms, while histology, mucosal gene expression, protein expression, and T cell phenotype showed differences as compared to N9 gel. Overall the RG 1% TFV gel was considered both acceptable and safe and has been advanced to Phase II clinical trials in the MTN-017 study [121]. In addition to MTN-017, a combination rectal microbicide gel is under investigation in the Combination HIV Antiretroviral Rectal Microbicide (CHARM) Program. This program is currently investigating the safety, acceptability, distribution, and pharmacokinetic (PK)/pharmacodynamic (PD) profiles of three 1% TFV gels (the original vaginal formulation, the RG formulation, and a rectal specific formulation) in two Phase I trials, Charm-01 and Charm-02 [121]. A third trial, Charm-03, aims to compare the safety, acceptability, and PK/PD of oral and rectal gel formulations of maraviroc, a CCR5 receptor antagonist.

Another more recently explored avenue for rectal microbicide is the development of a microbicide containing rectal douche (or enema). Many MSM currently used enemas prior to RAI, making this another PrEP method that requires little behavioral changes [131]. Most enemas are used within 0.5-8 h prior to receptive rectal intercourse, such that for a microbicide loaded enema no daily administration would be necessary. In addition to

providing little need for behavioral changes, enema formulations have been shown to reach significantly larger fractions of the colorectal surface compared to rectal gels [132-134]. In fact, Leyva et al demonstrated that an iso-osmolar enema led to fluid distributing into the descending colon, in some participants all the way to the splenic flexure, after only 2 h. In contrast, microbicide loaded gels required 24 h to reach the splenic flexure, a time that is much too long for a microbicide-loaded lubricant used during intercourse [133]. Leyva et al also showed that the osmolarity of the enema formulation played a critical role in its distribution; hypo-osmolar (tap water) and hyper-osmolar (Fleet ®) enemas remained localized to the recto-sigmoid colon 2 h after administration in stark contrast to the iso-osmolar enema. The basis of designing enema formulations optimal for STI prevention and the tunability of enema formulations for other diseases is topic of Chapter 4 of this thesis, and this work in combination with studies by Hendrix et al on use of enemas as rectal microbicides has recently been translated into clinical trials via the Development of Rectal Enemas as Microbicide (DREAM) Project.

A novel development in PrEP is the use of nanotechnology to provide sustained release and improve solubility of poorly water soluble drugs. Das Neves et al developed a dapivirine, a nucleoside reverse transcriptase inhibitor, loaded polymeric nanoparticles that, when coated with poly(ethylene glycol) (PEG), provided improved tissue penetration and no detectable epithelial toxicity [135-138]. Another nanocarrier explored as microbicide is the Starpharma's Vivagel ®, a gel containing the polylysine dendrimer known as SPL7013. Dezzutti et al found that a 5% SPL7013 gel was safe on Caco-2 cells and reduced HIV infection by over 85% [139]; however, this formulation also caused epithelial sloughing [140]. A 3% SPL7013 gel tested in pigtail macaques was found to be

safe after daily administration for three days [141]. Nanocarriers used as rectal microbicides will face a particular challenge: the mucus barrier, as already discussed in section 2.1. The development of a dapivirine nanoparticle that can traverse the mucus barrier is demonstrated in Chapter 5 of this thesis.

Table 2-1. Properties of mucus at various surfaces including thickness, primary mucin type, and turnover rate.

Mucosal surface		**Thickness (µm)**	**Mucin type**	**Turnover rate**
Cervicovaginal tract	-	NA	MUC4 MUC5B [142, 143]	3 – 7 h [144]
Respiratory tract	Airway	7 – 30 [145-147]	MUC5AC MUC5B [148]	10 – 20 min [149]
	Bronchi	50 – 60 [150]		
Eye	Mucus	0.02 – 0.05 [151]	MUC5AC MUC1 MUC4 [152]	5 – 8 min [153]
	Tear film	5 – 50 [151, 154, 155]		
Gastrointestinal tract	Stomach	50 – 450 [9]	MUC5AC MUC6 [31]	4-6 h [83, 156]
	Small intestine	10 – 40 [157, 158]	MUC2 [31]	
	Large intestine	110 – 160 [157-161]	MUC2 [31]	

3. EFFECT OF SURFACE CHEMISTRY ON NANOPARTICLE INTERACTION WITH GASTORINTESTINAL MUCUS AND DISTRIBUTION IN THE GASTROINTESTINAL TRACT FOLLOWING ORAL AND RECTAL ADMINISTRATION IN THE MOUSE[*]

[*] Reprinted from Journal of Controlled Release, Maisel, K. Ensign, L. Reddy, M. Cone, R. Hanes, J. Effect of surface chemistry on nanoparticle interaction with gastrointestinal mucus and distribution in the gastrointestinal tract following oral and rectal administration in the mouse, *In press*, Copyright 2014, with permission from Elsevier.

3.1 Introduction

More than 80% of drugs are taken orally, making the gastrointestinal (GI) tract the primary site of drug delivery [1-3]. Many potent small molecule drugs are hydrophobic and poorly water soluble, which often translates into poor oral bioavailability [3]. Micronization of hydrophobic drugs to increase surface area is a common method to improve drug dissolution, thereby enhancing uptake of poorly soluble drugs [3, 162-164]. Encapsulation within polymer nano- and microparticles is another approach that has been demonstrated to improve oral delivery of many types of drugs, ranging from small molecules to large proteins [1, 3, 165]. However, whether a poorly soluble drug is micronized into a suspension of hydrophobic particulates, or any drug is encapsulated within conventional polymeric nanoparticles, the final product is typically a hydrophobic particle that is strongly adhesive to mucus [4].

Current dogma suggests that mucoadhesion of particulates is beneficial for maximizing delivery in the GI tract. Mucoadhesion purportedly allows the particulates to leave the chyme by adhering to the mucus layers lining the GI tract [4, 166, 167]. It is widely agreed that enhanced drug delivery from the chyme to the entire (highly-folded) GI tract epithelium, including the highly absorptive jejunum, where fluid absorption greatly speeds nutrient uptake, is desired for maximum absorption into the systemic circulation [4, 168-171]. Furthermore, for treating diseases of the colorectum, such as ulcerative colitis (UC), and for preventing rectal transmission of sexually transmitted infections (STI), rectal, rather than oral administration, may be more effective [131, 133, 172, 173].

However, GI tract mucus is a continuously secreted barrier that traps and coats foreign particulates and pathogens to protect the underlying epithelium [4]. Thus, we

recently suggested that it is possible that the rapid clearance of the most superficial luminal mucus layers in the GI tract may limit the effectiveness of mucoadhesive particles [4]. Mucoadhesive nano- and microparticulate formulations have been shown to significantly improve delivery of several drug molecules in the GI tract compared to drugs administered without a delivery system, at least partly by increasing drug solubility, providing sustained release, and protecting the drug cargo. However, it has yet to be carefully tested whether mucoadhesive nano- and microparticles provide advantages over non-mucoadhesive particles in terms of partitioning from the chyme into the GI mucus layers. It also has not been established which type of particle provides the most uniform distribution over the absorptive epithelium in the GI tract.

In this paper, we sought to directly test the GI distribution of particles that were carefully confirmed to possess either strongly mucoadhesive or non-mucoadhesive surfaces. We hypothesized that particles smaller than the mucus mesh spacing and with non-mucoadhesive surfaces would penetrate the thick mucus barrier in the GI tract, leading to a more uniform delivery of the particles to the absorptive epithelium in healthy animals. We also tested these particle types in an animal model of ulcerative colitis (UC), a subset of inflammatory bowel disease (IBD) characterized by disruption of the epithelial barrier, increased mucus secretion, and increased inflammation, with the hypothesis that the non-mucoadhesive particles may more effectively penetrate through the mucus barrier and enter into the diseased tissues of the GI tract.

To test our hypotheses, we prepared nanoparticles of various sizes that possessed either unmodified hydrophobic surfaces, or hydrophilic, neutrally charged surfaces obtained via a dense coating with polyethylene glycol (PEG). We first confirmed in

mouse GI mucus *ex vivo* that the unmodified nanoparticles were mucoadhesive (mucoadhesive particles, MAP), whereas the PEG-coated particles were non-mucoadhesive (mucus-penetrating particles, MPP). Subsequently, we administered MAP and MPP to mice by oral gavage, ligated intestinal loops and by rectal enema, and observed their distribution in the jejunum, ileum, and colon. We further compared MAP and MPP distribution in inflamed regions of the small intestine and the associated ulcerated colonic tissue regions in two common mouse models of UC.

3.2 Materials and Methods

3.2.1 Animal model

Female 6-8 week old CF-1 mice were purchased from Harlan (Indianapolis, IN). Mice were placed on liquid diet for 24 h and starved for 24 h to produce reduced amounts of softer, more human-like feces, as opposed to the dry, hard pellets normally produced by mice. To induce TNBS-colitis, mice were anesthetized with isoflurane and dosed rectally with 0.125 mg/g of 2,4,6-trinitrobenzenesulfonic acid (TNBS, also known as picrylsulfonic acid, Sigma-Aldrich) in 50% ethanol as previously described [174]. To induce DSS-colitis, mice were given 4% w/v dextran sulfate sodium (DSS, Sigma-Aldrich) in their drinking water for four days, as previously described [175]. Only mice that lost at least 5% of their body weight, a common measure of disease induction, were used [174]. These procedures reliably produced mice with colorectal tissue with clear signs of inflammation, including thickening of the mucosa and loose stool. Mice with DSS- and TNBS-induced colitis were allowed access to food and water ad libitum. All procedures were approved by the Johns Hopkins Animal Care and Use Committee.

3.2.2 Nanoparticle formulation

Fluorescent, carboxylate-modified polystyrene nanoparticles (PS-COOH) of various sizes (40 nm, 100 nm, 200 nm, 500 nm) were purchased from Molecular Probes (Eugene, OR) and used as model conventional mucoadhesive particles (MAP). To produce mucus-penetrating particles (MPP), PS-COOH nanoparticles were densely coated with poly(ethylene glycol) (PEG), as previously described [176]. Briefly, 5 kDa methoxy-PEG-amine (Creative PEGworks), N-Hydroxysulfosuccinimide (Sigma), and 1-Ethyl-3-(3-dimethylaminopropyl) carbodiimide (EDC, Invitrogen) were dissolved in 200 mM borate buffer and added to PS-COOH to facilitate coupling of carboxylic acid and amine groups. Nanoparticle size was characterized using dynamic light scattering (90° scattering angle), and ζ-potential was determined via laser Doppler anemometry with a Zetasizer Nano ZS90 (Malvern Instruments, Southborough, MA) (Table 3-1). We have previously found that a near-neutral ζ-potential for these particles indicates that the surface is sufficiently coated with PEG to rapidly penetrate human cervicovaginal mucus (Table 3-1) [61]. All measurements were performed at 25°C and according to instrument settings.

3.2.3 Nanoparticle distribution in the mouse small intestine and colorectum

Nanoparticles were diluted to 0.2 – 0.02% w/v in water for distribution studies depending on particle size and mode of administration. For nanoparticle distribution in the small intestine, 50 μl of nanoparticles suspended in deionized (DI) water were administered via oral gavage. Sections of the jejunum were excised 1 h (colitis) and 2 h (healthy) post administration, and sections of the ileum were excised 6 h post administration and subsequently flash frozen in Optimal Cutting Temperature compound (OCT). For intestinal loop experiments, animals were anesthetized with avertin solution, and the

ileum was exposed from a small incision in the abdomen. A 2 cm region was tied off using surgical sutures, and 200 µl of fluid was injected into the loop using a syringe. The loops were excised 30 min after administration of nanoparticles and frozen in OCT. To assess colorectal distribution, nanoparticles were suspended in DI water as an enema vehicle. For transverse sections, 20 µl of nanoparticle solution was administered to mice under isoflurane anesthesia. After 5-10 min, their colorectal tissues were excised and immediately frozen in OCT. For all tissues, sections were cut 6 µm thick using a Leica CM-3050-S cryostat. The tissue sections were briefly fixed in 10% formalin, air dried, and stained with ProLong Gold antifade reagent with 4',6-diamidino-2-phenylindole (DAPI). Sections were imaged using an inverted epifluroescence microscope (Zeiss Axio Observer).

For surface coverage measurements in the jejunum, 50 µl of nanoparticles suspended in DI water were administered via oral gavage, and tissues removed after 2 h. The tissues were then sliced open longitudinally and flattened between two glass slides to expose the epithelial folds (colon) or villi (jejunum), as previously described [177]. For surface coverage measurements in the colorectum, mice were given a 200 µl DI water enema prior to nanoparticle administration to remove remaining pellets and ensure maximum tissue surface exposure. After 10 min, to ensure that all excess enema fluid was either expelled or absorbed by the epithelium, 50 µl of nanoparticle solution was administered rectally, and the tissues were excised within 5-10 min. Tissues were imaged using an inverted epifluroescence microscope (Zeiss Axio Observer). Control tissues (mice receiving no nanoparticles) were imaged to determine tissue background fluorescence levels to ensure that the fluorescent nanoparticle signal was above

background. For quantification, 6 images were obtained at regular intervals along the tissue surface. The images were threshholded and the % coverage was quantified using ImageJ as previously described [177]. Data represents the average for n ≥ 3 mice ± the standard error of the mean.

3.2.4 Ex vivo tracking of nanoparticles in small intestinal and colorectal mucus of mice

Mice were prepared as described above. On day 3 after TNBS treatment (UC colon) or after 3 days of liquid diet and a 24 h starvation period (healthy small intestine), *ex vivo* tracking experiments were performed as previously described [61, 178]. Briefly, the small intestine or colorectum was excised, longitudinally sliced open, and a 1 cm segment of tissue was placed in a custom-made 0.5 x 1 cm chamber. A volume of 0.5 μL of nanoparticles of various sizes (diluted to 0.02−0.08% w/v) was carefully pipetted on top of the mucus coating the tissues. The wells were then sealed by placing a cover slide was on top of the tissue and affixing it using superglue. Movies were obtained using an inverted epifluorescence microscope with a 100×/1.46 NA oil-immersion objective. Movies were taken using an EMCCD camera (Evolve 512; Photometrics) for 20 s at temporal resolution of 66.7 ms. Nanoparticle positional data was obtained using Metamorph software and the resulting trajectories were analyzed using MATLAB. At least 100 nanoparticles of each size and type were tracked for 50 frames or more to obtain nanoparticle mean square displacements (MSD) as a function of timescale calculated as $\langle \Delta r^2(\tau) \rangle = [x(t+\tau)-x(t)]^2 + [y(t+\tau)-y(t)]^2$ [178-181]. Our prior work has found that static error can be estimated to be 20 nm, much smaller than the size of the nanoparticle displacements [179, 182].

3.3 Results

3.3.1 Distribution of orally-administered MAP and MPP in the small intestines of healthy mice.

We first performed *ex vivo* multiple particle tracking (MPT) experiments, as previously described [61], to confirm that our model mucoadhesive particles (MAP) were adhesively trapped in mucus layers coating freshly excised mouse small intestine tissue. The trajectories of 200 nm MAP indicated adhesive immobilization (Fig 3-1A). In contrast, the trajectories of similarly-sized MPP indicated that MPP freely diffused in the mucus layers coating mouse small intestine tissue (Fig 3-1A). We then sought to determine whether adhesive interactions with small intestine mucus would impact nanoparticle delivery following oral administration by gavage. We used small gavage fluid volume (50 μL) to administer MAP and MPP to minimize volume-related artifacts [183]. As shown in Figure 3-1B, adhesion of MAP to luminal mucus layers resulted in exclusion of these particles from most of the epithelial surface (black in the image). In contrast, MPP were found distributed over much more of the epithelial surface, such that the impression of the flattened villus tips could be visualized to be nearly completely surrounded by MPP (Fig 3-1B). We then quantified the epithelial surface area covered by nanoparticles, and found that MPP covered 74 ± 4% of the epithelial surface of the jejunum, compared to only 35 ± 7% by MAP (Fig 3-1C).

Using the same oral administration methods, we then examined the cross-sectional distribution of the particles. We found that the adhesive MAP were clumped together in the lumen of the jejunum and ileum, unable to penetrate between the villi (Fig

3-2). In contrast, MPP distributed evenly throughout the tissue in both the jejunum and ileum, even though a small gavage fluid volume was used (Fig 3-2).

3.3.2 Impact of fluid volume and mode of administration on MAP and MPP distribution in the small intestines of healthy mice.

One challenge with interpreting and comparing literature reports of oral administration of nano- and microparticles is that the experimental protocols often differ significantly. We thus investigated the effects of fed state, administration method (oral gavage vs. intestinal loop), and gavage fluid volume on the GI distribution of MAP and MPP. Animals are almost always starved prior to oral administration experiments to avoid the confounding changes in transit time and absorption attributable to varied GI content. As shown in Figure 3-3A, not only was there little apparent effect on intestinal distribution of MPP after oral gavage to mice in the "fed" state, but the difference in distribution between co-administered MAP and MPP appeared even more pronounced in the fed state compared to the starved state. In the area close to the lumen (L), outlined at 10x magnification by a pink box and then shown at 20x, MAP were found in large aggregates sometimes colocalized with some MPP, whereas MPP were also dispersed between the villi. In the area far from the lumen and among the villi, outlined at 10x magnification by a yellow box and then shown at 20x, MAP were essentially absent in the villi, whereas MPP were dispersed throughout and between the villi (Fig 3-3A). Thus, in the fed state, in contrast to MAP, non-adhesive MPP appeared to leave the digesta, penetrate the entire mucus barrier, and become well distributed on the epithelial surfaces.

We next investigated whether the high fluid volumes often used with intestinal loops or oral gavage can impact the distribution of MAP or MPP. We anticipated that

administering particles in a large volume of fluid, that can distend the intestines and potentially cause viscous fingering through the mucus barrier [4], would enhance MAP distribution throughout the small intestine. As expected, filling the intestine with fluid containing MAP in an ileal loop model led to dispersion of MAP throughout the intestine and between the villi (Fig 3-3B). The distribution of MAP was very similar to MPP administered to intestinal loops (Fig 3-4). Similarly, when we administered MAP by oral gavage in 5-fold higher fluid volume (250 μL), although MAP appeared to aggregate to some extent, they became distributed in the jejunum and ileum as though the mucus barrier was not present (Fig 3-3B). Overall, the small intestine distribution of MAP in an intestinal loop model, and after high volume gavage of MAP (that would be impractical to scale to humans), was very similar to distribution of MPP, and was in stark contrast to the distribution of MAP administered by gavage in low fluid volume (Fig 3-2).

3.3.3 Distribution of MAP and MPP in the colorectum of healthy mice.

Prior to *in vivo* experiments to investigate MAP and MPP distribution in the colorectum of healthy mice following administration by enema, we first confirmed that MAP, regardless of particle diameter, were adhesively trapped in the mucus layers coating colorectal tissues freshly prepared *ex vivo*, whereas MPP <230 nm in diameter rapidly diffused through mouse colorectal mucus, as indicated by their trajectories (Fig 3-5). With this confirmation, we compared MAP and MPP distribution on the colonic epithelium when administered a hypotonic enema vehicle that causes osmotically-induced fluid absorption by the colonic tissue and, thus, fluid advection toward the epithelium [61]. MAP were trapped and aggregated within colorectal mucus *in vivo* regardless of particle size, leading to limited distribution to only select areas in the

colorectal lumen (Fig 3-5). In contrast, MPP uniformly coated the epithelial surface of the colorectum within only a few minutes after administration. MPP 40 nm and 100 nm in size reached all of the deep, folded surfaces, evenly coating the colorectal epithelium (Fig 3-5). MPP 200 and 500 nm in size also provided improved distribution compared to similarly sized MAP (Fig 3-5). However, 200 and 500 nm MPP did not distribute throughout the colorectal epithelium as uniformly as 40 and 100 nm MPP (Fig 3-5), a result consistent with the rapid diffusion of 40 and 100 nm MPP observed by *ex vivo* multiple particle tracking on freshly excised mouse GI tissue.

We then sought to quantify the colorectal distribution of MAP and MPP in the mouse colorectum after administration by hypotonic enema. MAP of all sizes were found to associate with luminal mucus bundles (Fig 3-6A), limiting the apparent colorectal surface coverage of 40, 100, 200 and 500 nm MAP to 39 ± 4%, 38 ± 2%, 38 ± 3%, and 36 ± 3%, respectively (Fig 3-6B). In contrast, MPP reached more of the colorectal tissue surface, with overall surface coverage decreasing as particle size increased (Fig 3-6A). MPP 40 nm in size provided a nearly uniform coating of the colorectal tissue surface (84 ± 1%), and while a significant portion of 100 nm MPP reached the tissue surface (leading to 80 ± 1% coverage of the colorectal surface), some 100 nm MPP remained in the luminal mucus gel (Fig 3-6A). MPP with diameters of 200 and 500 nm MPP were also found on the colorectal tissue surface (76 ± 2% and 55 ± 3% of the tissue surface, respectively; Fig 3-6B), however, an increasing amount appeared to be associated with the luminal mucus plug as MPP size increased (Fig 3-6A). Penetration of colorectal mucus by larger MPP was likely hindered by steric interactions with the mouse colorectal mucus mesh as MPP size increased, which is consistent with what we have observed

using *ex vivo* MPT (Fig 3-5 and [61]), as well as with the cross-sectional colorectal MPP distribution observed in Figure 3-5.

3.3.4 MAP and MPP transport in colorectal mucus from mice with TNBS-induced colitis.

Mucus hypersecretion and degradation is associated with UC, which may impact the structure of the mucus mesh and potentially alter the relative adhesive character of MAP or non-adhesive character of MPP. Thus, we first used MPT to quantify the transport of MAP and MPP in colorectal mucus on freshly excised *ex vivo* colorectal tissue obtained from mice with TNBS-induced colitis. The ensemble-averaged mean square displacement (<MSD>) of MAP in UC mouse colorectal mucus was decreased by >8,000-fold compared to the theoretical MSD of similarly sized nanoparticles in water, regardless of size, indicating adhesive immobilization (Table 3-2, Fig 3-7A). In contrast, MPP up to 200 nm in size readily diffused in colorectal mucus from mice with UC. Steric trapping of 500 nm MPP was observed in UC colorectal mucus, resulting in a low <MSD> that was similar to all sizes of MAP (Fig 3-7A). The distribution of the individual particle MSD values indicated that 100 nm MPP were uniformly diffusive, and >30% of 200 nm MPP diffused rapidly in UC colorectal mucus (Fig 3-7B). The <MSD> of 100 and 200 nm MPP in UC mucus were 2- and 25-fold increased, respectively, in UC colorectal mucus compared to in colorectal mucus from healthy mice (Table 3-2), indicating an increase in the overall pore size in UC colorectal mucus compared to healthy mouse colorectal mucus.

3.3.5 Distribution of MAP and MPP in the GI tract of mice with induced colitis.

After confirming that MAP were adhesively immobilized in GI mucus from mice with UC, while MPP were diffusive, we sought to evaluate the distribution of MAP and

MPP in the colorectum of mice with UC. Similar to the distribution observed in the healthy mouse colorectum, MAP of all sizes were adhesively trapped in mucin bundles in the colorectum of mice with TNBS-induced UC, thus limiting distribution over the tissue surface (Fig 3-8A). Mucin bundling induced by MAP also trapped some MPP that were co-administered with MAP, as evidenced by the low amount of individual MAP compared to co-localized MAP and MPP, and MPP alone (Fig 3-8A). Regardless, MPP of all sizes distributed over more of the colorectal tissue surface in both healthy mice and mice with UC (Fig 3-8A). There was an increase in the colorectal surface coverage by 200 nm MPP in mice with UC compared to in healthy mice (Fig 3-8A), which is consistent with the increase in the fraction of diffusive 200 nm MPP observed in UC mucus compared to in healthy colorectal mucus in the *ex vivo* MPT experiments (Fig 3-7B).

We next sought to test whether inflammation in the small intestine associated with IBD would impact the distribution of MAP and MPP after oral administration, but TNBS-induced colitis only locally affects the colorectum. It is generally accepted that DSS-induced colitis causes inflammation and mucus hypersecretion in the small intestine [175], so we used this model of induced colitis to observe nanoparticle distribution in the inflamed small intestine after oral administration. Inflammation was evident by the lack of organized alignment of cell nuclei and general damage to the small intestine villi compared to healthy mice. We found that, similar to our findings in healthy mice, 200 nm MAP aggregated in the lumen of the inflamed small intestinal regions, whereas MPP distributed throughout and between the villi (Fig 3-8B), following oral administration.

UC is also characterized by increased epithelial permeability and ulceration, such that nanoparticle uptake into the tissue has been hypothesized as a mechanism for improved and selective nanoparticle-based drug delivery to treat UC [89, 109, 111, 184-186]. We hypothesized that the ability of MPP to penetrate the mucus barrier would lead to increased accumulation of MPP compared to MAP in the tissue ulcerations. As shown in Figure 3-8, co-administration of MAP and MPP to mice by enema provided a stark visual contrast between the aggregated and poorly distributed MAP compared to the evenly distributed MPP in the healthy mouse colorectum, regardless of nanoparticle size. A similar contrast in colorectal distribution was seen for MAP and MPP in the colorectum of mice with TNBS-induced UC, and MPP also penetrated into damaged areas of the epithelium (Fig 3-9, green arrows) much more efficiently than MAP. MAP were also found near damaged areas of the epithelium, but tended to aggregate in the mucus or adhere only to the outer cell layer (Fig 3-9, red arrows).

3.4 Discussion

Enhancing the uniformity and proximity of drug-loaded particulates to the absorptive regions of the GI epithelium may improve both systemic drug absorption and local drug delivery for disorders such as IBD. Since most small molecule drugs are hydrophobic, strategies such as drug micronization and encapsulation within micro- or nanoparticle systems are used to overcome solubility limitations, leading to enhanced drug absorption [1, 3, 4, 162-164]. However, additional barriers to effective drug absorption in the GI tract exist, such as the mucus barrier lining the GI tract. Mucus can form multiple low-affinity interactions with particulate matter, including hydrophobic interactions, such that most types of drug particles and polymer particles stick to it [4, 8, 9, 82, 187]. There are many other

mechanisms by which mucoadhesion occurs, including electrostatic interactions and polymer interpenetration [9, 71, 72, 83], and these systems are all designed to facilitate strong adhesion to mucus. We demonstrated here that conventional hydrophobic mucoadhesive particles (MAP) stick to mucus and digesta, resulting in aggregation and limited distribution throughout the GI tract after oral and rectal administration. In contrast, non-mucoadhesive particles that penetrate through small and large intestine mucus (MPP) were able to reach nearly the entire tissue surface, which is likely to provide improved drug delivery for both local and systemic applications.

Mucoadhesion, which is generally defined as the interaction between a biological or synthetic material and the mucosa [188], is widely employed for drug delivery to mucosal surfaces. For example, mucoadhesion of pharmaceutical devices to surfaces that experience constant physical stress and drug clearance on the order of seconds to minutes, such as the buccal or ocular surfaces, can markedly improve drug delivery [189]. Also, devices generally larger in size than the thickness of the mucus barrier, such as micropatches [190, 191] and large microspheres functionalized with silicon nanowires [192], may be able to interact directly with the underlying mucosa to increase residence time in the GI tract. The distinction between *mucus* adhesion and *mucosa* adhesion is very important, and size scale is one factor that determines the efficiency by which a system designed to stick to the mucosal epithelium may contact the epithelium, as opposed to becoming trapped in the mucus gel instead. This paper shows that a typical mucoadhesive micro- or nanoparticle adheres to the luminal mucus gel before reaching the mucosa, thereby limiting particle distribution in the GI tract, and likely limiting GI residence time to the minutes to hours it takes for the mucus barrier to clear [4, 83]. It is not known at

present whether MAP or MPP would be retained longer in the GI tract. However, our other work in the lung [7] and vagina [177] demonstrated that MPP enter more slowly cleared mucus layers, leading to prolonged retention of MPP compared to MAP that stick to the luminal mucus layers (note that MAP were called conventional particles, or "CP", in these other papers). Carefully comparing the GI tract residence time of MAP and MPP will likely require the use of larger animals with GI transit times more similar to humans, such as dogs and pigs [193]. In rodents, the rapid GI transit time and production of a succession of hard, desiccated pellets (we have observed that mice produce a pellet once every 5-10 min) limits the ability to correlate particle retention in the rodent GI tract to what would be expected in humans. Assessing GI tract retention in a more physiologically relevant animal model is a high priority for future development of MPP for GI tract drug delivery.

It is important to recognize that numerous examples of mucoadhesive micro- and nanoparticle systems exist that provided improved drug delivery compared to the unencapsulated drug. For proteins where mucoadhesive particle systems have provided significantly improved bioavailability, such as insulin [194-198] and calcitonin [196, 199-201], encapsulation within the nanoparticle core shields the cargo from degradation in the harsh GI environment and can provide sustained release, which likely account for the enhanced protein uptake. However, while drug delivery to the GI tract via mucoadhesive particles may provide significant advantages compared to administration of unencapsulated drug, our work suggests that the extent of the advantage is limited by particle aggregation and adhesion to mucus *in vivo*. In other work, liposomes coated with a commonly used polymer for mucoadhesive formulations, chitosan, were shown to aggregate in simulated

GI fluid *in vitro*, and provided decreased cyclosporine A bioavailability *in vivo* compared to unmodified liposomes [202]. Also, the percentage of drug that was absorbed by GI tissues was increased when the mucus barrier was degraded prior to oral administration, and without an intact mucus barrier, drug delivery was improved for chitosan liposomes compared to unmodified liposomes [202]. Similarly, incubating invasin-coated PS nanoparticles in porcine mucin prior to oral administration led to decreased systemic absorption in rats [203]. Cell culture studies have also demonstrated decreased uptake of mucoadhesive nanoparticles in the presence of mucus [4, 204]. Indeed, we demonstrate here that MAP, in contrast to MPP, tend to aggregate in the GI tract lumen, where they are largely restricted from accessing the absorptive epithelium in the small intestine (both by poor surface coverage of the epithelium and by not penetrating to obtain close proximity to the epithelium). Our results suggest that drug delivery to the GI tract could be further improved by using non-mucoadhesive nanoparticles that distribute throughout the GI tract and reach nearly the entire epithelial surface. Definitive illustration of such improvement will await future studies seeking to test whether an improvement in systemic drug absorption will result from the increased access of drug in MPP to the absorptive epithelium, and/or improved efficacy of local drug treatment from increased uniformity of drug delivery to the affected tissues and cells.

We also demonstrate that methods commonly used for testing mucoadhesive particle systems may obscure the importance of the mucus barrier in the GI tract. For example, intestinal loop models have been used for decades to investigate systemic absorption of nanoparticles and drugs. In this model, a portion of the small intestine is excised from the abdominal cavity, thread is used to tie off the ends to make an isolated

"loop", and the test solution of interest is directly infused into the segment of intestine. The intestine is then placed back into the abdominal cavity, and absorption is allowed to occur over several hours. Using this model, as much as 67% of mucoadhesive nanoparticles were found in the blood and various organs, indicating systemic absorption [205]. However, as we demonstrate here, administering fluid into a tied-off loop distends the intestine and dilutes the mucus barrier, distributing MAP throughout the entire intestinal segment in a manner indistinguishable from MPP. Other studies have also demonstrated elevated absorption of nanoparticles after oral gavage. For example, more than 30% of 500 nm polystyrene nanoparticles were absorbed after oral gavage in one study [205]. However, the gavage volume used is important, as similar dilution effects can occur when large fluid volumes are gavaged to rodents. For example, Eyles *et al.* demonstrated that, with the same amount of 870 nm PS particles in each dose, a 5-fold increase in gavage volume from 0.1 mL to 0.5 mL in rats also caused a 5-fold increase in the percentage of nanoparticles found in the bloodstream [183]. Thus, when we administered MAP by gavage in 5-fold higher volume of fluid (0.25 mL as opposed to 0.05 mL for the rest of our studies), it is perhaps not surprising that the small intestinal distribution of MAP was indistinguishable from MPP. For most oral drug delivery systems, including pills, the driving force for absorption would not be large volumes of fluid forced into the intestines, but rather the natural digestive absorption processes, and we demonstrate here that MPP have a clear advantage over MAP in being drawn through the mucus barrier with the fluid as it is absorbed. We further demonstrated that the stark contrast between the small intestinal distribution of MAP and MPP was further enhanced when the nanoparticles were co-administered in the fed state. Nutrients that can penetrate the

mucus barrier are transported to the epithelium by the rapid absorption of water by the GI tract. This 'advective' transport by the flow of water rapidly transports nutrients into the highly infolded surfaces between villi. Water absorption increases in the fed state, increasing the speed of this advective transport process, and MPP take advantage of this process for efficient and uniform drug delivery. In contrast, MAP stick to the outer layers of mucus and aggregate in clumps in the center of the lumen, far from the epithelial surface.

For certain applications, such as rectal protection against sexually transmitted diseases with microbicides or treatment of UC, colorectal drug delivery may be preferable [173, 206-208]. Our work indicates that, when administered locally to the colorectum via enema, MPP of all sizes tested provided improved distribution over the epithelial surface compared to MAP. The hypotonic enema vehicle caused fluid absorption by the colorectal epithelium, thus advectively transporting MPP, but not MAP, through pores in the mucus mesh to reach the epithelial surface. We had previously observed similar results for MAP compared to MPP in the mouse vagina following administration in hypotonic aqueous vehicles [61].

UC has been associated with mucus hypersecretion and a reduction in mucus barrier properties [84, 89, 185]. Using MPP of various sizes, we showed that local inflammation in the TNBS-induced UC mouse model altered the structure of colorectal mucus, allowing larger (200 nm) MPP to penetrate more efficiently compared to penetration in healthy mouse colorectal mucus. However, despite the reduction in steric barrier properties, colorectal mucus in TNBS-induced UC maintained adhesivity toward MAP. It has been demonstrated in animal models of IBD that mucoadhesive

nanoparticles preferentially accumulate in inflamed areas of the GI tract due to increased mucus accumulation and potentially phagocytosis by macrophages [109, 209]. In addition to mucus gel hypersecretion, inflammation is associated with breakdown of the adherent mucus layer in the colon, which normally excludes bacteria in the healthy colon [210], leading to bacterial infiltration into the tissue [113, 211]. Increased tissue permeability may be a mechanism for selective particle uptake and retention in highly inflamed regions; indeed, a measureable decrease in epithelial resistance was observed in tissue biopsies obtained from patients with IBD compared to healthy controls, which led to accumulation of mucoadhesive particles (microparticles > nanoparticles) in ulcerated tissue regions [112]. The accumulation increased with increasing disease severity, but the accumulation was typically less than 1% of the field of view [112]. It was then demonstrated with Ussing chambers and tissue biopsies that chitosan-modified poly(lactic-*co*-glycolic acid) (PLGA) nanoparticles had even less penetration into tissue from IBD patients compared to PLGA nanoparticles [212]. In contrast, PEG-modified PLGA nanoparticles were found in the tissue specimens in greater amounts [212]. Ussing chamber models may be limited by the fact that the tissue and mucus are soaked in media; however, our *in vivo* results in a mouse model of UC confirmed that only small amounts of MAP penetrate into ulcerated tissue regions, whereas MPP penetrate the mucus and enter the ulcerated tissue regions in much greater amounts. Importantly, the use of a hypotonic enema vehicle likely enhanced MPP penetration into ulcerated tissue regions throughout the entire colorectum.

3.5 Conclusion

We systematically compared mucoadhesive nanoparticle (MAP) and non-mucoadhesive nanoparticle (mucus-penetrating particles, or MPP) behavior in the GI tract of mice. We

showed that the mucus barrier strongly limited the distribution and proximity of MAP to epithelial surfaces in both the small and large intestine. In contrast, MPP evenly coated the epithelial surfaces of the GI tract, achieved close contact to the underlying epithelium, and penetrated much more effectively into inflamed regions of UC tissues. Thus, the formulation of drugs into MPP may provide significant advantages in GI retention and drug absorption (owing to increased retention, distribution and proximity to the epithelium). In addition, unlike the clear difference of distribution between MAP and MPP when orally or rectally delivered, MPP and MAP distribute similarly when administered directly to the small intestine, as done in intestinal loop models, or in a high volume of gavage fluid. This indicates that care must be taken when choosing experimental methods for evaluating nanoparticle delivery to the GI tract, as some techniques are not representative of normal GI tract transit. Future studies will determine whether the improved mucosal distribution in the GI tract observed with non-mucoadhesive particles may lead to improved local drug treatments for diseases such as UC and colon cancer, improved microbicide-based protection against sexually transmitted infections, and/or improved oral absorption of drugs.

Table 3-1. Size and ζ-potential of various sized MPP and MAP used for oral and rectal administration of mice. Values are presented as the average of three runs ± SEM.

Particle Type	Size (nm)	ζ-potential (mV)
40nm MAP	56±2	-33 ±0.6
40nm MPP	60±1	-2.2 ±0.2
100nm MAP	88±1	-50±0.7
100nm MPP	120±2	-2.3±0.2
200nm MAP	190±3	-53±2
200nm MPP	230±4	-1.9±0.2
500nm MAP	500±11	-69±3
500nm MPP	530±11	-2.0±0.3

Table 3-2. Comparison of ensemble averaged MSD of MPP in colorectal mucus from healthy mice and mice with TNBS-induced colitis. Values are representative of $n \geq 3$ mice. MSDw denotes the theoretically diffusivity of similarly sized nanoparticles in water.

Particle Type	Healthy $MSD_w/\langle MSD \rangle$	Colitis $MSD_w/\langle MSD \rangle$	$MSD_{colitis}/MSD_{healthy}$
100 nm MPP	80	40	2
200 nm MPP	8,000	300	25
500 nm MPP	24,000	1,900	13

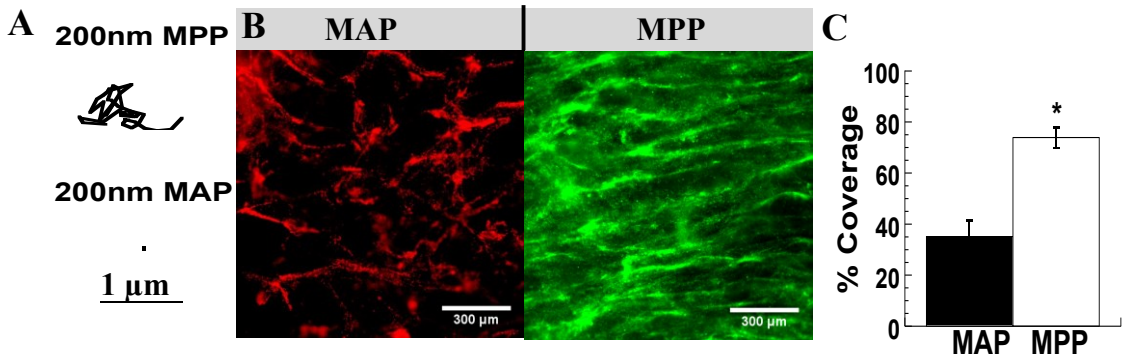

Figure 3-1. Distribution of MAP and MPP in the jejunum after low volume oral gavage. (A) Trajectories representative of 3 s of movement of 200 nm MAP and MPP in mucus on freshly excised mouse small intestine tissue. (B) Distribution of 200 nm MAP and MPP on flattened mouse jejunum tissues after oral administration. (C) Quantified surface coverage of 200 nm MAP and MPP on flattened mouse jejunum tissue. Images are representative of $n \geq 3$ mice. White scale bars indicate 300 µm. Data are calculated as means ± SEM. $^*P < 0.05$ as compared to CP, Students t-test.

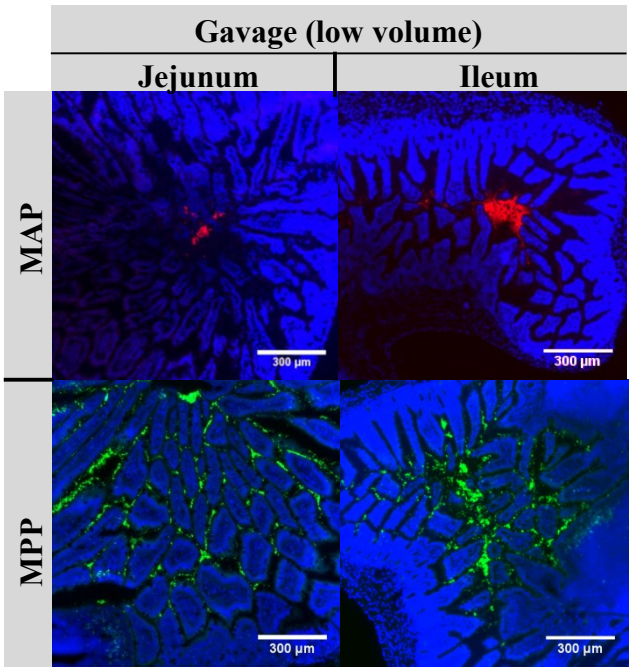

Figure 3-2. Distribution of MAP and MPP in the jejunum and ileum after low volume oral gavage. Distribution of fluorescent 200 nm MAP or MPP in the healthy mouse jejunum and ileum after low volume oral gavage. White scale bars indicate 300 µm. Images are representative of $n \geq 3$ mice.

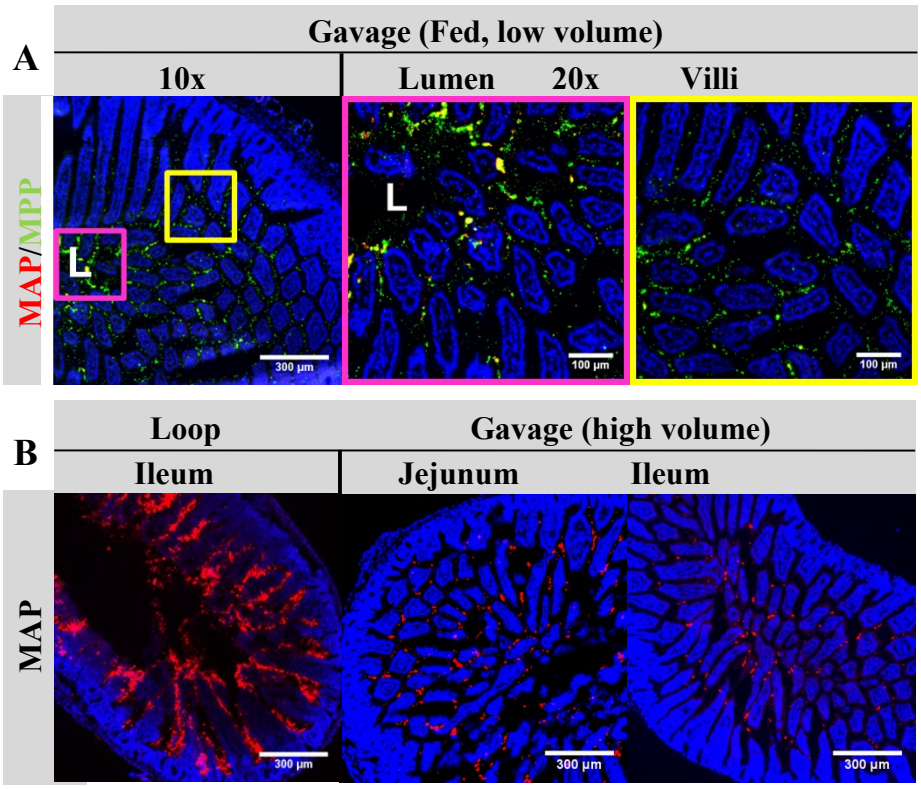

Figure 3-3. The impact of different experimental methods on the distribution of MAP and MPP in the jejunum and ileum. Distribution of fluorescent 200 nm MAP (red) or MPP (green) in: (A) the jejunum of healthy mice in the fed state after oral co-administration in a low volume gavage. In the 10x image, "L" denotes the lumen, the pink box outlines the luminal area (also shown outlined in pink at 20x), and the yellow box outlines the villi region (also shown outlined in yellow at 20x); and (B) the ileum of mice in the starved state after direct administration to an ileal loop, or in the jejunum and ileum after oral direct administration to an ileal loop, or in the jejunum and ileum after oral administration in a high volume gavage. Images are representative of $n \geq 3$ mice. White scale bars indicate 300 µm and 100 µm for 10x and 20x images, respectively.

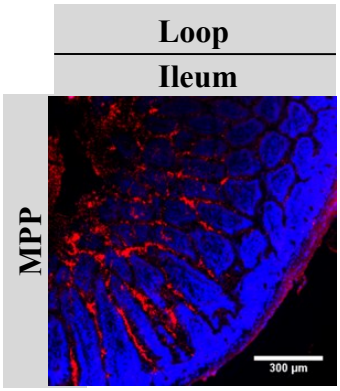

Figure 3-4. Distribution of MPP ileum after intestinal loop. Distribution of red fluorescent 200 nm MPP after direct administration into an ileal loop. White scale bar indicates 300 µm. Image is representative of $n \geq 3$ mice.

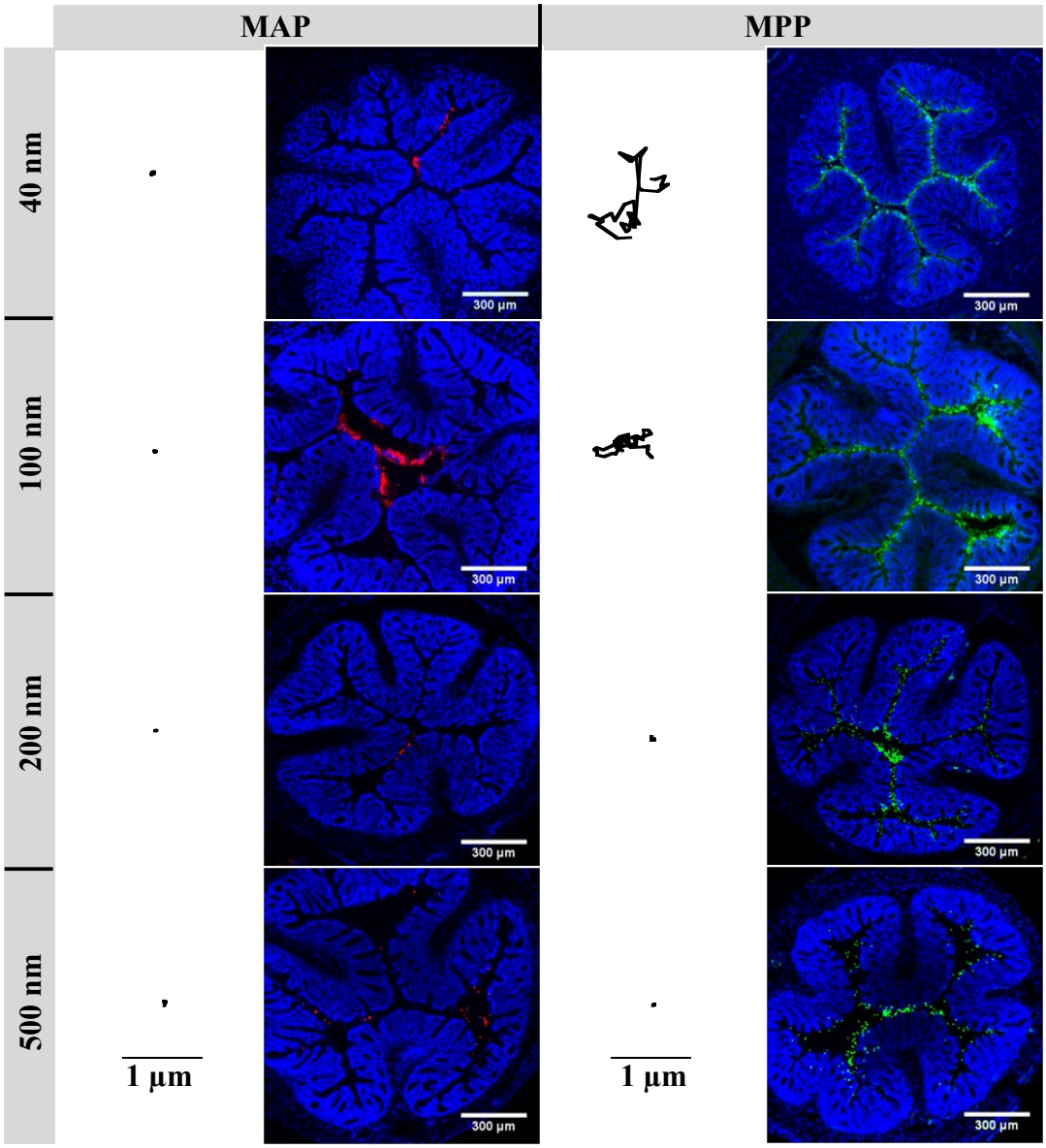

Figure 3-5. Trajectories in colorectal mucus and distribution of MAP and MPP in the mouse colorectum. Trajectories representative of 3 s of movement for 40, 100, 200, and 500 nm MAP and MPP in mucus on freshly excised mouse colorectal tissue. Black scale bars indicate 1 µm for all trajectories. Distribution in transverse colonic cryosections after rectal administration of 40, 100, 200, and 500 nm MAP (red) or MPP (green). Cell nuclei are stained with DAPI. White scale bars indicate 300 µm for all distribution images. Images are representative of $n \geq 3$ mice.

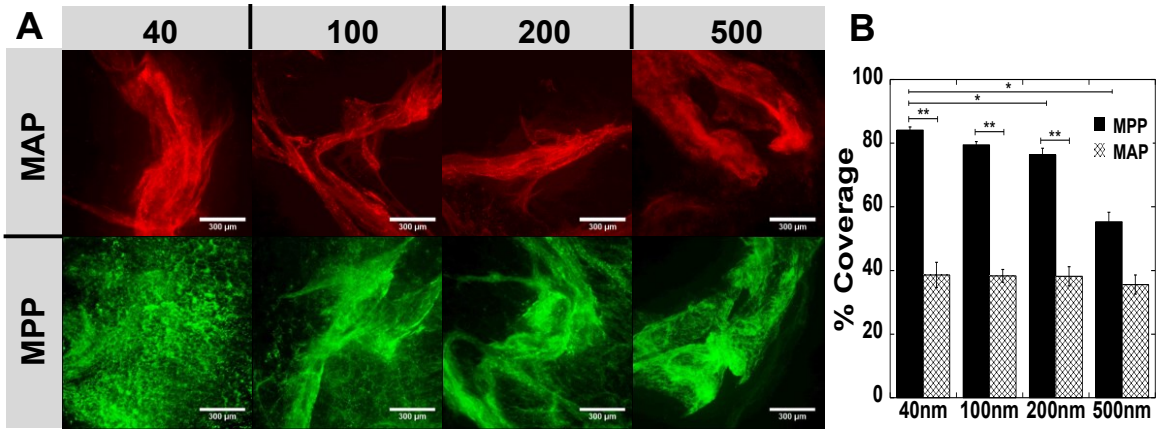

Figure 3-6. Quantified colonic distribution of MAP and MPP after rectal administration to mice. Distribution on flattened colonic tissue after rectal administration of 40, 100, 200, and 500 nm (A) MAP (red) or MPP (green). (B) Quantified surface coverage of various sized MAP and MPP on flattened mouse colonic tissue. Images are representative of $n \geq 3$ mice and 6 images per tissue. White scale bars indicate 300 µm. Data are calculated as means ± SEM. $*P < 0.05$ as compared to MAP, Student's t-test.

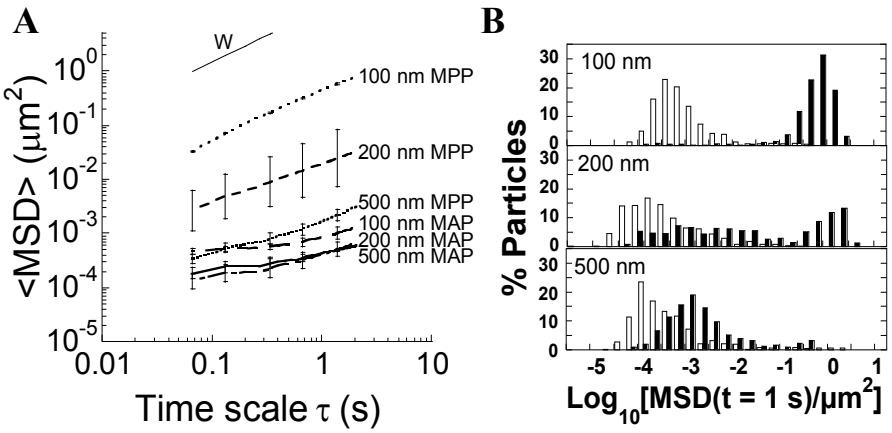

Figure 3-7. Transport of MAP and MPP in colorectal mucus on freshly excised ex vivo tissue from mice with TNBS-induced colitis. (A) Ensemble averaged mean-squared displacement (<MSD>) as a function of time scale for various sizes of MAP and MPP particles, including the theoretical MSD of 100 nm particles in water (W). (B) Distribution of the logarithms of individual particle MSD at a time scale of 1 s for various sized MAP (□) and MPP (■). Data is calculated as mean ± SEM (≥ 3 individual tissues with n > 100 particles per tissue).

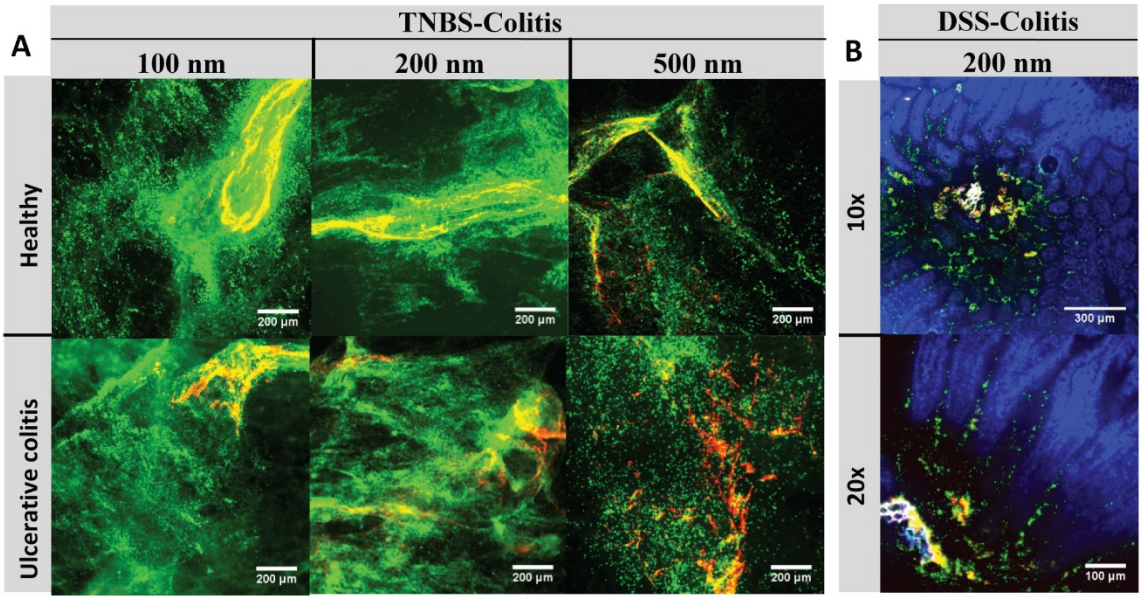

Figure 3-8. Distribution of various sizes of MAP and MPP after rectal co-administration to mice with TNBS-colitis and after oral co-administration to mice with DSS-colitis. Distribution of co-administered, fluorescent MAP (red) and MPP (green) (A) on flattened colonic tissue after rectal administration of various sizes (100 nm, 200 nm, 500 nm) to healthy mice and mice with TNBS-induced ulcerative colitis and (B) in the jejunum of mice with DSS-induced colitis after low volume oral co-administration of 200 nm particles (shown at 10x and 20x magnification). White scale bars indicate 200 µm in (A) and 300 µm for the 10x and 100 µm for the 20x images in (B). Cell nuclei are stained blue with DAPI. Images are representative of $n \geq 3$ mice.

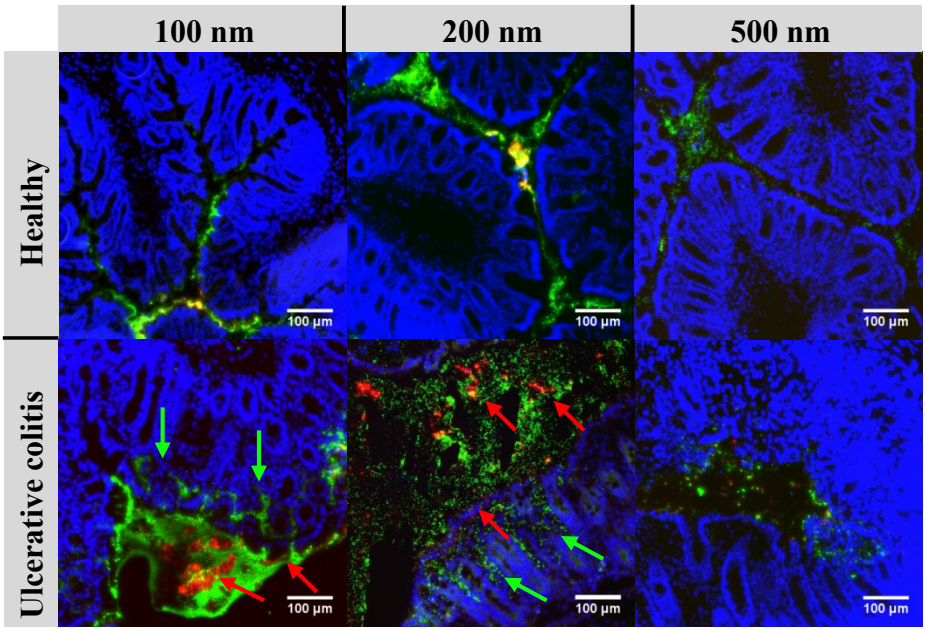

Figure 3-9. Distribution of various sizes of MAP and MPP after rectal co-administration to mice. Distribution of rectally co-administered, fluorescent MAP (red) and MPP (green) of various sizes (100 nm, 200 nm, 500 nm) in the colorectum of healthy mice and mice with TNBS-induced colitis. The red arrows highlight aggregates of MAP, while the green arrows highlight areas where the MPP have penetrated into the tissue. Cell nuclei are stained blue with DAPI. White scale bars indicate 100 µm. Images are representative of $n \geq 3$ mice.

4. OPTIMIZING LOCAL AND SYSTEMIC DRUG DELIVERY VIA THE COLORECTUM: TUNING ENEMA FORMULATIONS FOR SYSTEMIC OR LOCAL APPLICATIONS BY VARYING ION COMPOSITION

4.1 Introduction

Delivering drugs to the colorectum can provide several benefits. Systemic delivery via the colorectum is commonly used in children and also adults when drugs are either poorly bioavailable or oral ingestion is not possible [213-216]. Rectal delivery allows drugs to reach systemic circulation without degradation due to stomach acid, digestive enzymes, and hepatic first-pass metabolism. Colorectal delivery can also provide increased local tissue drug concentrations without systemic exposure to large drug doses taken orally. Stable, water-soluble drugs can be administered directly to the colorectum in aqueous enemas; poorly water soluble and/or easily degraded drugs can be packaged into nanoparticles, and then suspended into aqueous enemas. In either case, the enema itself, which is often ignored as a formulation component, can be optimized for improving colorectal drug delivery. The rational design of enema formulations can improve the bioavailability whole bypassing the barriers to oral administration. More effective drug delivery to the colorectum has the potential to improve therapy for diseases with local manifestations, such as inflammatory bowel disease (IBD) and colorectal cancer, and for preventing rectally transmitted infections such as HIV.

Many functions of the gastrointestinal (GI) tract use bulk fluid flow: in the small intestine, many liters of fluid are absorbed to rapidly transport nutrients through the mucus barrier covering the villi, and in the colon, additional water is withdrawn to dry the feces. Thus, we hypothesized that fluid absorption by the colorectum could be

harnessed for more effective drug delivery. However, nutrients can only be absorbed by the GI tract if they can pass through the "filter" formed by highly viscoelastic and adhesive layers of mucus. Nutrients, or drug-loaded nanoparticles, that adhere to the mucus barrier will be trapped before they reach the epithelium and be rapidly cleared along with outermost 'sloppy' layers of mucus [4, 9]. In contrast, we found that nanoparticles engineered to slip through the mucus barrier, or mucus penetrating particles (MPP), can be efficiently delivered to the entire colorectal epithelial surface [79]. Rapid and widespread distribution of MPP was driven by the rapid absorption of water from hypotonic vehicles "advectively" transporting MPP to the epithelium much faster than by diffusion alone [79]. Similarly, we found that hypotonic vehicles induced rapid fluid absorption by the vaginal epithelium that rapidly delivered water soluble drugs and MPP to the epithelial surface by advection [5, 61]. In contrast, MPP administered in isotonic vehicles (no fluid absorption) remained in the vaginal lumen and only slowly diffused through the mucosal barrier [61]. Thus, MPP provide a simple and sensitive method for observing the direction of fluid movement induced by the tonicity of the vehicle, as well as serving as carriers for improved mucosal drug delivery.

Here, we investigated the impact of enema composition (osmolality, ion composition) on fluid absorption/secretion and drug delivery in the colorectum. We explored the full range of hypotonic (pure water, 20 mOsm) to hypertonic (2200 mOsm Fleet® enema) as well as solutions that contained sodium or potassium ions. We found that the tonicity of a solution depends not only on the osmolality, but also on the ion composition as it relates to ion transport processes of the epithelium. Further, the properties of the enema and their effect on the mucosal environment can be harnessed to

enhance various types of drug delivery, whether the goal is systemic absorption or local tissue absorption. We demonstrate that a mildly hypotonic, sodium-based enema formulated with ion concentrations similar to those in feces (simulated colon solution, or SCS), provided enhanced colorectal distribution of both MPP and water soluble drug, improved tissue uptake of water-soluble drug, and caused no detected toxic effects in the colorectum. In addition, we show that pre-treatment using epithelial-damaging, strongly hypertonic enemas causes nanoparticle penetration *into* colorectal tissue. Our investigations illustrate the ability to tune enemas by varying ion content, thus making them suitable for local and/or systemic drug delivery.

4.2 Materials and Methods

4.2.1 Animal Model

Rodents are commonly used as animal models for delivery to the gastrointestinal tract. However, their defecation rate is much more rapid (every 5-10 min for mice) than typical for humans, and their hard, desiccated pellets do not resemble human feces. To simulate the softer stool consistency and less frequent defecation rate of humans, female 6-8 week old CF-1 mice (Harlan) were starved for 24 h to make the feces softer, more human-like, and less abundant. Mice were housed in cages with wire bottoms to prevent coprophagia. Various test solutions were administered intrarectally to mice with a Wiretrol (Drummond, Inc.) at volumes of 20 μL. Mice were anesthetized with the drop-method via isofluorane for shorter times, or injected with 300 mg/kg avertin (2, 2, 2-Tribromoethanol), using a 20 mg/mL working solution in phosphate buffered saline (PBS), when more extended anesthesia times were required. All mice were euthanized

while still anesthetized. All experimental procedures were approved by the Johns Hopkins Animal Care and Use Committee.

4.2.2 Nanoparticle formulation and characterization

MPP were synthesized as previously described [217]. Briefly, fluorescently labeled carboxylate-modified polystyrene (PS-COOH) nanoparticles 40 nm in diameter were purchased from Molecular Probes (Eugene, OR). To obtain a dense polyethylene glycol (PEG) coating, nanoparticles were suspended in 200 mM borate buffer and 5 kDa methoxy-PEG-amine was added in excess. N-Hydroxysulfosuccinimide (Sigma) and 1-Ethyl-3-(3-dimethylaminopropyl) carbodiimide (EDC, Invitrogen) were subsequently added to couple the carboxylic acid on the nanoparticles with the amine group on the PEG. Nanoparticle size and ζ-potential were measured in a Zetasizer Nano ZS90 (Malvern Instruments) after suspending nanoparticles in 10 mM NaCl solution, via dynamic light scattering (90° scattering angle) and laser Doppler velocimitry (or anemometry). Measurements were taken at 25°C according to instrument settings. A near-neutral ζ-potential indicates sufficient PEG surface coverage to make nanoparticles that penetrate mouse colorectal mucus (MPP) as previously described [79].

4.2.3 Enema formulations

To obtain sodium-based solutions of various osmolalities, concentrated (10x) tris-buffered saline (Mediatech; 1X TBS in 20 mM tris, 138 mM NaCl, pH 7.4) was diluted with DI water. Similarly, to obtain potassium-based solutions (KPO_4) of various osmolalities, potassium phosphate buffer (1 M K_2HPO_4 pH 5.5, Sigma) was diluted with DI water (e.g. 150 mOsm buffer was made by diluting 1M K_2HPO4 ~12 fold). The simulated colon solution (SCS) was made by dissolving sodium bicarbonate, potassium

chloride, dibasic potassium phosphate and monobasic potassium phosphate (Sigma) in DI water at the following ion concentrations: 75 mM K^+, 25 mM Na^+, 35 mM Cl^-, 30 mM PO_4^{3-}, and 25 mM CO_3^{2-} [40]. Solution osmolality was measured with a vapor pressure osmometer (Wescor Vapro) and measurements were reported as mean ± SEM for n = 3 measurements. Fleet® enema solution and Fleet® Naturals were purchased over the counter, and all enema solutions were sterile-filtered through a 0.2 μm filter prior to use *in vivo*. A 5% w/v glycerol gel was obtained by mixing the universal placebo hydroxyethylcellulose (HEC) gel (ReProtect, Inc.) with glycerol. The glycerol gel and Fleet® were serially diluted in DI water before measurements in the osmometer and osmolality was extrapolated from the obtained data points. Ion concentrations and osmolalities of the various formulations are listed in Table 4-1.

4.2.4 Nanoparticle and free drug distribution on tissues

MPP 60±1 nm in (hydrodynamic) diameter were diluted 1:10 in TBS and KPO_4 buffers of various osmolalities to make a range of sodium-based and potassium-based buffered solutions. To observe the colorectal distribution of anti-retroviral drug tenofovir (9-(2-Phosphonyl-methoxypropyly)adenine, TFV) now in clinical trials for preventing rectal transmission of HIV, fluorescein isothiocyanate (FITC) was covalently reacted to the amino group on the purine ring of TFV. FITC-labeled TFV (FITC-TFV) was then dissolved 1:10 with unmodified TFV in the various solutions at an overall concentration of 1% (w/v), the concentration of TFV tested in the (moderately successful) CAPRISA 004 trial. Mice were anesthetized using isofluorane during administration to ensure that the enema fluids would not be immediately expelled. To obtain cross-sectional images for assessing qualitative colorectal distribution, 20 μL of solution was administered

intrarectally to mice. The mice were sacrificed after 5-10 min. For distribution post Fleet® enema, mice were anesthetized with isoflurane and 200 µL of fleet was administered intrarectally. After 10-15 min to allow for fluid expulsion (confirmed visually), 20 µL of MPP diluted 1:10 in DI water was administered. Mice were sacrificed after 5-10 min. Segments of tissue 1-2 cm in length were flash-frozen in Optimal Cutting Temperature (OCT) compound. Transverse sections of tissue 6 µm thick were cut at various points along the length of the colorectum using a Leica CM-3050-S cryostat. Sections containing nanoparticles were fixed with formalin and stained for cell nuclei using ProLong Gold antifade reagent with DAPI (Invitrogen). Sections containing free drug were not fixed to reduce quenching of the fluorophore and stained with ProLong Gold antifade reagent with DAPI. Fluorescent images were obtained using an inverted epifluorescence microscope (Zeiss Axio Observer). To quantify nanoparticle distribution, one representative section was chosen per animal, and an outline of the epithelial perimeter was drawn. The percent overlap between the perimeter and fluorescence (% colocalization of nanoparticles with the epithelial perimeter) due to the presence of nanoparticles was then calculated for each image using the JACoP plugin for ImageJ, and the average with standard error of the mean (SEM) was reported for $n \geq 3$ mice.

4.2.5 Free drug uptake into plasma after administration to the mouse colorectum

Mice were anesthetized with avertin, and 20 µL of the various solutions containing 1% w/v unlabeled TFV and 1 µL of H^3-TFV (1 mCi/ml, suspended in ethanol, Moravek Biochemicals) was administered intrarectally. For the t = 0 time point, retro-orbital blood collection was used to collect blood immediately after administration of each solution; for the 30 min time point, blood was collected 30 min post administration. Whole blood was

centrifuged in heparinized tubes to obtain plasma, and 200 µL of plasma was dissolved in 5 mL of Solvable™ and bleached using hydrogen peroxide. 500 µL of plasma/Solvable™ solution was added to 10 mL of Ultima Gold, and H^3 content was analyzed using a scintillation counter. Concentrations were calculated using a calibration curve of free H^3-TFV. Separate standard curves for high and low count samples were made by serial dilution of H^3-TFV. The concentrations of H^3-TFV in the plasma samples were estimated using the standard curves, and the total drug concentration was calculated assuming that the H^3-TFV and TFV were absorbed similarly in the colorectum.

4.2.6 Pharmacokinetic studies of free drug in the mouse colorectal tissue

Mice were anesthetized with avertin, and 20 µL of the various solutions containing 1% (w/v) unlabeled TFV and 1 µL H^3-TFV (1 µCi/mouse) was administered intrarectally to mice. Colorectal tissue was harvested at 5 min, 30 min, 1 h, 2 h, and 4 h time points and processed as described above. H^3 tissue content was measured using a scintillation counter and normalized based on individual tissue weights. Values were obtained from n = 5 mice, and the highest and lowest values were removed from each group to obtain n = 3 per time point for each solution used.

4.2.7 Toxicity of enema formulations in the mouse colorectum

Mice were anesthetized with avertin, as described above, and 50 µL of tap water, SCS, or Fleet® was administered as an enema. Mice were kept in supine position for 15-30 min prior to sacrificing them and excising the tissues. For histological analysis, tissues were fixed in formalin and taken to the Johns Hopkins Medical Institutions Reference Histology Laboratory for standard paraffin embedding, sectioning, and hematoxylin and

eosin (H&E) staining. Images were obtained using a light microscope with a 10×/0.25 NA objective (Nikon E600).

4.3 Results

4.3.1 Effect of enema osmolality and ion composition on colorectal MPP distribution

We first investigated the effects of altering enema sodium concentration on MPP distribution in the mouse colorectum. It was evident that sodium-based enemas below a certain osmolality (~450 mOsm, ~210 mM NaCl) induce fluid absorption that results since MPP became uniformly distributes on essentially the entire the epithelial surface (Fig 4-1A). In contrast, sodium-based enemas with osmolality >350 mOsm caused fluid secretion and bowel distension, resulting in MPP remaining more centrally located in the lumen, rather than approaching close proximity to the epithelial surface (Fig 4-1A; 450, 600, 860, and 2200 mOsm). We next quantified MPP surface coverage as a function of absorption or secretion inducing formulations [61]. We found that MPP administered in sodium-based enemas with osmolalities below 450 mOsm provided >70% coverage of the colorectal epithelium, whereas MPP administered in solutions with an osmolality ≥450 mOsm did not enter the epithelial folds, reducing their surface coverage to < 45%, and as low as 0% when administered in a Fleet® enema (Fig 4-1B). Thus, we estimate that the effective isotonic point for sodium-based enemas in the mouse colorectum lies between 350 and 450 mOsm.

Potassium, in contrast to sodium, is pumped *into* the lumen of the colorectum, creating a potassium gradient opposite to sodium and producing a high potassium/sodium ratio in feces [40]. This led us to hypothesize that increasing the potassium concentration in an enema would slow fluid absorption by the epithelium. MPP administered in a 150

mOsm potassium buffer that is markedly hypo-osmolal with respect to blood, would be expected on the basis of osmolality to induce fluid absorption, but instead this enema did not induce absorption (Fig 4-2A). In contrast, a sodium-based enema with the same 150 mOsm osmolality, induced rapid absorption that advectively transported MPP to coat epithelial surface uniformly throughout the colorectum similarly to MPP administered in DI water (Fig 4-2A). Based on the drop in tissue coverage, the isotonic (no fluid flow) concentration for potassium phosphate was between 20 and 70 mOsm, and colorectal tissue coverage decreased as the osmolality of the potassium-based enema solution increased above this range (Fig 4-2B). As shown in Figures 4-1B and 4-2B, the sodium-based enemas were significantly more effective for achieving maximal tissue coverage by MPP.

4.3.2 Effect of osmolality of sodium-based solutions on colorectal drug distribution

We demonstrated previously that hypotonic solutions causing advective absorption may also be advantageous for improving the distribution of water soluble drugs in the mouse vagina, leading to uniform drug delivery to the entire epithelial surface [61]. Here, we explored colorectal delivery of TFV in a hypotonic enema for HIV pre-exposure prophylaxis (PrEP). We fluorescently labeled TFV with FITC (TFV-FITC) and mixed it at a 1:10 ratio with unlabeled TFV to visualize distribution. We first compared sodium-based enemas of varying osmolality: deionized water (20 mOsm), iso-osmolar saline (264 ± 1 mOsm, iso-osmolar to the blood), TBS buffer at the osmolality in isotonic range (450 mOsm), and slightly hypertonic TBS buffer (650 mOsm) that should induce fluid secretion. As shown in Figure 4-3, fluorescently-labeled TFV distribution was consistent with MPP distribution: colorectal tissue coverage (and therefore access to target cells and

tissues) was improved by using an absorption inducing enema. Bulk fluid flow transported the water-soluble, small molecule drug through the mucus barrier and to the epithelium, and also transported the drug deep into the folds of the (collapsed) colorectum.

We then developed an SCS enema formulation that has sodium and potassium concentrations similar to those found in feces, which is likely optimal for safe water absorption in the colorectum. The osmolality of the SCS was approximately 150 mOsm. Since the solution contained both sodium (25 mM) and potassium (75 mM), we investigated the individual contributions of these ions to bulk fluid flow. We found that fluid absorption only occurred if sodium was present in the solution (Fig 4-4). If sodium was removed, leaving potassium unchanged at 75 mM (SCS, K^+ only), no fluid absorption occurred and TFV-FITC remained in the lumen. In contrast, if potassium was removed, leaving sodium unchanged at 25 mM (SCS, Na^+ only), fluid was rapidly absorbed by the colorectal epithelium, distributing TFV-FITC throughout all of the folds of the mouse colorectum (Fig 4-4).

4.3.3 Effect of tonicity on colorectal drug uptake into plasma and tissue

We previously documented that very hypotonic delivery of a water soluble drug led to reduced vaginal retention, likely due to the drug being driven advectively all the way through the epithelium to reach systemic circulation [61]. Here, we investigated the effect of enema tonicity on movement of drugs from the colorectal lumen into the plasma. We compared drug delivered in a variety of solutions, including: tap water, SCS, TBS (a sodium chloride based tris buffer) in isotonic range (450 mOsm), and the highly hypertonic Fleet® enema. In addition, we tested a mild secretion-inducing (hypertonic)

solution containing 5% glycerol in DI water, which is the concentration of glycerol used in the *reduced*-glycerol TFV gel formulation now being tested in clinical trials for rectal PrEP [218]. No TFV was detected in the plasma after 30 min if administered in isotonic and mildly hypotonic SCS solution; however, ^{3}H-TFV could be found in the plasma 30 min after enema administration in very hypotonic (DI water) as well as very hypertonic (Fleet®) solutions (Table 4-2).

To investigate how enema composition impacts drug levels in the tissue, we compared the amount of ^{3}H-TFV associated with colorectal epithelial tissue when administered in the same set of solutions. Based on published cell migration data and the number of cell layers these cells need to ascend through the crypts in the mouse colorectum, we calculated that the surface epithelial layer, which would absorb drug, renews approximately every 2 h [219, 220]. For this reason, we assessed tissue concentration up to 4 h, at which time TFV tissue concentrations became low and indistinguishable between the different solutions. The initial tissue TFV concentrations were highest when administered in Fleet® and in SCS compared to administration in isotonic (450 mOsm) TBS. But at 2 h, tissue concentrations of TFV administered in Fleet® or isotonic TBS were significantly lower than when administered in SCS (Fig 4-5). The area under the curve (AUC) for TFV administered in SCS, isotonic 450 mOsm TBS, Fleet® enema, and 5% glycerol gel were 330, 120, 72, and 21 μg·h/g, respectively. Even though the 5% glycerol gel was only moderately hypertonic, it decreased the amount of TFV taken up by colorectal tissue by more than 10-fold.

4.3.4 Toxicity of enema formulations

Previous results have shown that hypertonic vehicles (gels, lubricants, enemas, etc.) are toxic to the human colorectal epithelium [221]. We investigated acute tissue effects of hypotonic and hypertonic enemas. We compared tap water (strongly hypotonic), strongly hypertonic Fleet®, and our moderately hypotonic SCS enema in the mouse colorectum. As shown in Figure 4-6, Fleet® enema caused distension and epithelial disruption (red arrows) within 10 min of administration. In addition, the damage induced by the Fleet® enema allowed nanoparticles to penetrate into the tissue regions where the epithelial integrity was compromised (Fig 4-6B), which may be useful for other drug delivery purposes, but not for prophylaxis. Tap water and moderately hypotonic SCS did not induce any detectable epithelial damage (Fig 4-6A).

4.4 Discussion

The human colon absorbs 1.4-1.8 L of water every day, driven by active ion transport [222]. Water absorption is accomplished by electrogenic $3Na^+/2K^+$ ATPase pumps in the basolateral membranes, and high conductance sodium, potassium, and chloride channels in the apical membrane of epithelial cells. This robust physiological mechanism provides an opportunity to optimize fluid absorption to provide more effective colorectal drug delivery. We have previously demonstrated that MPP, which rapidly diffuse through mouse colorectal mucus, have enhanced distribution when administered hypotonically in the colorectum [79]. Unlike model MPP that neither entered the epithelium nor were drawn through epithelial at short time points, small molecule drugs can be rapidly drawn into and through the epithelial layer [61]. Thus, strongly hypotonic solutions, such as DI water, can cause drug to reach systemic circulation (Table 4-2) [61, 133]. Similarly, hypertonic

solutions such as Fleet can also cause drug to reach systemic circulation (Table 4-2) [133], and thus, to achieve setmatic drug delivery, either strongly hypertonic or hypotonic solutions can therefore be used for rectal administration. A moderately hypotonic enema, in contrast, resulted in no detectable rapid systemic drug absorption (Table 4-2), but showed optimal tissue drug levels compared to isotonic and hypertonic formulations. In humans, Leyva et al showed that systemic drug levels are highest when using tap water (strongly hypotonic) and similarly high in a iso-osmolar enema (300 mOsm, a formulation that likely causes moderate fluid absorption in the human colon), while Fleet ® (strongly hypertonic) resulted in significantly lower systemic drug absorption [133]. Differences in systemic drug absorption in humans compared to our murine model were likely due to the differences in colorectal surface area exposed to the enema formulations (higher area exposed in mice than humans). Fleet ® damage may have caused a temporary increased permeability in the mouse tissue, and since a relatively larger area was affected, significant amounts of drug were able to reach systemic circulation. Leyva et al reported that tissue concentration were highest in the iso-osmolar (mildly hypotonic) formulation, which correlates with our findings in mice [133].

For certain applications, systemic delivery is desirable. Rectal delivery has long been used to administer medications, such as anti-arthritic, anti-emetic and anti-angiogenic agents, to the systemic circulation [213-216]. Most of these medications have improved bioavailability when administered intrarectally, which avoids first-pass metabolism and degradation by stomach acid and digestive enzymes. Our findings indicate that both strongly absorbing and secreting enemas cause detectable systemic drug concentrations within 30 min of rectal administration, but only if they are strongly

hypo- or hypertonic, respectively. However, the toxicity induced by advectively secreting (hypertonic) enemas in the colorectum may limit the utility of hypertonic enemas, particularly if epithelial toxicity would be detrimental. On the contrary, extremely hypotonic enemas may be able to transport drug through the epithelium by both paracellular and transcellular fluid absorption and deliver drug to the blood that can increase drug plasma levels. The previously mentioned clinical data also suggest that strongly hypotonic delivery is favorable for systemic delivery, and intestinal epithelial cells show increased transport of hydrophilic molecules when the molecules are applied in a 50% hypotonic solution [133, 223]. A strongly hypotonic enema formulation may thus be optimal for systemic drug delivery via rectal administration

When high tissue drug levels and low systemic drug exposure are desired, mildly hypotonic solutions may be optimal. These solutions can provide robust fluid flow and result in increased local drug levels, while avoiding overly rapid trans-epithelial advection and systemic absorption (Table 4-2). Sodium drives fluid absorption in the colorectum as long as levels are below 205 mM NaCl (450 mOsm) in the mouse, similar to the 220 mM NaCl (theoretical osmolality: 440 mOsm) found to cause fluid secretion in humans [224]. Potassium, on the other hand, seems to induce colorectal fluid secretion even at very low levels. By varying the amounts of each of these two ions, optimal concentrations can be found that lead to the highest drug tissue levels. Tissue levels may depend on the interaction of a specific drug with mucus and the epithelium, and enema products could be fine-tuned by varying potassium and sodium concentrations [11, 16, 224]. An enema with only *mild* advective absorption can provide improved colorectal drug distribution and tissue uptake without excessive loss of drug to systemic circulation

(Table 4-2, Fig 4-6). Our SCS matches ion concentrations found in feces, making it an optimal starting point due to a low chance of causing toxicity while still inducing sufficient advective fluid absorption to create rapid local drug levels and uniform distribution.

An especially useful application for rectal drug delivery is HIV PrEP. Rectal risk for HIV transmission is 10 – 20 fold higher than vaginal transmission, and enema use is widespread for cleansing the bowel prior to receptive anal intercourse (RAI) [117, 131, 218, 225-229]; a microbicide-loaded enema would thus require minimal behavioral changes. Currently available OTC enema formulations like Fleet, as well as the tenofovir (TFV) gels now in clinical trials [221, 230], are hypertonic in the colon, and induce rapid secretion of fluid that likely opposes effective drug delivery [61]. Moreover, hypertonic formulations cause epithelial toxicity that may significantly increase susceptibility to infection, as indicated by the increased delivery of particulates (similar to HIV in size and surface properties, unpublished observations) to penetrate into epithelial tissue when they are damaged by Fleet® (Figure 4-6B) [129, 221, 231]. To provide maximal protection drugs such as TFV must be effectively delivered to all of the susceptible cells and tissues, including deep into the folded surfaces of the colorectum without inducing epithelial toxicity, a task that unlikely to be achieved with current microbicide formulations [5, 61, 230]. A hypotonic enema vehicle may provide the desired uniform coverage of drug or drug-loaded MPP of the epithelial surface of the colorectum while minimizing epithelial damage.

In addition, the hypotonicity could be tuned based on whether or not systemic drug exposure is desirable – a moderately hypotonic formulation such as the iso-osmolar

formulation used by Leyva et al could provide both high systemic and high local drug levels, while SCS could provide only high local and low systemic drug exposure [133].

While epithelial toxicity is undesirable in PrEP, it may be advantageous for other applications. A strongly hypertonic enema could be used as a pre-treatment to hypotonically delivered nanoparticles that could then penetrate deep into the damaged tissue (Fig 4-6B). Tissue penetration may in turn improve drug uptake into systemic circulation as well as local tissue uptake. In addition, increased inflammation and tissue damage may provide a way to target the immune system via the rectal route. Nano- or microparticles could be taken up by the immune cells residing in a tissue that has received "danger signals" through Fleet® exposure. The exposure of vaccine-loaded nanoparticles to increased numbers of immune cells present could potentially enhance the effectiveness of rectal vaccines, such as those currently under investigation to prevent STIs and other mucosal infections [232-235].

4.5 Conclusion

Systemic delivery via the colorectum is commonly used in children and for medications rapidly degraded in the GI tract. Local delivery is preferred at the mucosal surfaces when treating and preventing diseases that locally manifest at these surfaces. Here, we report that hypotonic, sodium-based enemas improve the distribution of MPP and hydrophilic free drugs on the colorectal epithelial surface compared with isotonic and hypertonic enemas and potassium-based enemas. We demonstrate that enema formulations can be tuned to cause drugs to rapidly reach systemic circulation or remain local in the tissue by varying the ion content: Hydrophilic free drug was rapidly taken up into systemic circulation when administered in strongly hypotonic or hypertonic solutions, while a

moderately hypotonic enema (SCS) significantly improved local drug levels and reduced systemic exposure. We also found that hypotonic enema formulations caused no detected epithelial damage, while hypertonic enemas significantly damaged the colorectal epithelium while improving penetration of nanoparticle into the damaged tissue.

Table 4-1. Ion concentrations and osmolalities of various formulations. Osmolalities were measured using a vapor pressure osmometer and are reported as mean ± SEM of n = 3 measurements.

	Composition							
Formula-tion	**Na^+ (mM)**	**K^+ (mM)**	**PO_4^{3-} (mM)**	**Cl^- (mM)**	**CO_3^{2-} (mM)**	**Glycerol (w/v)**	**HEC (Y/N)**	**Osmolality (mOsm)**
1x TBS	70	0	0	70	0	0	N	260 ± 20
SCS	25	75	30	35	25	0	N	150 ± 1
SCS K^+ only	0	75	30	35	0	0	N	130 ± 1
SCS, Na^+ only	25	0	0	0	25	0	N	55 ± 1
0.9 % saline	150	0	0	150	0	0	N	260 ± 1
1.5x TBS	205	0	0	205	0	0	N	450 ± 2
5% glycerol	0	0	0	0	0	5	N	600 ± 2
5% glycerol gel	150	0	0	150	0	5	Y	760 ± 3
Fleet®	~1600	0	~1400	0	0	0	N	≥2200 ± 1
Fleet naturals®	NA	0	0	NA	0	0	N	260 ± 3

Table 4-2. Plasma levels of TFV after administration in various enema solutions. Amount of TFV present in 200 µL of plasma 0 min and 30 min after administration to mouse colorectums. 1% TFV (1:100 H3-TFV:TFV) was administered in DI water (20 mOsm), TBS (450 mOsm), 5% glycerol (600 mOsm) and Fleet® (2200 mOsm) enema. Total amounts were calculated assuming tritiated and unlabeled TFV entered circulation at the same rate. Studies were performed in $n \geq 5$ mice.

	Time after dosing			
	0 min		**30 min**	
Formulation (osmolality)	**TFV (µg)**	**# signal/# total**	**TFV (µg)**	**# signal/# total**
DI water 20 mOsm	0 ± 0	0/5	7.4 ± 3.4	6/8
SCS 150 mOsm	0 ± 0	0/5	0 ± 0	0/5
1.5x TBS 450 mOsm	0 ± 0	0/5	0 ± 0	0/5
5% Glycerol in DI water 600 mOsm	0 ± 0	0/5	0.1 ± 0.1	1/5
Fleet® enema 2200 mOsm	0 ± 0	0/5	42±18	4/5

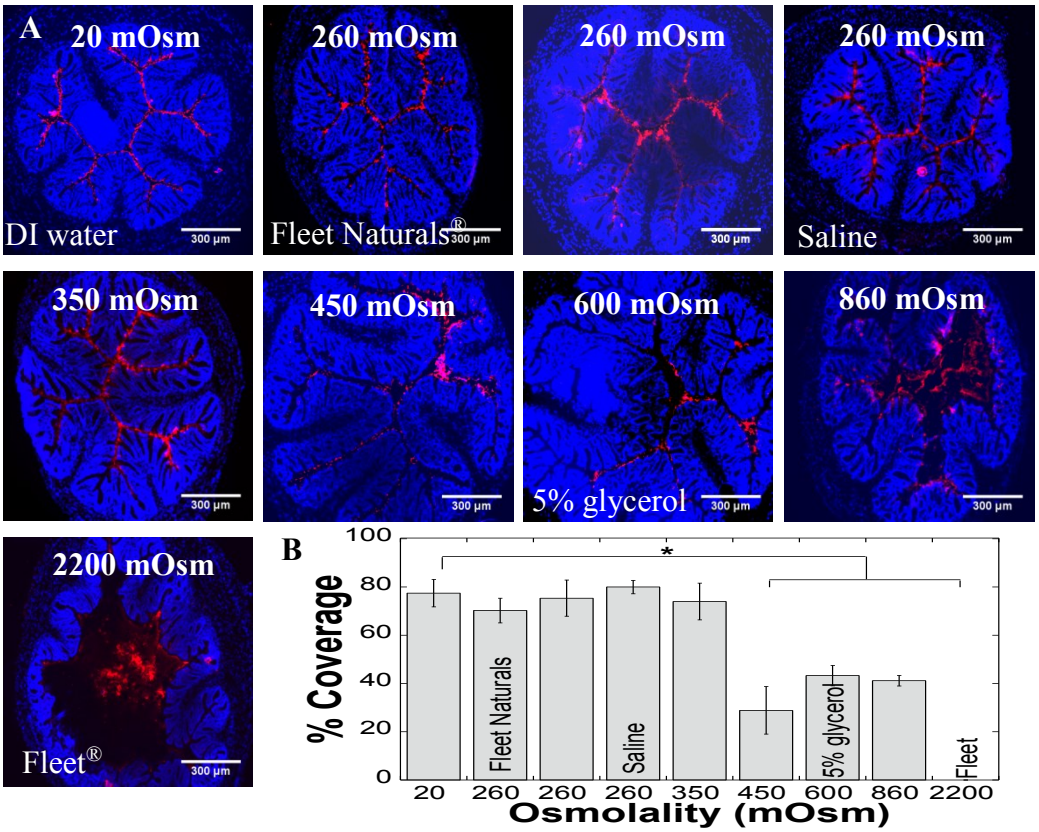

Figure 4-1. Distribution of MPP administered in sodium-based solutions with various osmolalities. (A) Distribution of 40 nm MPP in transverse colorectal cryosections after intrarectal administration in DI water (20 mOsm); sodium-based tris buffers (TBS) with osmolalities of 20, 260, 350, 450, and 860 mOsm; 5% glycerol in DI water (600 mOsm); clinical iso-osmolal saline (260 mOsm); Fleet Naturals® (260 mOsm); and regular Fleet® (2200 mOsm). Cell nuclei in transverse crysections were stained with DAPI. (B) Quantified surface coverage of MPP administered in various solutions on flattened mouse colorectal tissue. Images are representative of $n \geq 3$ mice. White scale bars = 300 µm. Data are calculated as means ± SEM. $*P < 0.05$ as compared to DI water (20 mOsm), Student's t-test.

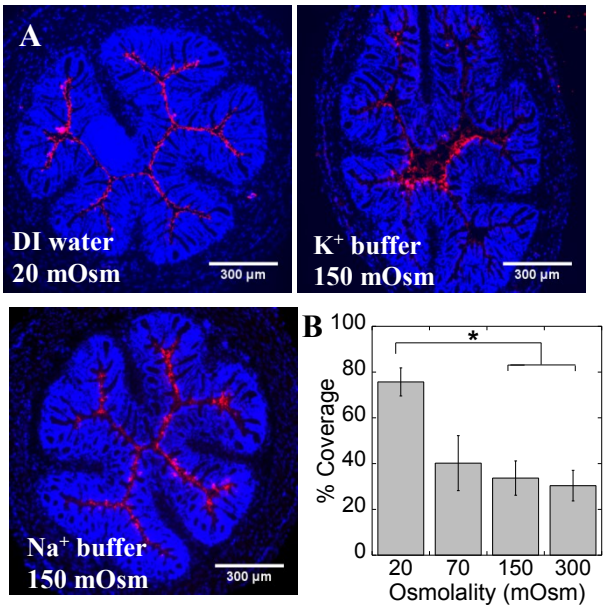

Figure 4-2. The impact of potassium on the colorectal distribution of MPP. (A) Distribution of 40 nm MPP in transverse colorectal cryosections after intrarectal administration in DI water (20 mOsm), potassium phosphate buffer (K+, 150 mOsm), and sodium-based tris buffer (Na+, 150 mOsm). Cell nuclei in transverse crysections are stained with DAPI. Images are representative of n ≥ 3 mice. White scale bars = 300 µm. (B) Quantified surface coverage of MPP administered in potassium phosphate buffers with various osmolalities on mouse colorectal tissue. The images in (A) do not correspond with quantified surface coverage in (B), but are illustrative of the difference in distribution of MPP after administration in sodium and potassium based enemas. Data are calculated as means ± SEM. *$P < 0.05$ as compared to DI water (20 mOsm), Student's t-test.

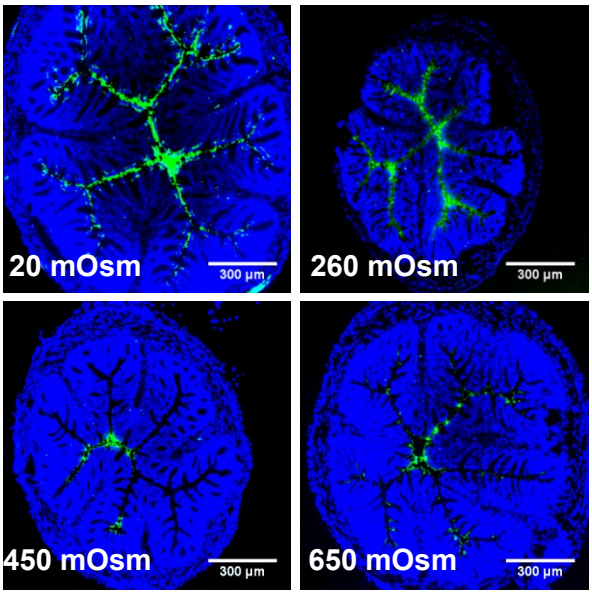

Figure 4-3. Distribution of TFV administered in sodium-based solutions with various osmolalities. Distribution in transverse colorectal cryosections after intrarectal administration of 1% TFV (1:10 TFV-FITC:TFV) in sodium-based tris buffers (450 and 650 mOsm), DI water (20 mOsm), and iso-osmolal saline (260 mOsm). Cell nuclei are stained with DAPI. Images are representative of $n \geq 3$ mice. White scale bars = 300 µm.

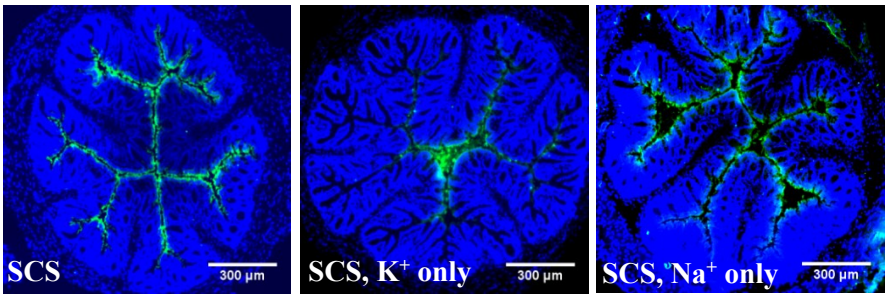

Figure 4-4. Distribution of TFV in SCS, SCS with only potassium, and SCS with only sodium ions matched to those in feces. Distribution in transverse colorectal cryosections after intrarectal administration of 1% TFV (1:10 TFV-FITC:TFV) in SCS, SCS without sodium (SCS, K+ only) and SCS without potassium (SCS, Na+ only). Cell nuclei in transverse cryosections are stained with DAPI. Images are representative of n ≥ 3 mice. White scale bars = 300 µm.

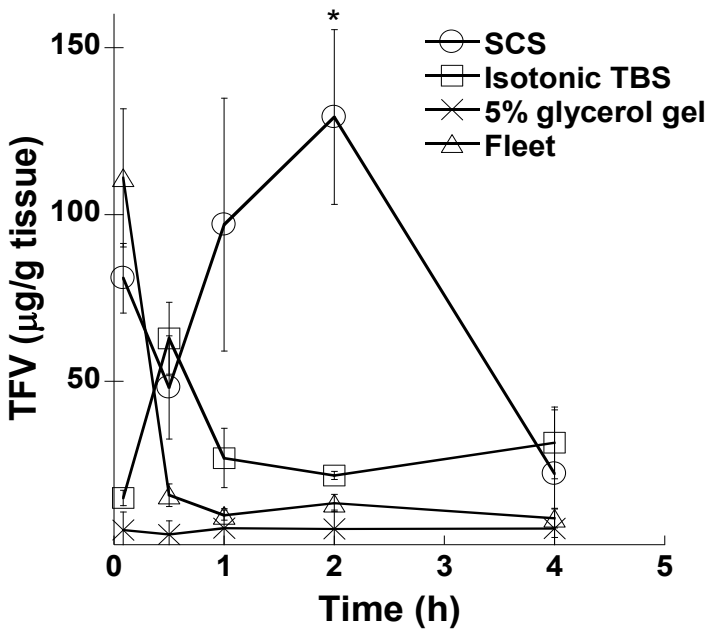

Figure 4-5. Pharmacokinetic analysis of TFV in mouse colorectal tissue. The calculated amount of TFV present in mouse colorectal tissues is shown for up to 4 h after administration. 1% TFV was administered in the simulated colon solution (SCS) (150 mOsm), isotonic TBS (450 mOsm), 5% glycerol gel (760 mOsm), and Fleet® enema (2200 mOsm). Total amounts were calculated assuming tritiated and unmodified TFV entered the cells at the same rate Studies were performed in $n \geq 5$ mice with highest and lowest value excluded to yield a total of $n \geq 3$ sample points. Data is shown as mean ± SEM. *$P < 0.05$ using Student's t-test.

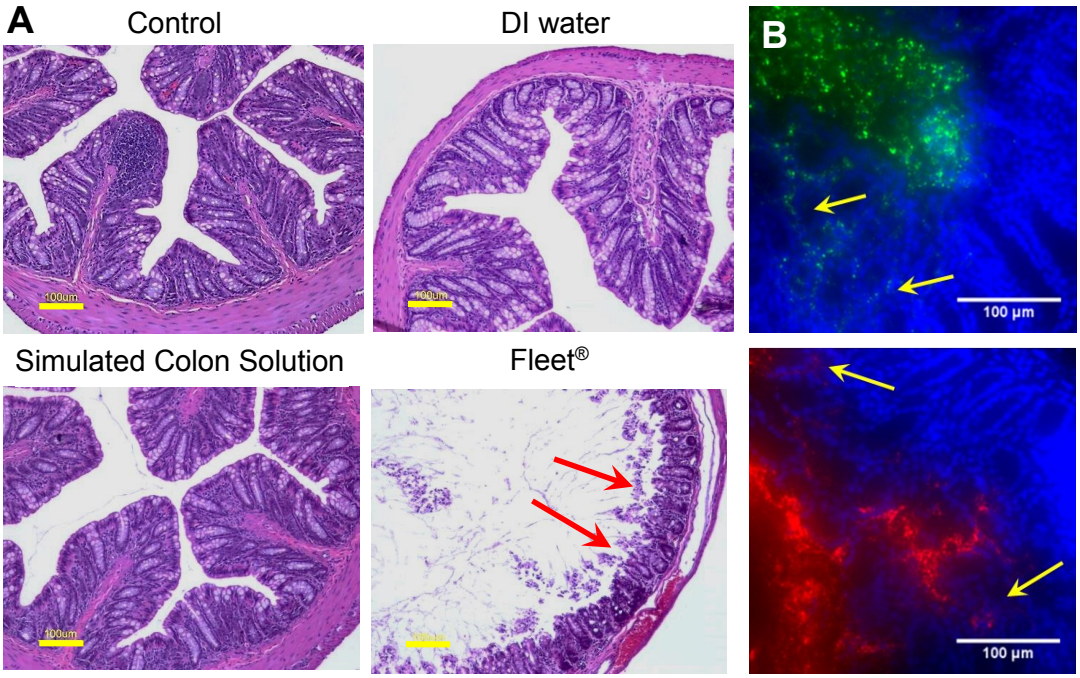

Figure 4-6. Acute toxicity of various enemas in the mouse colorectum. (A) Hemotoxylin and eosin (H&E) stained mouse colorectal tissue excised 10-15 min after intrarectal administration of DI water, simulated colon solution (SCS), or Fleet® enema. Red arrows indicate epithelial tissue that has separated from the tissue surface. Yellow scale bars = 100 µm. (B) Distribution of 40 nm (green) and 200 nm (red) MPP administered in a hypotonic solution 10 min after pretreatment with Fleet® enema. Yellow arrows indicate areas where MPP have penetrated into the damaged tissue. White scale bars = 100 µm. All images are representative of $n \geq 3$ mice.

5. A NOVEL NON-MUCOADHESIVE DAPIVIRINE NANOCRYSTAL FORMULATION IN A NOVEL OSMOTIC THERMOSENSITIVE GEL FOR IMPROVED VAGINAL AND RECTAL PRE-EXPOSURE PROPHYLAXIS

5.1 Introduction

According to UNAIDS, More than 35 million people are currently living with HIV infection and ~3 million new infections occur every year [117]. Unprotected vaginal and/or rectal intercourse are the two main sources of these new infections, with risks of 0.08-0.3% per sexual act for vaginal transmission and 1.8% per sexual act for rectal transmission [228]. Currently, neither preventative vaccines nor treatments have successfully eradicated the virus. The key strategy under investigation for ending the HIV epidemic is chemoprevention, or pre-exposure prophylaxis (PrEP) [121, 236-238]. A promising initial step in PrEP development was the recent US FDA approval of Truvada®, an oral pill that combines two antiretroviral drugs, for use by high risk populations [122, 239]. Truvada® and other systemic drug treatments, however, can have significant adverse side effects and some researchers have also voiced concerns that systemic drug exposure may lead to an increase in drug-resistant HIV strains [122, 239, 240]. Topical PrEP provides a unique opportunity, as it can achieve therapeutic drug levels directly at potential sites of infection, while avoiding side effects from systemic PrEP.

A number of topical delivery systems are currently under investigation for PrEP including vaginal rings, vaginal or rectal gels, and vaginal films [121, 122, 236, 241-243]. Vaginal rings have the advantage of providing long-term drug release over several weeks, but they are less discrete, thus limiting their applicability in third world countries [242]. Gels and films are more discrete and have high user acceptability, particularly in sub-Saharan

Africa [243-245]. However, research has shown that the incomplete epithelial coverage provided by many gels is a major failure mode of vaginal microbicide products [246]. In addition, rectally applied gels are unable to reach all internal surfaces potentially affected by HIV, since gels mostly remain in the rectosigmoid colon after rectal application [132, 134]. In contrast, we have previously found that fluid-absorption inducing (hypotonic) vaginal and rectal aqueous fluid formulations cause hydrophilic drugs and non-mucoadhesive nanoparticles to evenly coat the vaginal and rectal epithelium [61, 79]. In addition, Leyva et al have demonstrated that moderately fluid-absorption inducing enema formulations can reach all the way to the splenic flexure of the large intestine in a matter of 2 h [133]. Aqueous formulations thus have the advantage of providing drug to the entire surface that may come in contact with HIV.

Many of the antiretroviral drugs currently under investigation for PrEP are strongly hydrophobic and will poorly dissolve in an aqueous vehicle at therapeutic concentrations. Micronization is commonly used to help solubilize hydrophobic drugs in aqueous solutions. However, we have previously shown that large micron-sized (and down to 40 nm), hydrophobic particulates will become entrapped in the mucus barrier [15, 79]. Mucus is a highly viscoelastic hydrogel that coats the entire GI tract and effectively traps most pathogens and foreign particulates by hydrophobic and electrostatic interactions [8, 9]. Nanoparticles that are larger than the mucus mesh spacing or are mucoadhesive do not provide uniform coverage of the colorectal or vaginal epithelium even when administered in strongly hypotonic aqueous vehicles (Chapter 4 and [5, 79]). We have therefore designed nanoparticles that can slip through the mucus barrier, or are mucus penetrating, by densely coating them with poly(ethylene glycol) (PEG) and

ensuring their size is smaller than the mucus mesh spacing [15]. We have found that these mucus penetrating nanoparticles (MPP) can uniformly coat the colorectal and vaginal epithelium when administered in a hypotonic aqueous vehicle.

Dapivirine (TMC120) is one of the strongly hydrophobic antiretroviral candidates currently under investigation for PrEP. We here investigat the development of a novel dapivirine mucus penetrating nanocrystal formulation (TMC120 NC) made from all generally regarded as safe (GRAS) materials as dual-compartment vaginal and rectal product, and test its application in a murine model. To ensure that the TMC120 NC formulation reaches all areas HIV can reach as delivered in human seminal plasma, we also investigate the properties of human seminal plasma as a delivery vehicle. Our results demonstrate that human seminal plasma is hypotonic to the mouse vagina and colorectum. We also show that TMC120 NC evenly coat the colorectal and vaginal epithelium, and are able to cover all areas that HIV can reach on the colorectal tissue. In addition, we illustrate a novel method to osmotically deliver free drug or nanoparticles in a thermosensitive gel (thermogel). Thermogels have recently received considerable attention due to their ability to form a gel only once administered, making their administration easier than that of regular gels [245, 247-249]. However, when used in sub-Saharan Africa, where outdoor temperatures are well above body temperature, these gels are rendered useless. For this reason, we developed a novel method to form thermogels: when solutions containing thermogel below critical gelling concentrations (CGC) are administered hypotonically, the fluid absorption will cause the materials to both evenly coat and concentrate to CGC or above at the epithelial surface. We determined that F127 (a thermogel at 18% w/v) [249, 250], when delivered as osmotic thermogel effectively traps

HIV, evenly coats the cervicovaginal and colorectal epithelium, and significantly improves the retention of both TMC120 NC and free drug surrogate in the cervicovaginal tract. Our investigations illustrate that a mucus penetrating TMC120 NC formulation and a novel osmotic thermogel can improve colorectal and vaginal drug delivery by providing uniform epithelial coverage and prolonging retention time.

5.2 Materials and Methods

5.2.1 Nanocrystal and MPP formulation and characterization

Dapivirine nanocrystals (TMC120 NC) were fabricated by milling. Dapivirine was dissolved in methanol or acetone at 1% w/v and injected into a 1% F127 solution containing 10% polystyrene milling beads ranging from 0.4-0.6mm in diameter. Nanocrystals were covered and spun at 990 rpm for 4 days. Milling beads were removed and the resulting solution was filtered using a 0.22 μm filter. Fluorescein was conjugated to dapivirine to formulate fluorescent TMC120 NCs containing 10% w/w dapivirine-fluorescein. FITC-TMC120 NCs were fabricated by the same method described above.

MPP were formulated as previously described [176]. Briefly, carboxylate-modified polystyrene beads (PS-COOH, Molecular Probes) were suspended in 200 mM borate buffer containing 5 kDa methoxy-polyethylene glycol-amine (mPEG-NH_2), N-Hydroxysulfosuccinimide (Sigma) and 1-Ethyl-3-(3-dimethylaminopropyl) carbodiimide (EDC, Invitrogen) to couple the amine group on the mPEG-NH_2 with the carboxylic acid groups on the PS-COOH. Nanoparticles were washed and resuspended in deionized water.

For both nanocrystals and MPP, size (z-average) and polydispersity index (PDI) were determined using a Zetasizer Nano ZS90 (Malvern Instruments), via dynamic light

scattering (90° scattering angle). Measurements were taken at 25°C according to instrument settings and are presented as average ± standard error of the mean (SEM). Final drug concentration in TMC120 NC solution was determined via a high pressure liquid chromatography (HPLC) [251]. Images of TMC 120 NC were obtained using a Hitachi H7600 Transmission Electron Microscope (TEM). GFP labeled X4-HIV was graciously provided by the Siliciano lab at the Johns Hopkins University.

5.2.2 Nanocrystal stability and release

TMC120 NC were tested for long-term shelf life and stability in our previously developed SCS enema formulation. For long term shelf life, NC were lyophilized and stored at room temperature for up to 20 months. Size and PDI were measured at 2 weeks, 1 month, 3 months, and 20 months. For stability in SCS enema, previously lyophilized NC were suspended in SCS and 20 μL were extracted for size and PDI measurements immediately after suspension and at 30 min, 1 h, 2 h, 4 h, 6 h, 24 h , and 48 h.

TMC 120 NC release was determined by suspending 100 μL of nanocrystals in a sink of PBS containing 2% polysorbate 80 [137, 251]. Solution was removed at 0h, 1 h, and 2 h and spun down at 13000 rcf to remove any undissolved nanocrystals. The solution was analyzed for TMC120 concentration using HPLC.

5.2.3 Animal Model

Female CF1 mice were used for both colorectal and vaginal distribution and retention experiments. For vaginal distribution, mice were selected for estrus phase, in which the mucus has been shown to be most similar to human cervicovaginal mucus [5, 64]. For colorectal distribution, mice were starved for 24 h, and were given a 50 μL deionized water enema 15-20 minutes prior to administration of vehicle for quantified distribution.

For vaginal retention, animals were subcutaneously injected 2.5 mg of Depo Provera® (UpJohn) to induce a diestrus-like state [5]. All experiments were approved by the Johns Hopkins Animal Care and Use Committee (ACUC).

5.2.4 Distribution of nanoparticles, virus, nanocrystals, and osmotic thermogels on mouse vaginal and colorectal tissues

For nanoparticle or virus distribution in the colorectum, 30-50 μL of vehicle (hypotonic pure water, human seminal plasma, or osmotic thermogel in form of 10% F127 in pure water) containing either 60 nm mucus penetrating nanoparticles, TMC120 NC, or X4-HIV was administered intrarectally. For vaginal distribution of virus or nanoparticles, 5-10 μL of vehicle (hypotonic pure water, human seminal plasma, or osmotic thermogel in form of 10% F127 in pure water) containing 120 nm mucus penetrating nanoparticles or labeled TMC120 NC was administered intravaginally. Tissues were excised after 5-10 mins. For quantified colorectal distribution, tissues were cut open longitudinally, flattened between two glass slides, and 6 images were obtained along the tissue as previously described and quantified for fluorescence coverage using ImageJ [79]. The percent surface coverage for each animal was averaged over the six images, and an overall average was calculated for $n \geq 3$ mice. For qualitative distribution, tissues were excised, flash frozen in optimal cutting temperature compound (OCT), sliced into 6 μm slices using a Leica CM-3050-S cryostat, and cell nuclei were stained using ProLong Gold antifade reagent with DAPI (Invitrogen). All images were obtained using an inverted epifluorescence microscope (Zeiss Axio Observer).

5.2.5 Scanning electron microscopy (SEM) of colorectal tissue

For determining the honey-comb pattern evident on flattened colorectal epithelial tissue, colorectal tissue was dried and prepared for scanning electron microscopy. Tissues were excised from healthy mice, fixed overnight, washed, and incubated in 1% w/v osmium (OsO_4) for 1h. Tissues were again washed and incubated in 2% w/v aqueous uranyl acetate for 1h, and subsequently washed in 30% ethanol (EtOH), 50% EtOH, 70% EtOH, 90% EtOH, 100% EtOH, 1:1 HMDS:100% EtOH and HMDS. Tissue bits were then dried in a dessicator overnight, mounted, and coated with silver for imaging using a LEO/Zeiss Field-emission SEM.

5.2.6 HIV tracking on ex vivo tissue in the mouse colorectum and vagina pre and post osmotic gel administration

To determine if HIV can diffuse in mouse vaginal and colorectal mucus, mice were either starved for 24 h for rectal application or selected for naturally cycling estrus for vaginal application. Mice were anesthetized with isoflurane, tissues were excised, and placed into custom made 1x0.5 cm wells, and 0.25 µL of mCherry-HIV solution was pipetted on top of the tissue. To determine if a thermogel was formed in the colorectum, mice were anesthetized using isoflurane and 50 µL of 10% F127 solution was administered intrarectally. Mice were sacrificed at 5 min and 1 h, colorectal tissues were excised and placed into custom-made 1 x 0.5 cm wells, and 0.25 µL of mCherry-HIV solution was pipetted on top of the tissue. To determine if a thermogel was formed in the cervicovaginal tract, mice were anesthetized using isoflurane, and 10 µL of 10% F127 solution was administered intravaginally. Mice were sacrificed at 5 min and 1 h, vaginal tissues were excised and placed into custom-made 1x0.5 cm wells, and 0.25 µL of

mCherry-HIV solution was pipetted on top of the tissue. For all procedures, slides were covered with a cover slip, sealed with superglue and nanoparticle movement was imaged at 100x magnification over 20 s at 66.7 ms per frame using an EMCCD camera (Evolve 512; Photometrics) on an inverted epifluorescence microscope. Nanoparticle movement was analyzed. Nanoparticle centroids were tracked for ≥ 30 frames using MATLAB to obtain trajectories and mean squared displacements (<MSD>) calculated as $\langle \Delta r^2(\tau) \rangle = [x(t+\tau) - x(t)]^2 + [y(t+\tau) - y(t)]^2$ [81, 178-181]. Static and dynamic errors have previously been estimated to be below 20 nm, making them lower than the average nanoparticle displacement [179, 182].

5.2.7 Retention of free drug and nanocrystals in the mouse vagina

Fluorescein, a fluorescent free drug simulant, was dissolved at 1mg/mL in DI water, 18% F127, or 10% F127 solution with 1% v/v DMSO to ensure complete dissolution. Similarly TMC 120 NC were resolubilized in 1% or 10 % F127 solutions. Mice were anesthetized using isoflurane and restricted from grooming, which could alter retention results. 10 µL of fluorescein or TMC120 NC solutions were administered and mice were sacrificed immediately or after 24 h. Cervicovaginal tracts were excised and the fluorescence retained was analyzed using a Xenogen IVIS spectrum optical imaging device (Caliper Life Sciences, Inc., Hopkinton, MA) at 1s exposure time. The average fluorescence normalized based on area was measured and percent retained was calculated based on the amount of fluorescence at 0 h [5]. Statistical differences were calculated using a 2-tailed student's T-test assuming unequal variance.

5.3 Results

5.3.1 TMC120 NCs stability and drug release

The novel TMC120 NCs contained only dapivirine and 1% w/v F127, an FDA approved pluronic. Their z-average size was 200 ± 1 nm with a PDI of 0.122 ± 0.004 (Fig 5-1A & B). TMC120 NC size was stable for 48 h when suspended in a moderately hypotonic enema formulation (SCS) (Fig 5-1A), indicating their stability when exposed to ion-containing solutions prior to administration. However, TMC 120 NCs exhibited an increase to a stable size of 280 ± 3 nm and PDI of 0.198 ± 0.01 (Fig 5-1 B) when left as dry powder at room temperature for 20 months, likely due to spontaneous crystal assembly since dapivirine naturally crystallizes (unpublished observation) [252]. As shown in Figure 5-1C, TMC120 NCs also dissolved rapidly, with no crystals remaining after 2 h. TEM images reveal smaller crystals <50 nm radius along with larger, more oval crystals with dimensions of 170 ± 10 nm by 125 ± 10 nm (Fig 5-1D).

5.3.2 TMC120 NC distribution on mouse vaginal and colorectal tissue

To ensure that the NC formulation is indeed mucus penetrating, we next assessed their distribution on the vaginal and colorectal epithelium. Fluorescein-labeled TMC120 NC evenly coated both the vaginal and colorectal epithelium when administered in a hypotonic solution, similar to model MPP (Fig 5-2) [5, 79]. When developing an effective microbicide one must also consider what cells could come in contact with the pathogens. For this reason we investigated whether or not human seminal plasma, in which these pathogens are delivered, is hypotonic to the vaginal or colorectal tissue. Indeed human seminal plasma transports MPP to the murine vaginal and colorectal epithelial surfaces within minutes, evenly coating their surfaces with MPP (Fig 5-2). These results illustrate

that human seminal plasma is hypotonic in nature to both the vaginal and colorectal epithelium.

5.3.3 HIV distribution on mouse colorectal tissue

When we then administered HIV in a hypotonic solution, as it would be in human seminal plasma, we found that it evenly coats the colorectal epithelial surface, covering >80% (Fig 5-3). To ensure that our nanocarriers are also able to reach all areas HIV reaches, we also determined the coverage of TMC120 NCs and model 60 nm MPP. Both of these nanocarriers have similar distribution to HIV (Fig 5-3A), with >80% of the epithelial surface coated (Fig 5-3B). In addition, the distribution of all three, MPP, TMC120 NCs, and HIV, results in a honeycomb pattern that we have identified as the colonic crypts (Fig 5-3C) [113], again indicating that there is no difference in distribution.

5.3.4 TMC120 NC distribution in a thermogelling vehicle on colorectal and vaginal tissue

We next investigated the distribution of the hypotonically delivered thermogel F127, which becomes a thermogel at 18% w/v (Fig 5-4A). When we administered 10% w/v F127, a concentration below CGC (Fig 5-4A), to the mouse colorectum or cervicovaginal tract, we found that a thick F127-mucus gel mixture forms (Fig 5-4B). In addition, when we administered TMC120 NC in 10% F127, they evenly coated both the vaginal and colorectal epithelium (Fig 5-4C).

5.3.5 HIV diffusion on mouse colorectal and vaginal tissue with and without the presence of a thermogel

In order to prove that a complete gel was indeed formed, we observed the movement of HIV on mouse tissue with and without the presence of thermogel (F127 in these studies).

HIV is able to rapidly diffuse through mouse colorectal (Fig 5-5A) and vaginal (Fig 5-5B) mucus, as indicated by the high <MSD> (Fig 5-5). HIV diffuses only 6-fold slower in vaginal and 70-fold slower in colorectal mucus compared to its diffusion in water. To illustrate that fluid absorption is occurring and causes F127 to concentrate and form a gel, we observed HIV movement on *ex vivo* colorectal and vaginal tissues 5 min and 1 h after administration of the F127. When we compared HIV movement in untreated mouse colorectal and vaginal mucus with movement in thermogel-treated tissues, HIV movement was similar to that in mucus 5 min after thermogel administration. In contrast, HIV movement was significantly inhibited 1 h after thermogel administration for both tissues (Fig 5-5), indicating that fluid absorption had sufficiently concentrated the gelling vehicle to trap HIV.

5.3.6 Model drug and TMC120 NC retention with and without osmotic thermogel in the mouse vagina

We investigated whether or not the osmotic thermogel improves the retention of both TMC120 NC and free drug. Here, we used fluorescein as surrogate drug molecule. When TMC120 NC or free fluorescein were administered in simple hypotonic formulations, their 24 h retention was 21 ± 3% for TMC120 NC (in 1% F127) and 7 ± 4% for free fluorescein (Fig 5-6). Administration in 10% F127, however, yielded 35 ± 2% TMC120 NC and 23 ± 6% fluorescein retained over a 24 h period, a 70% increase for TMC120 NC and 230% increase for free fluorescein (Fig 5-6). In addition, the retention of free fluorescein delivered in osmotic thermogel was indistinguishable from its administration in the original 18% F127 formulation, namely 23 ± 6% in 10% F127 and 24 ± 9% in 18%

F127 (Fig 5-6B), indicating that the process of fluid absorption prior to gelling did not negatively affect drug retention.

5.4 Discussion

Formulating effective delivery vehicles for hydrophobic microbicides like TMC120 presents a unique challenge. Unlike their hydrophilic counterparts, hydrophobic drugs will not simply dissolve in a hydrogel or douche formulation and thus require the addition of potentially harmful additives to ensure drug dissolution. Formulating TMC120 in a nanosuspension, as we have done in this work, eliminates the need for such additives, providing the basis for a versatile range of delivery vehicles. Many rectal and vaginal formulations have not been designed with epithelial health in mind [129, 253]. In fact, many of the gels currently under investigation for vaginal or rectal microbicides have been highly strongly hypertonic, formulations which have recently been shown to cause significant epithelial toxicity [128, 129, 221, 230]. Many commercially available lubricants and enemas are also hypertonic, and recent evidence has linked use of such products to an increased susceptibility to STIs [253]. We have previously shown that hypotonic vehicles do not cause damage to the colorectal and vaginal epithelium. In addition, we have found that MPP are also non-toxic to the vagina. All materials used in our TMC120 NC formulation and in the osmotic thermogel are either GRAS or have been shown to be non-toxic, thus likely making the formulation non-toxic as well.

We have previously shown that uniform coating of mucosal surface can significantly improve protection against STIs as well as treatment of diseases including cystic fibrosis in inflammation [5-7]. Prior methods to determine distribution have only shown products to evenly distribute longitudinally along the vagina [5]. However, Achilles

et al (unpublished data) as well as our previously published work have illustrated that even longitudinal distribution will not account for distribution into all of the folds, or rugae, of the cervicovaginal tract [5, 246]. The incomplete coverage of the vaginal epithelium is likely a major pitfall in microbicide design [246]. Here, we demonstrated that TMC120 NC administered hypotonically (with or without osmotic thermogel) evenly coat the vaginal epithelium. In addition, we have previously shown that mucus penetrating nanocrystals made from acyclovir monophosphate, an anti-herpes (HSV) drug, and coated with F127 improved protection against HSV infection compared to free drug [5]. It was further concluded that this was due to the improved distribution and retention of the nanocarriers. The distribution of our TMC120 NC is similar to that of the model MPP used in these previous studies. Das Neves et al have also shown that dapivirine nanoparticles coated with PEG penetrate into vaginal tissue and improve drug retention compared to free dapivirine [136]. Our results illustrate that using an osmotic thermogel can further extend the vaginal retention of drugs and drug-loaded nanoparticles. TMC120 NC delivered in an osmotic thermogel would therefore likely also lead to prolonged protection against HIV infection.

In the colorectum, we found that the TMC120 NC penetrated deeply into the tissue. Similar results were obtained by das Neves et al who encapsulated TMC120 into polymeric nanoparticles coated with polyethylene glycol (PEG) [136, 137, 251]. The TMC120 nanoparticles were able to penetrate into vaginal and colorectal epithelial tissue 2 h after incubation with tissue [137]. While this group saw significant uptake of their nanoparticles into the epithelium, it is uncertain whether or not this was due to the particles ability to be transferred into the epithelium or if the tissue was simply becoming more permeable to

nanoparticles after removal from the physiological environment. In addition, the large amount of liquid that was incubated on only 1.8 cm^2 of tissue likely significantly diluted the mucus layer [137]. It is possible that this allowed nanoparticles to directly access the epithelial layer. While their methods may not be representative of the in vivo environment, their results still correlate with ours in that PEG coated nanoparticles can penetrate into vaginal and colorectal tissue. Recent results from Dezzutti et al has suggested that a thermogel formulation containing 1% w/v tenofovir, a hydrophilic antiretroviral drug, in 15% w/v F127 provided the best protection against HIV on human *ex vivo* biopsies, without causing any epithelial toxicity [248]. Also, Wang et al have illustrated that using a F127-based thermogel will improve colorectal drug retention in a rabbit model [247]. Their results demonstrate that both systemic and local drug levels are highest when using a thermogel administered in an enema compared to drug administered in a suppository or intravenously. These results indicate the promise of pluronic osmotic thermogels as PrEP drug delivery vehicle.

The importance of properly designing a drug delivery vehicle to reach the entire epithelial surface becomes more evident when we consider the vehicle in which HIV and other sexually transmitted infections are delivered. Most research has focused on understanding the mechanisms through which HIV infects cells in the vaginal and colorectal tissue and beyond [254, 255]. However, the vehicle with which HIV reaches those cells has not been investigated thus far. Our data indicate that human semen serves as a hypotonic delivery vehicle for pathogens and particulates that are non-adhesive to mucus in both the vagina and the colorectum. Since HIV is able to diffuse in both colorectal and vaginal mucus (Fig 5-5), the distribution of MPP and HIV delivered in human semen is

likely very similar. Indeed, we here showed that HIV administered in a hypotonic vehicle as it would be in human seminal plasma, distributes to the same areas that are reached by hypotonically delivered free drug, MPP, and MPP or free drug delivered in osmotic thermogel. Our results further support the hypothesis from Achilles et al that a conventional gel will not provide sufficient drug coverage of the epithelial tissue [246]. The osmotic thermogel formulation discussed here uniformly coats the epithelial surfaces of the colorectum and vagina and would thus present an improved drug delivery vehicle for microbicide candidates.

5.5 Conclusion

We have developed a novel mucus penetrating TMC120 NC formulation that remains stable in solution over 48 h and rapidly releases drug when sufficiently diluted. The formulation evenly coats the murine vaginal and colorectal epithelial surfaces when administered hypotonically. In addition, we found that thermogels can be administered below CGC and will be concentrated to or above CGC when administered in a hypotonic, fluid-absorption inducing vehicle. The concentrated material will gel at the epithelial surface and can effectively trap HIV particles. In addition, TMC120 NC administered in the osmotic thermogel evenly coat the epithelial surface. We also determined that the addition of an osmotic thermogel to both free drug formulations and TMC120 NC leads to increased drug and nanocrystal retention in the cervicovaginal tract. Formulating dapivirine into mucus penetrating nanocrystals delivered in an osmotic thermogel has the potential to significantly improve drug delivery to the cervicovaginal tract and colorectum, and thus may enhance protection against HIV in both compartments.

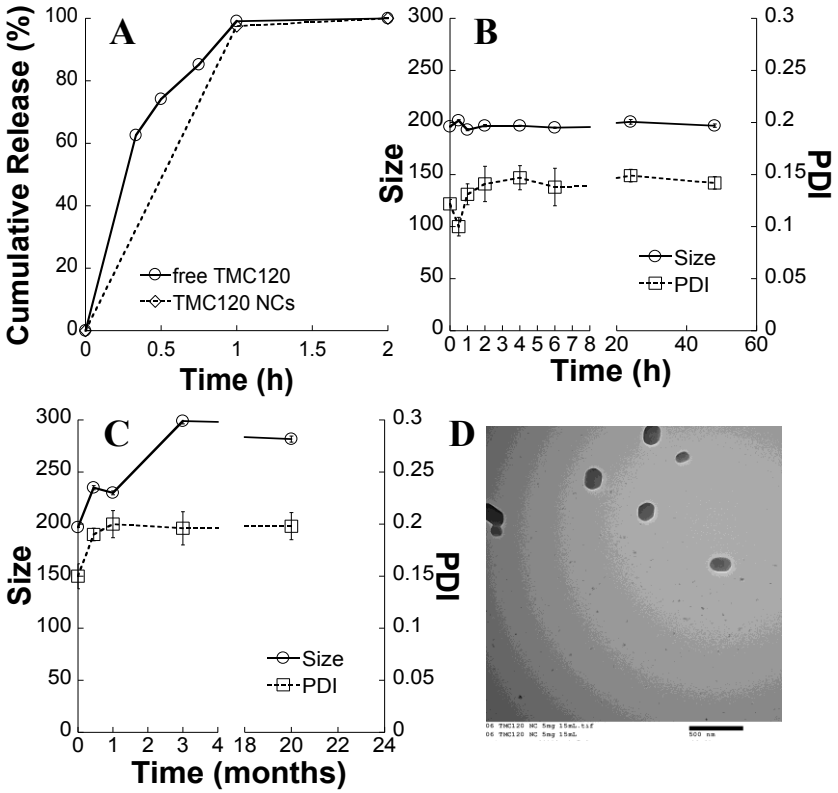

Figure 5-1. Size, stability, and drug release of TMC120 NC. (A) TMC120 NCs or free drug were suspended in PBS with 2% P80 and their drug release was determined over time via HPLC. TMC120 NC were lyophilized for size stability, and their size and PDI was assessed (B) after incubation in simulated colon fluid (saturated) or (C) after resuspension at various time points. (D) TEM image of TMC120 NC. Black scale bar represents 500 μm. Data are representative of $n \geq 3$ measurements and values are presented as mean ± SEM

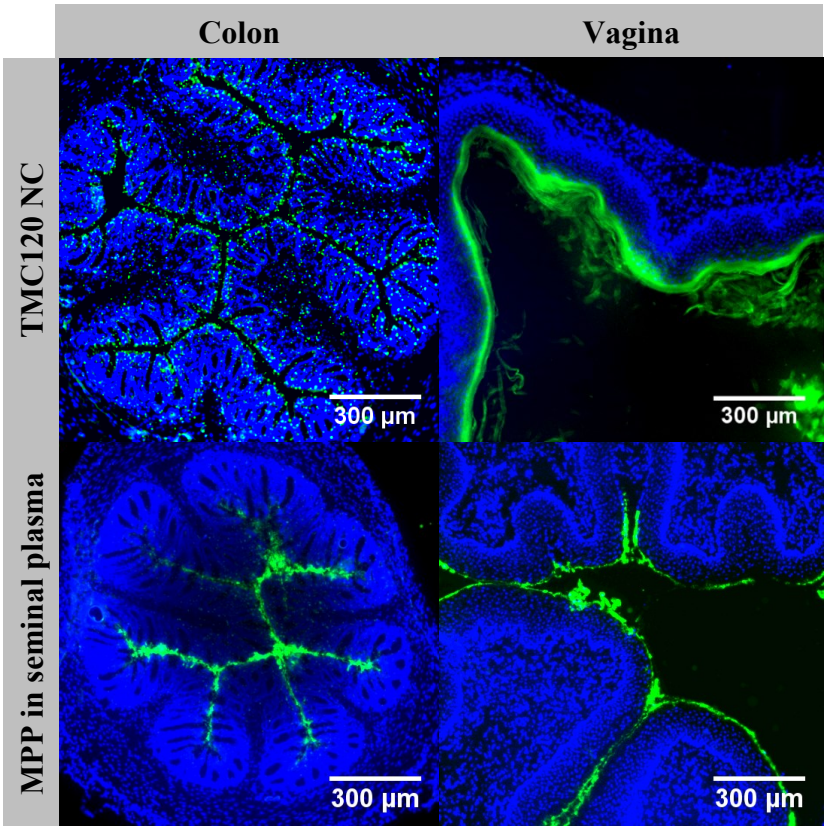

Figure 5-2. Distribution of TMC120 NC in hypotonic solution and MPP in human seminal plasma after rectal or vaginal administration. Distribution of TMC120 NC with 1% F127 in DI water after rectal or vaginal administration, or 60 nm MPP after rectal or 100 nm PSPEG after vaginal administration in human seminal plasma. White scale bars represent 300 µm. Images are representative of $n \geq 3$ mice.

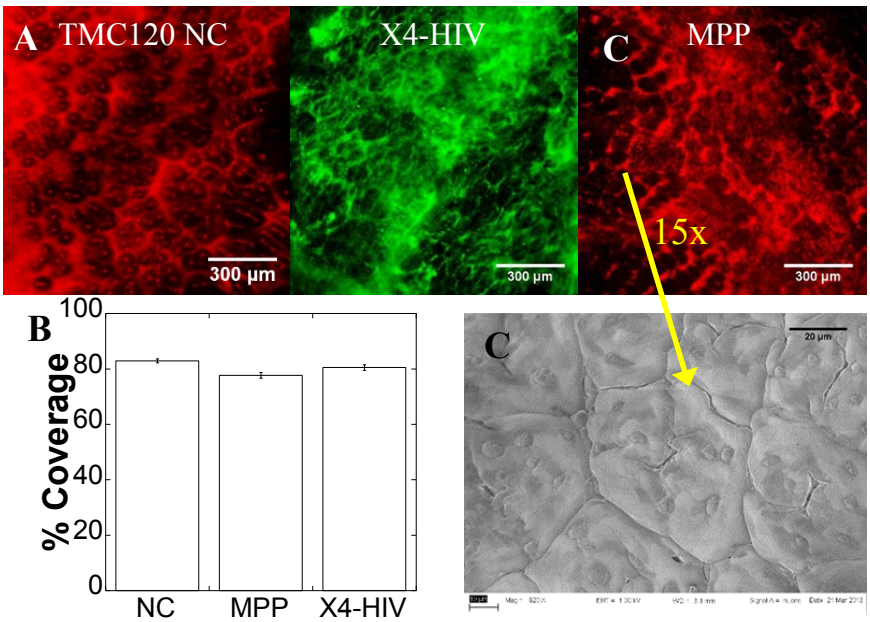

Figure 5-3. Distribution of TMC120 NCs, X4-HIV, and MPP on mouse colorectal crystal, and SEM of the colonic crypts. (A) Distribution of fluorescein-labeled TMC120 NC (200 nm), X4-HIV (160 nm), and MPP (60 nm) after rectal administration in a hypotonic fluid and (B) their quantification. (C) SEM image of the colonic tissue showing the colonic crypts that are outlined by the nanocarriers in (A). White scale bars represent 300 µm and black scale bar represents 20 µm. Images are representative of n ≥ 3 mice. Data represents averages over n ≥ 3 mice (n = 6 images per mouse) ± SEM.

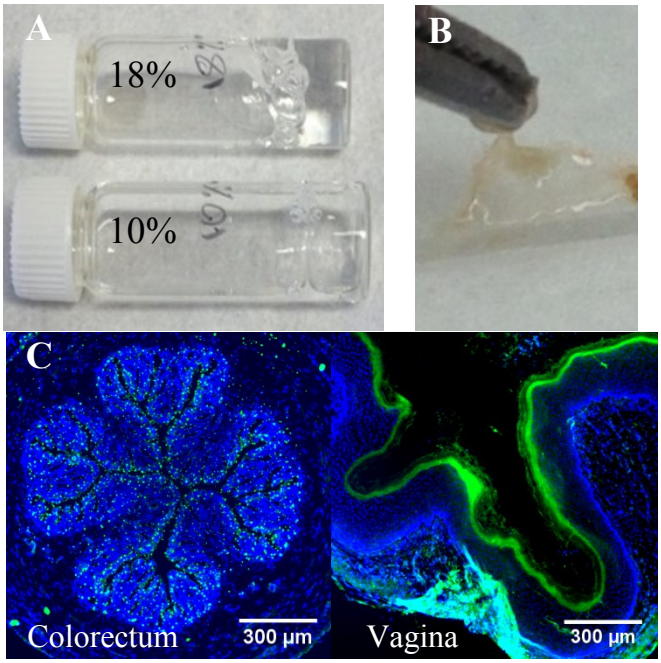

Figure 5-4. Gelling behavior of F127 gels and distribution of TMC120 NC in osmotic thermogel after rectal or vaginal (estrus) administration. (A) gelling behavior of 10% and 18% F127 at 37 C ex vivo. (B) gelling behavior of 10% F127 (osmotic thermogel) after hypotonic administration to the mouse colorectum. (C) Distribution of fluorescein-labeled TMC120 NCs after rectal or vaginal administration of 10% F127. White scale bars represent 300 µm. Images are representative of $n \geq 3$ mice.

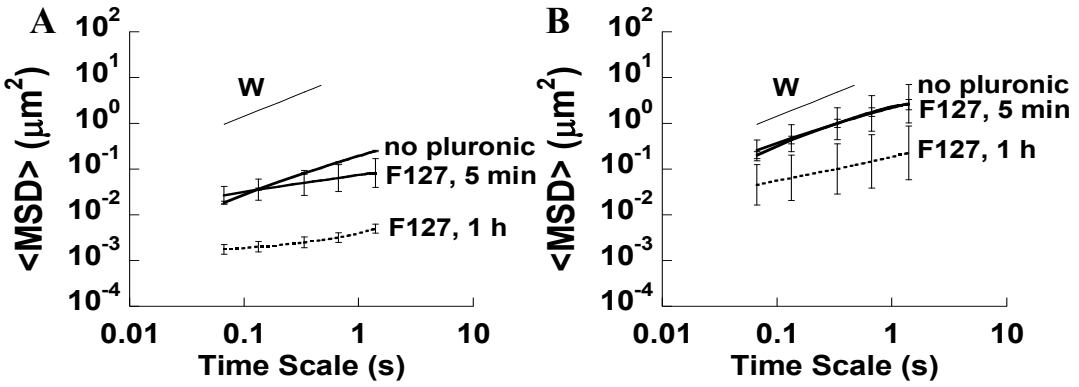

Figure 5-5. Transport properties of fluorescently labeled HIV after vaginal or rectal administration. Ensemble mean-squared displacement (<MSD>) with respect to time up to 3 s for (A) HIV moving in mouse colorectal mucus or on colorectal tissue 5 min or 1 h post administration of 10% F127 (thermogelling vehicle) and (B) HIV moving in mouse vaginal mucus or on vaginal tissue 5 min or 1 h post administration of 10% F127 (thermogelling vehicle). W indicates the movement of a 100 nm nanoparticle in water. Values are representative of $n \geq 3$ mice.

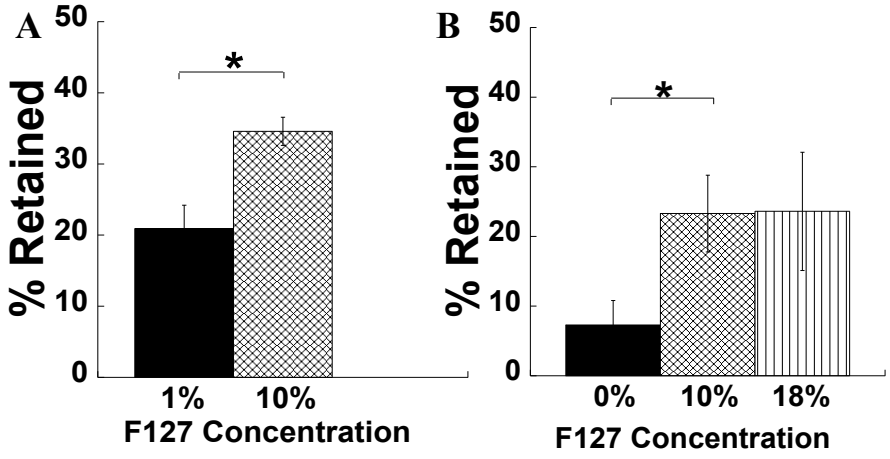

Figure 5-6. Vaginal retention of TMC120 NCs or free fluoresceine after 24 h.

Distribution of (A) fluorescein-labeled TMC120 NCs in 1% F127 or 10% F127 or (B) free fluorescein in DI H_2O, 10% F127, or 18% F127 24 h after vaginal administration in 1% (no gel) or 10% (hypotonic gel) F127. Values represent $n \geq 5$ mice and are normalized to the average of the 0+ time point (0+h = 100%). $*P < 0.05$ compared to 1% F127 (NC) or DI H_2O (fluorescein), Students t-test.

6. FUTURE OUTLOOK

In this thesis, I have shown the properties necessary to make nanoparticles rapidly diffuse through mouse GI mucus, including their size and surface charge; I have illustrated that these particles can be used as tools to assess whether or not fluid absorption is occurring, and I have developed a novel all GRAS MPP formulation for use in HIV prevention. There is, of course, much more to do.

A critical step to translating MPP to the clinic is to determine the properties necessary for nanoparticles to diffuse through *human* GI mucus. This will allow the proper design of drug-loaded nanocarriers that can provide uniform distribution on small and large intestinal tissues. Nanoparticles to develop include ones carrying poorly water soluble drugs and drugs with poor GI bioavailability in order to improve systemic delivery of these drugs, as well as ones carrying medications to treat local diseases such as IBD via both the rectal or oral routes. Moreover, the use of the microbicide-based nanocarrier (dapivirine MPP) for PrEP developed in Chapter 5 must be further investigated. This will include testing for toxicity and pharmacokinetics after colorectal administration and compared to free drug and current gel-based formulations. All developed nanoparticles, including the dapivirine MPPs, first need to be tested in murine models, but translation to a larger animal with GI tract function and transit times more similar to humans, such as pigs, will provide more insight into the improvements of MPP compared to MAP or free drug.

In addition to continuing the development of MPP for application in GI diseases and for improvement of oral-to-systemic drug delivery, developing proper delivery vehicles for these nanoparticles (and free drugs) is also essential. One such step is the

DREAM project, which focuses on developing and optimizing a microbicide-containing enema formulation as PrEP. The work in this project will translate the work from Chapter 4 into humans. Another delivery vehicle for both drugs and drug-loaded nanoparticles are gels. The novel osmotic gelling method discussed in Chapter 5 only shows initial steps toward developing better gel vehicles for vaginal and colorectal drug delivery. I illustrate that both free drug and nanocarriers can benefit from an osmotic thermogel. We have also found that the osmotic thermogel can serve as a barrier to the diffusion of infectious agents including HIV and HSV, though to this point the formulations tested so far have not increased protection from HSV infection vaginally. Further investigation for the use of an osmotic thermogel as a physical barrier against infections is still needed. The idea of using osmosis to form a gel right at the epithelial surface is not only limited to thermogels. My findings can easily be translated to gels including the hydroxyethylcellulose (HEC) based gels used in vaginal products. New gel products, especially dual-compartment gels, that provide uniform coverage of the vaginal and rectal epithelium may be particularly useful for prevention of STIs as well as for treatment of local vaginal and colorectal infections.

I. APPENDIX I – THE MUCOADHESIVITY PARADOX REVISITED: NANOPARTICLES DENSELY COATED WITH HIGH MOLECULAR WEIGHT POLYETHYLENE GLYCOL (PEG) ARE NOT MUCOADHESIVE AND RAPIDLY PENETRATE HUMAN MUCUS

I.1 Main Text

Mucus, the first line of defense on all mucosal surfaces, is a sticky, viscoelastic gel that effectively traps many pathogens, preventing them from reaching and infecting the underlying tissue. The trapping mechanisms (mucoadhesion, sieving, and unstirred adherent mucus layers) can significantly interfere with drug delivery to epithelial surfaces by preventing particulates from reaching the epithelial surface if they are larger than the mucus mesh or if they adhere to the mucus mesh [5, 8, 9, 15, 19]. Most nanoparticles designed for mucosal drug delivery are designed to be mucoadhesive, but we have shown that such particles provide incomplete distribution on vaginal, lung, and colorectal tissues [5, 7, 61, 79], whereas nanoparticles densely coated with polyethylene glycol (PEG), are able to penetrate the mucus barrier to reach and evenly coat the entire epithelial surface [5, 7, 15, 79]. In addition, mucus penetrating nanoparticles (MPP) are retained for longer periods of time in the cervicovaginal and respiratory tracts compared to mucaodhesive particulates [5, 7], indicating that MPP are more suitable for distributing drug to the entire epithelial surface and prolonging drug retention [5, 7, 79].

Research has shown that adding PEG to hydrogels and hydrogel microparticles causes their surfaces adhere to mucus [72-74, 256-259]. PEG was shown to act as a kind of mucoadhesive "glue" that could entangle with mucin fibers [73, 257] or form hydrogen bonds to the carbohydrate regions of the mucin fibers [260]. In our previous work, we

hypothesized that dense coatings of lower molecular weight (MW) PEG would not entangle with mucins and the hydrophilic and uncharged nature of PEG would allow nanoparticles to avoid adhesion [15]. Indeed, we showed that nanoparticles with a high surface density of low MW PEG (2 kDa and 5 kDa) rapidly diffused in human cervicovaginal mucus (hCVM) [15, 67, 68, 76]. We found that dense surface coverage by neutrally-charged PEG produced nanoparticles with a near-neutral surface charge (ζ-potential) that have a "mucoinert" surface that is non-mucoadhesive and non-inflammatory [5, 7, 261]. In contrast, nanoparticles with positively charged surfaces, and/or uncoated hydrophobic surfaces, were adhesive to mucus and also inflammatory [5, 15]. When we attached PEG with higher MW, 10 kDa, the particles became mucoadhesive, which we expected may be due to PEG entanglement with the mucus gel and/or insufficient PEG coverage on the nanoparticle surface [75]. We have recently optimized reaction conditions that can achieve higher PEG surface densities on nanoparticle surfaces as compared to our previous methods [78, 176]. Here we report that by using these new methods we can increase surface density of higher MW PEG (up to 40 kDa), and nanoparticles coated with PEG up to 40 kDa can rapidly penetrate hCVM.

To compare directly our prior and current PEGylation methods, we coated carboxylate-modified polystyrene (PS) nanoparticles with 10 kDa PEG using two different buffers: pH 7.4 200 mM borate buffer [176], and pH 6, 50 mM 2-(N-morpholino)ethanesulfonic acid (MES) buffer [15]. We found that PS coated with 10 kDa PEG using the borate method (PS-PEG_{borate}) were able to rapidly diffuse through hCVM. The ensemble-averaged mean squared displacement (<MSD>) of PS-PEG_{borate} (260 ± 7 nm; -0.7 ± 0.5 mV) was 1,000-fold higher than either uncoated PS or PS coated with 10

kDa PEG using the MES method (PS-PEG_{MES} ; 220 ± 10 nm; -12 ± 0.4 mV; Fig I-1A, Table I-1). The <MSD> and the logarithmic distribution of individual MSD values for PS-PEG_{MES} were similar to those of mucoadhesive, unmodified PS (180 ± 1 nm; -59 ± 2 mV) in hCVM (Fig I-1A, B) as we reported previously [75]. Nanoparticle trajectories representing 3 s of movement in hCVM further emphasize the difference in transport in hCVM, as PS-PEG_{borate} moved in a diffusive random walk, while PS and PS-PEG_{MES} remained immobilized, moving less than their diameter. In addition, the PS-PEG_{borate} moved only 11-fold slower than in water (Table I-1), whereas PS-PEG_{MES} were >10,000-fold slowed in hCVM compared to their theoretical diffusion rates in water (Table I-1). To further understand the difference between the diffusion abilities of PS-PEG_{borate} vs PS-PEG_{MES}, we determined the PEG density on PS-PEG nanoparticles. We previously used a fluorimetric method for determining PEG density, where we conjugated fluorescent dyes to the free carboxylic acid groups on the PS beads after coating them with PEG [75]. When using this method, PEG density on the surface of PS-PEG_{MES} coated with 5 kDa PEG was slightly higher than that of PS-PEG_{MES} coated with 10 kDa PEG [75]. These results were confirmed with our more sensitive, previously published NMR method for measuring PEG surface density [78, 176]: PS coated with 10 kDa PEG using the MES method seemed to have slightly lower PEG densities than PS coated with 5 kDa PEG using the borate method. In addition, we found that PS-PEG_{borate} coated with 10 kDa PEG also had slightly higher PEG density, calculated as unconstrained area covered by PEG chains/total surface area (Γ/SA), namely 1.3 ± 0.1 for PS-PEG_{MES} compared to 1.5 ± 0.1 for PS-PEG_{borate} (Table I-1). The Γ/SA values correspond to 2.9 ± 0.3 PEG chains per 100 nm^2 for PS-PEG_{MES} compared to 3.3 ± 0.1 for PS-PEG_{borate}. Theory has shown that PEG

surface density (Γ/SA) < 1 will lead PEG to be in mushroom conformation, in which neighboring PEG chains do not overlap, which may leave some of the hydrophobic nanoparticle core exposed and allow the PEG chains to interpenetrate with mucin or extracellular matrix fibers [71, 73, 74]. When Γ/SA > 1, PEG chains begin form a brush regime, where neighboring PEG chains are able to overlap, the hydrophobic nanoparticle core is likely no longer exposed and PEG chains are more constrained from interacting with surrounding tissue fibers [262]. We have previously shown that PS-PEG with Γ/SA < 1.7 were unable to penetrate brain tissue [176], indicating that a PEG density threshold exists for nanoparticles to be non-adhesive to the brain parenchyma. Similarly, it seems that a PEG density threshold must be exceeded to make nanoparticles mucus penetrating since a small increase in PEG density allowed the PS-PEG_{borate} rapidly diffuse through hCVM.

Using the optimized method to coat PS nanoparticles with PEG, we tested the effect of PEG MW on nanoparticle diffusion in mucus. We found that 200 nm PS coated with up to 40 kDa PEG (with sizes ranging from 230 – 300 nm, refer to Table I-1) were able to rapidly penetrate hCVM, as indicated by the high <MSD> (Fig I-2A). The logarithmic MSD distribution of these nanoparticles in hCVM showed a high fraction of moving nanoparticles for all MWs (Fig 2b). In addition, the 3 s trajectories indicated a random walk, in stark contrast to the mucoadhesive PS that remain in place (Fig I-2C). All non-mucoadhesive nanoparticles also had high PEG density (Table I-1). It is evident that the number of PEG/ 100 nm^2 decreases as PEG MW increases, as the # PEG/100 nm^2 was 7.1 ± 0.4 and 1 ± 0.1 for 5 kDa and 40 kDa PEG, respectively (Table I-1). The decrease can be attributed to the changes in space occupied by each PEG chain; the area

occupied by one unconstrained 5 kDa PEG chain is ~23 nm^2 and increases 8-fold to ~180 nm^2 for unconstrained 40 kDa PEG molecules. Thus a smaller total number of PEG chains is needed to cover the surface of the particles completely as PEG MW increases.

Similar to our results for 200 nm PS-PEG_{borate} (ranging between 230 – 300 nm, Table 1), 100 nm PS-PEG_{borate} (ranging between 110 – 170 nm, Table I-1) coated with 5 kDa, 10 kDa, 20 kDa, and 40 kDa all possessed high PEG density ($\Gamma/SA > 2$ [176], Table I-1) and were able to rapidly diffuse through hCVM. The high <MSD> of each of these particle types, and the large fraction of diffusive nanoparticles (Fib 3a and b), suggest that PEG MW (ranging from 2 – 40 kDa) does not directly affect the ability of nanoparticles to penetrate hCVM. Particle trajectories indicate a random walk, in stark contrast to the immobilized PS (Fig 3c). Both 100 nm and 200 nm PS-PEG coated with 5kDa - 40 kDa MW were all < 20 fold slowed in hCVM compared to their diffusion in water (Table I-1).

Higher MW PEG has been previously associated with increases in mucoadhesion [72-74, 257, 259, 260, 263, 264]. Peppas et al. have suggested that tethering PEG to different polymers and gels makes them more mucoadhesive by providing chains that are capable of entangling with and interpenetrating into the mucus gel [73, 257, 260]. They have reported that PEG will, over time, diffuse into the mucin network, due to its hydrophilic nature, where it can undergo hydrogen bonding with the polysaccharide groups found on mucins, and thus provide an anchor for the material it is attached to [260] In addition, DeAscentiis et al determined that for poly(hydroxyethyl methylcellulose) (pHEMA) microparticles, coatings with 1 kDa PEG actually led to increased mucoadhesion compared to 100 kDa PEG [256]. They hypothesize that because 100 kDa PEG chains could theoretically form significantly more entanglements than 1 kDa or 10 kDa PEG, this would lead to less

interpenetration by 100 kDa into the mucin gel and thus less mucoadhesion [256]. These results correspond with our previous findings that 10 kDa PEG leads nanoparticles to adhere to mucus [75]. However, our findings here illustrate that when a dense enough PEG layer is formed on a nanoparticle surface, the nanoparticles will no longer adhere to mucus. The increased number of PEG molecules present on the nanoparticle surface likely sterically hindered PEG molecules from interacting with mucus, and thus kept them from interpenetrating into or forming hydrogen bonds with the mucins. In addition, it is not surprising that larger MW PEG will more effectively prevent nanoparticles from interacting with biological surfaces, as He et al. have reported that using 20 kDa PEG can improve systemic nanoparticle immunogenicity and circulation times compared to nanoparticles coated 5 kDa PEG due to better stealth properties [265].

We have previously seen indications that mucus penetrating nanoparticles (MPP) more effectively improve treatment and prevention of diseases at mucosal sites, including preventing herpes (HSV) infection in the CV tract and asthmatic lung inflammation as well as treating diseases like cervical cancer and cystic fibrosis [5, 7, 266, 267]. Using PEG with MW $\leq$ 40 kDa allows for additional flexibility in formulating drugs into nanoparticles, and thus a more versatile range of drug-loaded MPP is possible. We have also observed that the use of MPP in a vehicle that causes fluid uptake by the epithelium improves distribution on vaginal and colorectal tissue compared to mucoadhesive particles [5, 61, 79]. Here we have investigated whether nanoparticles coated with higher MW PEG that diffuse in hCVM can also improve distribution in the cervicovaginal tract and colorectum compared to mucoadhesive nanoparticles. We administered 5 μL of nanoparticle solutions to the vagina of mice in the estrus phase of their estrous cycle, in

which the mucosa and mucus layer are most similar to those in the human vagina and hCVM, and 20 L of nanoparticle solutions to the colorectum of mice that had been starved for 24 h [5]. Nanoparticles were administered with hypotonic solutions that cause rapid fluid uptake from the vaginal and colorectal lumen [61]. We found that mucoadhesive PS remained in the lumen (Fig I-4), but non-mucoadhesive 40 nm (colorectum) and 100 nm (vagina) PS-PEG_{borate} with PEG MW $\leq$ 40 kDa were transported rapidly to the epithelial surface and evenly coated virtually the entire mouse colorectal and vaginal epithelium. This demonstrated that PS-PEG that diffuse rapidly in hCVM *ex vivo* mucus are also advectively transported through mucus *in vivo* by the flow of water toward the epithelium.

I.2 Materials and Methods

I.2.1 Nanoparticle formulation

PEG-coated nanoparticles were synthesized using the two methods previously described. For the "MES method", excess methoxy-polyethylene glycol (mPEG)-amine (10 kDa) was dissolved in 50 mM 2-(N-morpholino)ethanesulfonic acid (MES) buffer at pH 6 (Sigma). 200 nm carboxylate-modified polystyrene (PS) beads (Molecular Probes) were added to the MES/PEG mix and sonicated. 1-ethyl-3-(3-dimethylaminopropyl)-carbodiimide (EDC, Sigma) and N-Hydroxysulfosuccinimide (NHS, Sigma) were added to make a ratio of 0.1:1:1:1 COOH:PEG:EDC:NHS. The mixture was incubated at 37°C overnight, and then the nanoparticles were washed twice with DI water. For the borate method, 40 nm, 100 nm, or 200 nm carboxylate-modified PS beads (Molecular Probes) were coated with polyethylene glycol (PEG) with molecular weight of 5 kDa, 10 kDa, 20 kDa, or 40 kDa. PS beads were suspended in DI water with 200 mM borate buffer (pH

7.4) and respective methoxy-PEG-amine was added in excess. Excess amounts of NHS and EDC were added. The nanoparticle mixtures were incubated at room temperature overnight and subsequently washed twice with DI water. Nanoparticles were suspended in a 10 mM NaCl solution, and characterized with dynamic light scattering (DLS) for size and laser Doppler anemometry for ζ-potential measurements using a Zetasizer Nano ZS90 (Malvern Instruments). DLS was performed at 90° scattering angle and all measurements were taken at 25°C, in accordance with the instrument settings. ζ-potential close to 0 mV indicate PEGylation was complete [15, 176].

I.2.2 PEG surface density measurements

PEG density was calculated as previously described [78, 176]. Briefly, nanoparticles were fully dissolved in deuterated chloroform ($CDCl_3$, Sigma), trifluoroacetic acid-d (TFAd, Sigma), and a known concentration of Tetramethylsilane (TMS, 1% w/v). H-NMR spectra were obtained using a Bruker REM400 at 400 mHz. PEG density, or Γ/SA, was calculated from the integral of the PEG peak (3.6 ppm) and the internal standard TMS peak (0 ppm). To calculate the area occupied by the PEG chains on each particle, a random walk statistics model was used to find the area occupied by PEG of a certain length. These calculations yield a sphere with diameter $d = 0.76 (m_b)^{0.5}$ where m_b is the molecular weight of the PEG in question, yielding an area occupied by PEG of $A = \pi(d/2)^2$ [70]. The areas occupied were then used to calculate the number of PEG chains per 100 nm^2 and area occupied by PEG chains/total particle surface area (Γ/SA). PEG 5 kDa was used for calibrating PEG concentration in solution. For PEG surface density calculations, it was assumed that the nanoparticles' surfaces are smooth and their diameter is equivalent to that measured by DLS.

I.2.3 Multiple particle tracking in human cervicovaginal mucus

Human cervicovaginal mucus (CVM) samples were obtained by self-collection using a menstrual collection device as previously described [15, 268] and approved by the Institutional Review Board of the Johns Hopkins Medical Institution. Up to 2 μL of particle solution (0.02-0.08% w/v) was added to a volume of 30 μL hCVM in a custom made well. Wells were sealed with a coverslip that was affixed with superglue. Movies were obtained with a 100x/1.46 NA oil-immersion objective via an EMCCD camera (Evolve 512; Photometrics) as part of an inverted epifluorescence microscope setup (Zeiss Axio Observer). Movies were 20 s in time and had a 66.7 ms temporal resolution. Nanoparticle trajectories and mean squared displacements (MSD) were obtained using MATLAB [67] with a minimum of 30 frames tracked for each particle, and MSD calculated as $\langle \Delta r^2(\tau) \rangle = [x(t+\tau) - x(t)]^2 + [y(t+\tau) - y(t)]^2$ [15, 81, 180]. Our prior work has indicated that static error can be estimated to be below 20 nm, much smaller than the average particle displacement [7, 81].

I.2.4 Nanoparticle distribution in the mouse vagina and colorectum

Female CF-1 mice 6-8 weeks old were housed in a reverse light cycle facility (12 h light, 12 h dark) for one week to allow acclimatization. For vaginal distribution, mice were selected for naturally cycling estrus by visual appearance of their introitus as previously described [269], as this phase makes the vagina most similar to the human vagina [270, 271], and gives their mucus similar barrier properties to human CVM [64]. For colorectal distribution, mice were starved for 24 h, as this decreases the number and hardness of the pellets [79]. Mice were anesthetized using isoflurane, and 5 μL (vaginally) or 20 μL (rectally) of 0.02% w/v nanoparticles in DI water were administered into the vagina or colorectum [5].

Mice were sacrificed after 5-10 min (dissection speed) and tissues were excised, flash frozen in Tissue-Tek O.C.T. Compound, and sectioned into 6 μm slices along the entire length of the vagina and colorectum with a Leica CM-3050-S cryostat. Slices were fixed with 10% formalin and stained using ProLong Gold antifade ® reagent with DAPI to stain nuclei and retain particle fluorescence. Images were obtained using the inverted epifluorescence microscope setup (Zeiss Axio Observer). All experiments were approved by the Johns Hopkins University Animal Care and Use Committee.

Table I-1. Surface, size, and diffusional properties of PS and PS-PEG. Size, ζ-potential, PEG surface density (area covered by PEG/total surface area, or Γ/SA), and the comparison of the ensemble averaged MSD in mucus (<MSD>) to the theoretical MSD of similarly sized particles in water (MSD_w) (indicating how much slower the nanoparticles move in mucus, MSDw/<MSD>), of 100 and 200 nm PS and PS-PEG prepared by various methods. Unless otherwise indicated, PS-PEG are prepared via the borate method. Values are averaged over n ≥ 3 samples.

Size (nm)	**Type**	**PEG MW (kDa)**	**Hydrodynamic diameter (nm)**	**ζ-potential (mV)**	**Γ/SA**	**# PEG chains/ 100 nm²**	**MSD_w/ <MSD>**
100	PS	-	90 ± 1	-51 ± 1.6	0	0	>10,000
	PS-PEG	5	110 ± 2	-3.1 ± 0.3	>2*	~9*	10
		10	120 ± 7	-0.5 ± 0.1	2.0 ± 0.1	4.4 ± 0.2	18
		20	130 ± 4	-0.4 ± 0.1	3.3 ± 0.1	3.3 ± 0.1	6
		40	170 ± 8	-1 ± 0.1	2.1 ± 0.2	1.2 ± 0.1	20
200	PS	-	180 ± 1	-59 ± 2	0	0	>10,000
	PS-PEG	5	230 ± 5	-1.6 ± 0.1	1.6 ± 0.1	7.1 ± 0.4	9
		10	260 ± 7	-0.7 ± 0.5	1.5 ± 0.1	3.3 ± 0.1	11
		10 (MES)	220 ± 10	-12 ± 0.4	1.3 ± 0.1	2.9 ± 0.3	>10,000
		20	270 ± 7	-2 ± 0.7	1.7 ± 0.1	1.9 ± 0.2	10
		40	300 ± 5	-1 ± 0.6	1.7 ± 0.1	1 ± 0.1	15

*based on literature [176]

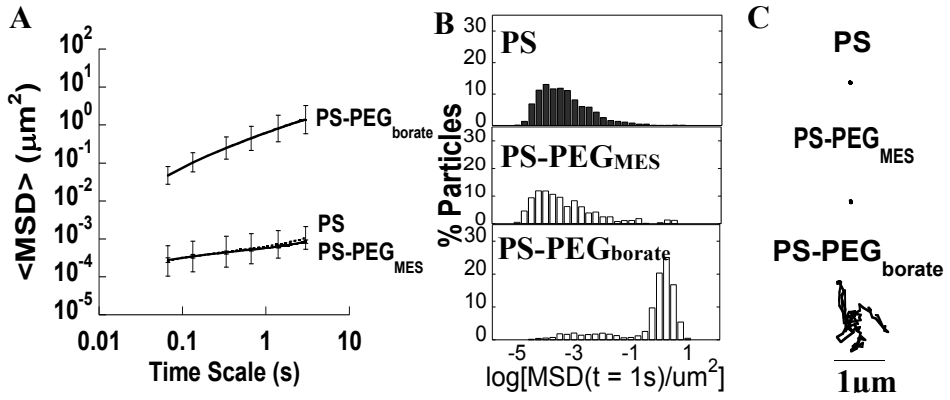

Figure I-1. Transport in hCVM of 200 nm PS and PS coated with 10 kDa PEG using borate or MES method. (A) Ensemble mean-squared displacement (<MSD>) with respect to time up to 3 s for PS and PS-PEG. (B) Distributions of the logarithms of individual particle MSD of PS and PS-PEG at a time scale of 1 s. (C) Representative trajectories for 3 s of motion of PS and PS-PEG. Data are representative of $n \geq 3$ samples.

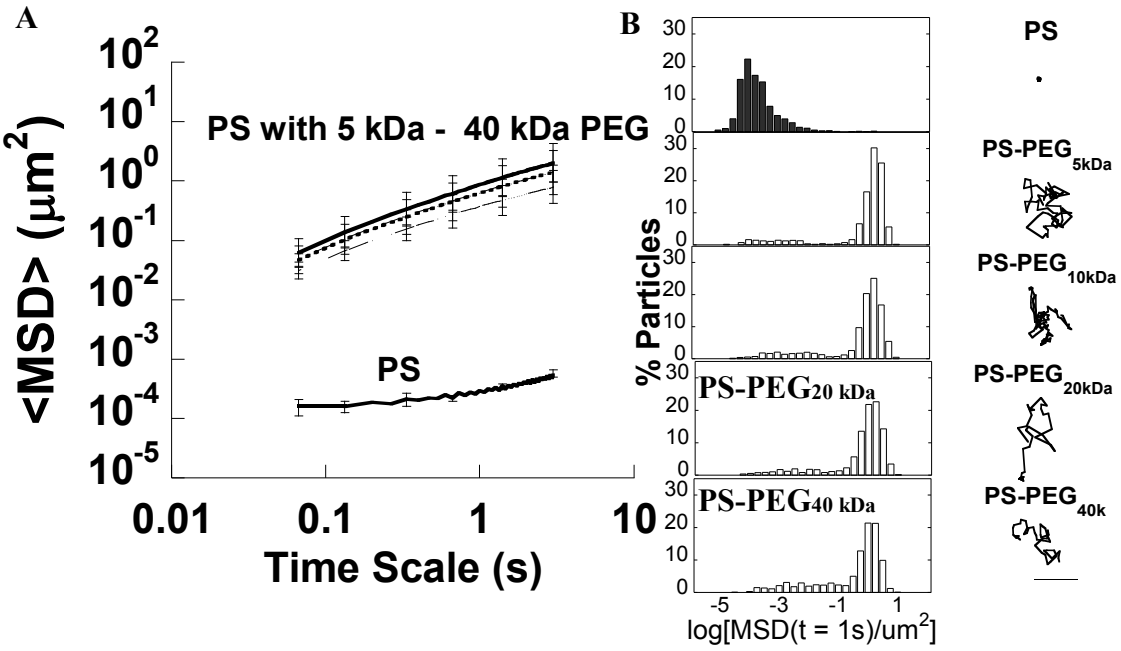

Figure I-2. Transport in hCVM of 200nm PS and PS-PEG with varying MW PEG. (A) Ensemble averaged mean-squared displacement (<MSD>) as a function of time up to 3 s for PS and PS-PEG_{borate} coated with 5 kDa, 10 kDa, 20 kDa, and 40 kDa PEG. (B) Distributions of the logarithms of individual particle MSD of PS and PS-PEG at a time scale of 1 s. (C) Representative trajectories for 3 s of motion of PS and PS-PEG. Data are representative of $n \geq 3$ samples.

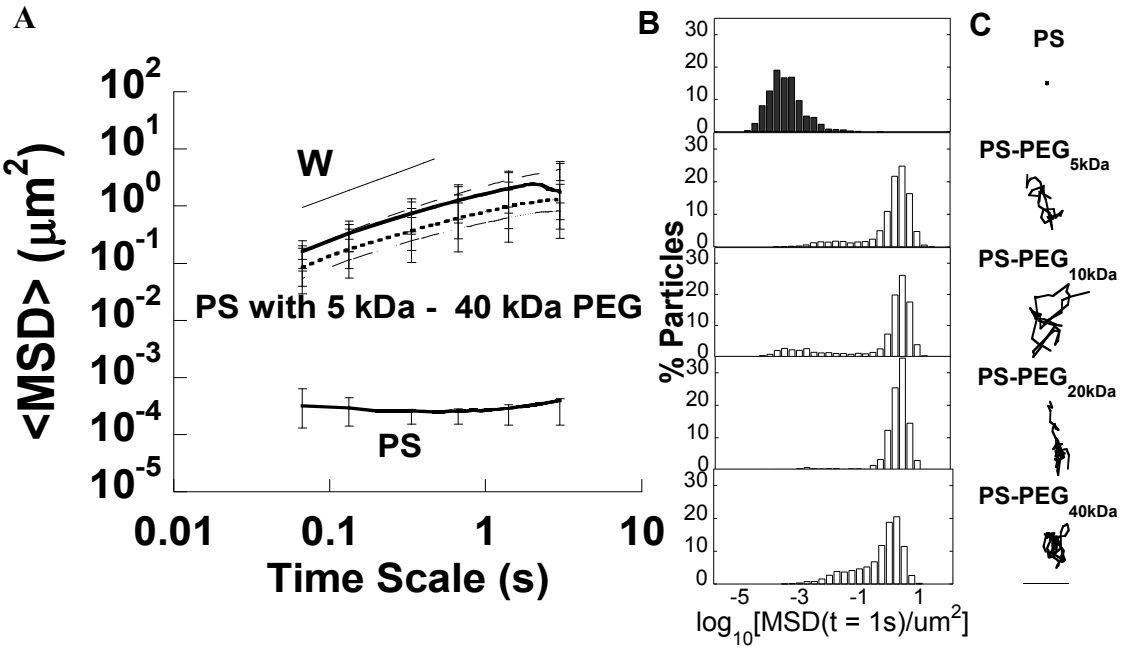

Figure I-3. Transport in hCVM of 100 nm PS and PS-PEG with varying MW PEG. (A) Ensemble averaged mean-squared displacement (<MSD>) as a function of time for PS and PS-PEG_{borate} coated with 5 kDa, 10 kDa, 20 kDa, and 40 kDa PEG, including the theoretical MSD of 120 nm particles in water (W). (B) Distributions of the logarithms of individual particle MSD of PS and PS-PEG at a time scale of 1 s. (C) Representative trajectories for 3 s of motion of PS and PS-PEG. Data are representative of $n \geq 3$ samples.

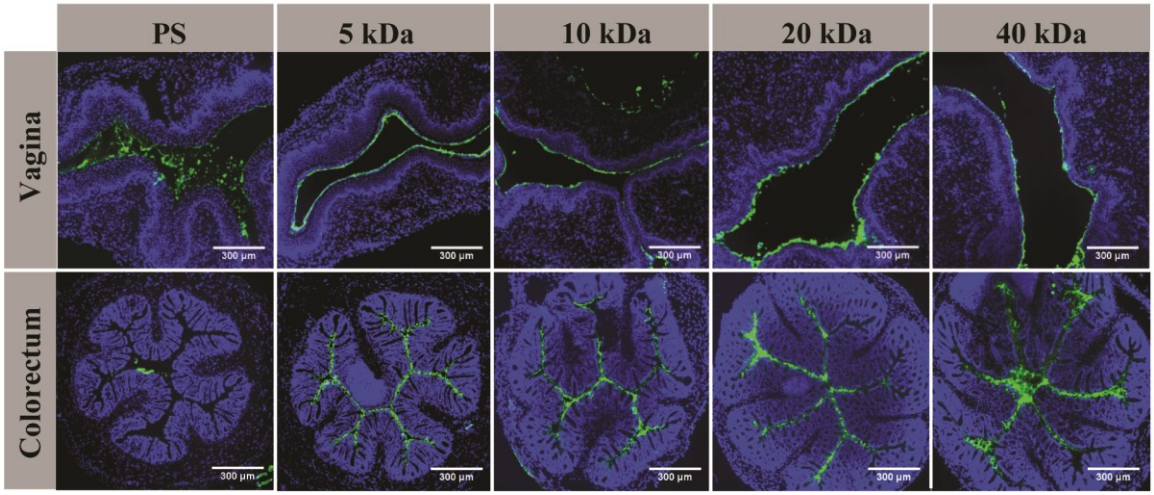

Figure I-4. Distribution of PS and PS-PEG with varying MW PEG in the mouse vagina and colorectum immediately after administration. Fluorescent images (10x magnification) of transverse vaginal and colorectal cryosections after administration of solutions containing either PS, or PS-PEG_{borate} coated with various MW PEG (5 kDa, 10 kDa, 20 kDa, 40 kDa). Cell nuclei are stained blue with DAPI and scale bars represent 300 µm. Images are representative of $n \geq 3$ mice.

II. APPENDIX II – HYDROXYL-FUNCTIONAL PAMAM DENDRIMERS EVENLY COAT MUCOSAL SURFACES AND HAVE HIGH CELLULAR UPTAKE IN THE COLORECTUM

II.1 Introduction

Nanoscale drug delivery systems may overcome many barriers faces by drugs, facilitate localized drug targeting and thus improve therapeutic efficacy [272-274]. Nanoparticles are particularly versatile in as they can provide controlled and sustained release, protect drug from enzymatic and acidic degradation in the body, allow surface conjugation of targeting moieties and improve tissue penetration and cellular transport[206, 207, 274-278]. In fact, several nanotherapeutics have been approved by the US Food and Drug Administration for treatment of a variety of diseases including cancer (*e.g.* ovarian cancer and myeloma) and infectious diseases (*e.g.* hepatitis C, fungal infections) [279]. Considerable interest lies in the development of local drug delivery to mucosal surfaces including the gastrointestinal (GI), cervicovaginal (CV), and respiratory tracts, since research has shown that local treatment of mucosal diseases improves drug concentrations in the affected tissues [280-284] while preventing undesired systemic effects [206, 207, 280, 285]. However, nanocarriers face one main obstacle from reaching their target cells at the mucosal sites: the mucus barrier.

Mucus is a highly viscoelastic substance that effectively traps many pathogens and particulate matter, and lubricates the surface in order to protect the underlying epithelial layer. Mucin fibers make up most of the gel structure and are highly entangled, forming a mesh that allows only molecules smaller than the average mesh spacing to pass through. In addition, mucins have highly glycosylated, negatively charged regions and regions of hydrophobic clusters coated with lipids, causing trapping through charge and hydrophobic

interactions [8, 9]. Mucus is rapidly cleared, on the order of hours in the CV, GI and respiratory tracts, clearing any trapped particulates or pathogens with it [8, 9]. Current strategies for local delivery of nanocarriers to the mucosal surfaces focus on increasing cell uptake via cellular targeting mechanisms [286], which often ignore the mucus barrier that must be traversed in order to reach the underlying cells. Mucoadhesion strategies have also been suggested to improve mucosal drug delivery; however, mucoadhesion can lead to incomplete coating of the epithelial surface and thus rapid clearance from mucosal surfaces, which can make treatments less effective [261, 287]. In addition, it may not lead to the cellular uptake, which is a key requirement for the treatment of many mucosal diseases [286].

We have previously shown that a dense layer of polyethylene glycol (PEG) makes nanoparticles non-mucoadhesive, allowing them to slip through the mucus if they are smaller than the mucus mesh spacing, and thus reach the underlying epithelial layer [7, 15, 287, 288]. In addition, we have shown that these nanoparticles are able to take advantage of advective fluid flow induced by hypotonic liquids that allow the nanoparticles to be dragged through mucus, and thus rapidly form an even coating on epithelial surfaces [61]. Because of the ability to evade mucosal clearance, mucus penetrating particles (MPP) have improved efficacy in treatment and prevention of diseases, including cervical cancer, herpes simplex virus infection, and cystic fibrosis [261, 287, 289]. While MPP bring drug more efficiently to the epithelium, the PEG coating can shield nanoparticles from cellular interaction and uptake.

Some classes of smaller nanocarriers, such as dendrimers, are actively taken up by cells [290-292]. Dendrimers (size ~3-12 nm, soft globular nanospheres) are emerging as

promising candidates for imaging and targeted drug/gene delivery, for diverse indications including cancer and central nervous system disorders [293-301]. The small size, branching architecture, and high density of tailorable surface functional groups may provide significant advantages for organ and cell-specific transport [302]. Polyamidoamide (PAMAM) dendrimers are widely studied due to their commercial availability. Recent studies have shown that PAMAM dendrimer size can have a significant impact on biodistribution and blood circulation time [303-305]. Many studies have been conducted on their *in vitro* cellular uptake by mucosal epithelial cells [290-292, 306]. These have indicated that dendrimers are well-suited for drug delivery to the mucosal surfaces, but only few have been translated into *in vivo* studies. Recent findings suggest that, with appropriate surface functionality, dendrimers help improve both oral and pulmonary drug delivery. Dendrimer-drug conjugates improve transport, increase drug solubility, and provide sustained release [303, 307-311]; however, none of these studies have directly correlated surface functionality to *in vivo* distribution and cellular uptake at the mucosal surfaces. Here, we investigate for the first time the interaction of PAMAM dendrimers with mucus, and the effects of surface functionality on the *in vivo* dendrimer distribution and cellular uptake at mucosal surfaces, with particular focus on the gastrointestinal tract.

II.2 Materials and Methods

II.2.1 Dendrimer conjugates

Ethylene diamine core polyamido amide (PAMAM) dendrimers (generation 4 hydroxyl, D-OH, and amine-terminated, D-NH_2, as well as generation 3.5 carboxyl terminated, D-COOH) were obtained (Dendritech, Inc.) and labeled with either fluorescein isothiocyanate (FITC, Sigma; D-OH, D-COOH, and D-NH_2) or Cy5 (Sigma; D-OH, D-COOH, and D-

NH_2) as previously described [302, 306, 312]. These conjugates have 1-2 molecules of the fluorescent agent per dendrimer, and fluorophore and dendrimer are linked via a stable amide bond that has been previously shown to resist hydrolysis [313]. The conjugates are highly soluble in water, have been shown to be stable in PBS and plasma for up to 24 h at 37C, and can be extracted intact from tissue [312, 313].

II.2.2 Animal models

Female CF-1 mice 6-8 weeks old were obtained (Harlan) and housed for 1 week for acclimatization. For colorectal distribution, mice were starved for 24 h prior to administration of dendrimer. For vaginal distribution, naturally cycling mice were selected to be in estrus phase, which we have previously shown to be most similar to the human epithelial thickness and the mucus is most similar to human CV mucus [64, 287]. For all routes of administration, mice were anesthetized using isoflurane. Experiments were approved by the Animal Care and Use Committee of the Johns Hopkins University.

Distribution of dendrimers on colorectal, vaginal and lung surfaces

For colorectal distribution, 20 μL of 1 mg/mL FITC-labeled dendrimer solution (D-OH, D-COOH, or D-NH_2) was administered intrarectally using a Wiretrol (Drummond). For vaginal distribution, 5 μL of 1 mg/mL Cy5-labeled dendrimer (D-OH, D-COOH, or D-NH_2) solution was administered. Tissues were excised immediately (with dissection times between 5-10 min), flash frozen in optimal cutting temperature compound (OCT), and cut into 6 μm thick sections. For distribution in the trachea, 50 μL 1 mg/mL Cy5-labeled dendrimer solution (D-OH, D-COOH, or D-NH_2) was administered intranasally. Lungs were excised after 30 min, flash frozen in OCT, and cut into 10 μm thick sections. All sections were cut using a Leica CM-3050-S cryostat, and subsequently washed and stained

with ProLong Gold antifade reagent with DAPI (Invitrogen). Tissues were imaged using an inverted epifluorescent microscope (Zeiss Axio Observer).

For semi-quantitative distribution, mice were given 200 μL deionized (DI) water enemas prior to administration of 50 μL 1 mg/mL of respective FITC-labeled dendrimer (D-OH, D-COOH, or D-NH_2) solutions. Mice were sacrificed after 5-10 min (dissection time), and tissues were excised, longitudinally sliced open, and flattened between two glass slides. Tissues were then imaged using an inverted epifluorescent microscope (Zeiss Axio Observer). To ensure fluorescence levels were above autofluorescence, control tissues were imaged prior to tissues containing dendrimers. For quantification, 6 images were taken per tissue. Images were threshholded, and analyzed for fluorescence coverage using ImageJ as previously described [287]. Data is reported as average ± SEM, and corresponds to $n \geq 3$ mice.

II.2.3 Methods for determining dendrimer cell uptake in the colorectum

The initial cell extraction method was adapted from Boothe et al [314]. Mice were anesthetized using avertin and 50 μL of 1 mg/mL FITC-labeled dendrimer solution (D-OH or D-NH_2) was administered intrarectally. Tissues were excised after 2 h, sliced open longitudinally, cut into 1cm pieces, and placed into a 1.5 mL tube. A solution of DMEM with 10% FBS and 4 mg/mL was added and tissues were incubated at 4°C over night. Tissues were transferred into a 1:1 mixture of 0.05% trypsin-EDTA and Versene and incubated at room temperature for 3 h. The reaction was stopped by adding DMEM/10% FBS and tissue pieces were removed. Cells remaining in the tubes were spun down and half of control tissue cells were incubated with SYTO® green fluorescent nucleic acid stain (Molecular Probes) for 15 minutes. Cells were incubated with red blood cell lysis buffer,

and then were washed with cold PBS and filtered through a 60 μm cell strainer. % fluorescent cells were obtained via flow cytometry using an Accuri C6 flow cytometer (BD).

For cell uptake studies using only the mucosa, following a method adapted from Bjerknes et al, mice were anesthetized using avertin and 30 μL of 2 mg/mL FITC-labeled dendrimer solution (D-OH, D-COOH, or D-NH_2) was administered intrarectally [315]. Tissues were excised after 30 min or 4 h, and inverted onto a glass wiretrol. Tissues were incubated in 30 mM EDTA in HBSS with 4 mg/mL dispase at 37°C under rotation for 1 h. Tissues were removed, cell sheets spun down and resuspended with DMEM/10% FBS and 4 mg/mL dispase at room temperature for 30 min. Cells were spun down and filtered through a cell strainer. Positive controls were incubated with 5 μL SYTO ® green fluorescent nucleic acid stain (Molecular Probes) and all samples were subsequently washed with cold PBS. % fluorescent cells were obtained via flow cytometry using an Accuri C6 flow cytometer (BD).

II.2.4 Semi-quantitative method for determining dendrimer retention in the colorectum

Dendrimer retention was assessed based on fluorescence retained 2 h after administration. Mice were anesthetized using averting, and 50 μL of 2 mg/mL D-OH, D-COOH, or D-NH_2 were administered to the colorectum. Mice were allowed to wake up, sacrificied after 2h, and the entire colorectum was excised and subsequently washed with PBS to remove any luminal contents. Tissues were then lyophilized, crushed, and incubated in methanol (D-OH and D-COOH) or phosphate buffered saline (PBS, D-NH_2) to extract the remaining dendrimers. Solutions were sonicated, spun down, and finally analyzed for fluorescence content using a Shimadzu RF-5301 spectrofluorometer. This method has been validated

and optimized to ensure that no significant amounts of dendrimer were used in the processing of the tissue (ref).

Statistical Analysis

Statistical significance was analyzed using student's t-test assuming unequal variance. Values compared resulting in p-values ≤ 0.05 were considered significantly different.

II.3 Results

II.3.1 Dendrimer distribution on mouse colorectal tissue

We have previously demonstrated the importance of sufficient PEG coverage of mucosal surfaces for efficient drug and gene delivery [261, 287, 289], and that hypotonic delivery can significantly enhance the distribution of non-mucoadhesive, but not of mucoadhesive, nanocarriers [61]. Here, we first investigated whether PAMAM dendrimers are mucus-penetrating in colorectal tissue, and what effect dendrimer surface functionality had on their distribution on the epithelial surface. When administered intrarectally, D-OH evenly coated the colorectal epithelial surface. We previously determined that non-mucoadhesive, or mucus-penetrating nanoparticles (MPP) evenly coat the colorectal epithelial surface and showed here that MPP distribute similarly to D-OH, indicating that D-OH also penetrate mouse colorectal mucus (Fig II-1) [7, 261, 287, 288]. In contrast to D-OH, D-NH_2 poorly distributed (<50% coverage) on colorectal tissue (Fig II-1), similar to mucoadhesive nanoparticles (MAP), indicating that D-NH_2 may stick to mouse colorectal mucus [7, 261, 287, 288]. D-COOH had intermediate distribution (50%-70% coverage) on the epithelial surface (Fig II-1). Based on these results, we determined that PAMAM dendrimer distribution increases in the following order: D-NH_2<D-COOH<D-OH (Fig II-2A). Our studies also suggest that D-NH_2 and D-COOH interact with mucus, as already indicated by their less

even distribution in Fig II-1; both D-NH_2 and D-COOH aggregated in mucin bundles, similar to MAP (Fig II-2A, red arrows) [288]. In contrast, D-OH penetrated through the mucus, reached the epithelial layer, and outlined the colonic crypts (honeycomb pattern) [316, 317]. Semi-quantitative assessment, using dendrimer fluorescence suggested that, D-NH_2, D-COOH, and D-OH respectively coat <45%, 67 ± 5%, and >80% of the epithelial surface respectively (Fig II-2B).

II.3.2 Cell uptake of dendrimers in colorectal epithelial tissue

Researchers have shown that dendrimers are actively taken up by epithelial cells via clathrin and non-clathrin mediated internalization, depending on their surface functionality [290-292, 306]. We investigated whether surface functionality affects cellular uptake when dendrimers are exposed to epithelial surfaces *in vivo*. First, we used a method for tissue extraction that includes digesting the entire colorectal tissue, we found that D-OH had significantly improved cell uptake after 2 h, compared to D-NH_2 (Fig II-3A). Due to the large errors of the complete tissue dissolution method (Fig II-3A), and the potential for dendrimer exocytosis from cells due to the lengthy incubation times (>24 h), we sought to test another method. We investigated a second method that only extracts the mucosal epithelium from the colorectal tissue, a method provides mostly epithelial cells for analysis [315]. Our data suggested that the PAMAM dendrimer surface functionality influences cell uptake, 30 minutes after topical administration to the colorectum. D-OH had significantly higher uptake than D-NH_2, with >40% of cells showing presence of fluorescence from D-OH, while <20% of cells showed presence of fluorescence after D-NH_2 administration (Fig II-3B). D-COOH had intermediate cell uptake, ranging between D-NH_2 and D-OH with ~30% of cells showing fluorescence (Fig II-3A). The uptake correlates well with the

distribution seen in Figure II-1, such that the amount of cells containing PAMAM dendrimer increased in the same order as the distribution: D-NH_2<D-COOH<D-OH. Since the outer most layer of the colonic epithelium turns over rapidly [219, 220], we also investigated if D-OH remained in cells after several hours. When tissues were excised 4 h post administration, D-OH showed even higher uptake with >50% of cells showing fluorescence (Fig II-3B), indicating that D-OH may be able to penetrate past the outermost layer of colonic mucosal epithelial cells.

II.3.3 Dendrimer retention in the colorectum

In order to reach optimal therapeutic drugs levels, it is important to know the amount of drug carrier, and thus drug, present in the target tissue. Given that surface functionality of PAMAM dendrimers significantly affects their distribution as well as cellular uptake, we sought to determine the effects of dendrimer surface functionality on their retention in colorectal tissue. Interestingly, both D-OH and D-NH_2 were retained at significantly higher levels than D-COOH (Fig II-4), despite our finding that D-NH_2 reached less of the cells (Fig II-3). The amounts remaining in the tissue were 1.4 ± 0.9 μg/g, 1.7±0.6 μg/g, and 7 ± 0.1 μg/g for D-OH, D-NH_2, and D-COOH respectively (Fig II-4). The differences between D-NH_2 and D-OH were not significantly different due to variability between animals.

II.3.4 Dendrimer distribution on various mucosal surfaces

Having found that not all functional groups on dendrimers lead to even coating of the colorectal epithelial surface, we further investigated whether the distribution pattern of D-NH_2<D-COOH<D-OH translates to other mucosal surfaces such as the cervicovaginal tract and the lungs. In both the CV and respiratory tracts, D-OH completely coated the epithelial surface; D-OH evenly coated the trachea after intranasal administration and evenly coated

the vaginal epithelium after intravaginal instillation (Fig II-5). This result is similar to our results in the colorectum (Fig II-1). In case of the CV and respiratory tracts, D-OH distribution was also similar to that of MPP on these surfaces (Fig II-5) [261, 287, 289], indicating that D-OH can penetrate respiratory and CV mucus as well. In addition, in the CV tract, D-OH penetrated past the initial cell layers and got deeper into the CV epithelium (Fig II-5, red arrows).

In contrast to the evenly distributed D-OH, D-NH_2 coated both the tracheal and the vaginal epithelium unevenly, and thus reached a smaller fraction of the epithelial surface (Fig II-5). Based on prior data, D-NH_2 distribution is similar to mucoadhesive particle distribution in the CV and respiratory tract [7, 261, 287], suggesting that D-NH_2 sticks to respiratory and CV mucus. Similar to our results in the colorectum, D-COOH distribution in the respiratory tract was intermediate between D-OH and D-NH_2. Interestingly, D-COOH distributed more evenly in the CV tract (Fig II-5), and coated a significant fraction of the epithelial surface (yellow arrows), but not as much as D-OH.

II. 4 Discussion

Our results indicate the interaction of water soluble PAMAM dendrimers with mucus is highly affected by their surface chemistry. In the colorectum, D-NH_2 distribution is poor, while D-COOH distribution is intermediate, and D-OH distribution is the best, suggesting a hierarchy of distribution that follows D-NH_2<D-COOH<D-OH. This relative distribution also correlates with the % cellular uptake of each of these dendrimers in the colorectum. Interestingly, the semi-quantitative assessment of cell uptake differed in that more D-NH_2 and D-OH were retained, compared to D-COOH. The high D-OH retention is likely due to the uniform distribution of D-OH that allowed for more cells to uptake and retain the

dendrimer. On the other hand, the rapid and efficient uptake of D-NH_2 into the cells they were able to reach likely caused the high D-NH_2 retention. D-COOH had similar uptake efficiency to D-OH but poorer distribution on the epithelial surface [290-292, 304, 307, 318, 319]. Our results indicate that D-OH may serve as superior nanocarriers for intracellular delivery to the mucosal epithelium, while D-NH_2 and D-COOH are better suited for extracellular delivery.

We have previously shown that surface distribution of nanocarriers can be indicative of their ability to penetrate through mucus [7, 287, 288]. Nanocarriers that distribute poorly on mouse colorectal, vaginal, and tracheal tissues, such as hydrophobic polystyrene beads, were highly mucoadhesive, whereas non-mucoadhesive nanocarriers evenly coat the epithelial surface [261, 287, 289]. The poor distribution of D-NH_2 is indicative of its mucoadhesive properties. It is likely that the cationic surface causes D-NH_2 to interact with the highly negatively-charged glycosylated regions on mucin strands (red arrows, Fig II-2A), trapping D-NH_2 that comes in contact with them. Prior work has indicated the negatively charged nanocarriers should penetrate mucus [156]; however, our results suggest that D-COOH associated with mucins (red arrows, Fig II-2A), indicating that there is some interaction between mucus and D-COOH. This is somewhat in contrast to previous studies that have indicated that D-OH and D-NH_2 interact similarly with ocular mucin, while D-COOH interact significantly less [320]. It is well-established that mucin composition differs at the various mucosal surfaces, likely altering the interaction with nanocarriers [8]. In addition, experiments in those studies were performed with isolated mucin, where other components of mucus (such as lipids, proteins, or dead cell matter) that may alter the interactions between mucin and dendrimer were absent. In this study, we used intact mucus

that is more representative of physiological conditions, indicating that *in vivo* D-OH are least affected by the mucus barrier. D-OH is thus a potential candidate for intracellular delivery to the mucosal epithelium.

Epithelial uptake and paracellular transport of PAMAM dendrimers has been extensively studied *in vitro* and *ex vivo*. El Sayed *et al* studied the effects of dendrimer surface charge on cell layer permeability by assessing mannitol permeability. They found that D-OH cause nearly no increase in permeability [318, 319], while D-COOH and D-NH_2 significantly increased paracellular permeability. Hubbard *et al* showed that D-NH_2 had greater tissue uptake and was poorly transported via the paracellular route, while D-COOH had increased paracellular transport but less tissue uptake [307]. These previous studies help explain the difference in retention between D-COOH and D-NH_2, as D-COOH would be translocated through the cells they reach while D-NH_2 gets taken up. There are some significant limitations to using cell culture and *ex vivo* models, with respect to studying mucous transport. Most cell culture methods do not include the presence of mucus-producing cells, leaving the epithelial cells completely unprotected and exposed to the dendrimers. In addition, many *ex vivo* models require the mucosal surface to be submerged in a significant amount of liquid, leading to dilution, excessive hydration, or removal of the mucus layer on the epithelial surfaces. Without a mucus layer, dendrimers can directly reach the epithelial layer and are more easily taken up by cells. Based on our current study, D-NH_2 is trapped by the highly negatively charged mucin fibers in vivo within 5-10 minutes. This is in contrast with previous studies that have indicated that uptake follows the order: D-COOH>D-NH_2>D-OH [290, 291]. Our results confirm that for the large intestine,

in vivo cellular uptake follows the order D-OH>D-COOH>D-NH_2, indicating that D-OH may be most suited for local drug delivery.

Dendrimers have been studied for therapeutic and preventive applications in various mucosal surfaces. In fact, a class of polylysine dendrimer, Vivagel ®, is currently in clinical trials for the prevention of genital herpes virus infection [321]. PAMAM dendrimers have also been shown to be effective for treatment of vaginal bacterial infections. Wang et al found that PAMAM dendrimers have significant antibacterial properties against *E. Coli*, leading to inhibition of bacterial infection of amniotic fluid when dendrimer was applied vaginally [322]. In their studies, both neutrally charged D-OH and positively charged D-NH_2 caused significant bacterial death, but cytotoxicity was associated with 100-fold lower concentrations of D-NH_2 compared to D-OH, indicating the potential for use of D-OH in vaginal applications. Our studies further confirm that D-OH may be more suitable for vaginal applications, as improved nanocarrier distribution has been shown to lead to better retention and efficacy in a mouse model of HSV [287].

PAMAM dendrimers have also been used as drug carriers and absorption enhancers across the pulmonary epithelium [298, 323]. Landers et al found that sialic acid conjugated to dendrimers successfully inhibits infection by influenza virus when delivered intranasally to mice [323]. Inapagolla et al showed that FITC-labeled D-OH was retained in the lungs to a significant extent for up to six days[298]. In addition, these studies found that lower doses of methylprednisone (MP) are necessary for the same decrease in pulmonary inflammation when MP is conjugated to D-OH dendrimers compared to free drug [298]. Suk *et al* have shown that non-mucoadhesive gene carriers that evenly coat the respiratory epithelium have longer retention than mucoadhesive gene carriers, and improved gene expression

compared to free DNA [7]. It is therefore not surprising that D-OH, which distribute similarly to non-mucoadhesive nanocarriers, are retained longer than free drug.

Previous work has already indicated the benefits of dendrimers as drug carriers to the mucosal surfaces. Our results further elucidate the role of surface functionality and its effects on dendrimer-mediated drug delivery to mucosal surfaces. Based on our studies, D-OH have the best distribution and % cellular uptake at various mucosal surface, and since D-OH have little cytotoxicity [302, 324], they have great potential for the treatment and prevention of diseases at mucosal sites in the CV tract, GI tract, and lungs.

II.5 Conclusion

We investigated the biodistribution of cationic (NH_2), anionic (COOH), and neutral (OH), surface functional, generation-4 PAMAM dendrimers for potential drug delivery to various mucosal epithelial surfaces. Our results suggest that D-OH has significantly better distribution (>80% surface coating, and cellular uptake, >50% of extracted cells, on the colorectal epithelium) compared to D-NH_2 (<45% of the surface, and <20% cell uptake). D-COOH has an intermediate distribution (~67 surface coverage, and 31% cell uptake). D-NH_2 and D-OH are retained in higher amounts than D-COOH in the colorectum after 2 h, likely due to rapid cell uptake of D-NH_2 and a larger number of cells reached by D-OH. We also determined that D-OH evenly coats the epithelial surface of the lungs and CV tract, while D-COOH and D-NH_2 do not. Our results indicate the suitability of D-OH dendrimers compared to D-COOH and D-NH_2 as drug delivery vehicle to mucosal surfaces for both treatment and prevention of local diseases.

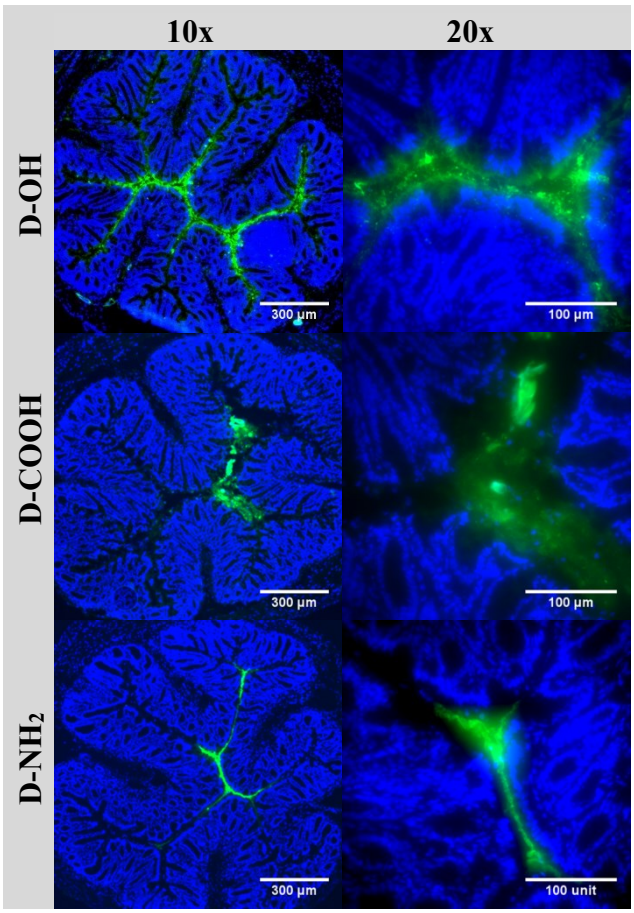

Figure II-1. Colonic distribution of PAMAM dendrimers after intrarectal administration to mice. Distribution in transverse colonic cryosections after hypotonic intrarectal administration of D-OH, D-COOH, and D-NH_2 with 10x and 20x magnification. Cell nuclei are stained with DAPI. Images are representative of $n \geq 3$ mice.

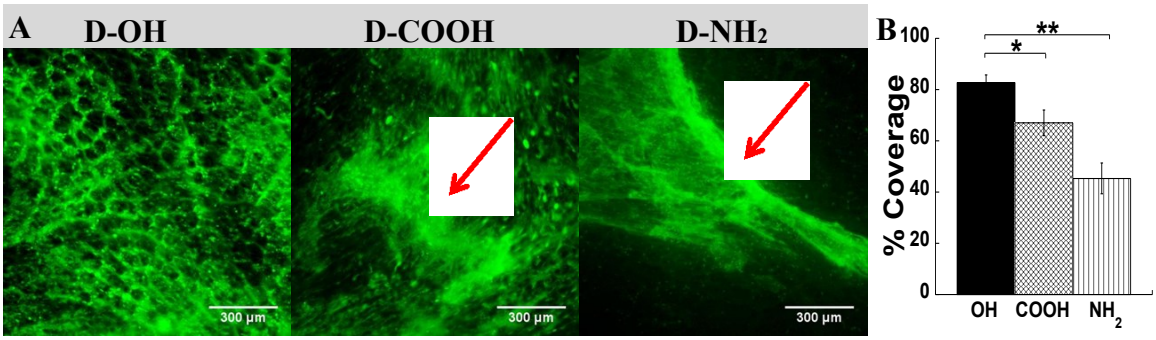

Figure II-2. Semi-quantified colonic distribution of PAMAM dendrimers after intrarectal administration to mice. (A) Distribution on flattened colonic tissue after intrarectal administration of D-OH, D-COOH, and D-NH_2. Red arrows indicate dendrimers aggregated in mucus. (B) Semi-quantified surface coverage of D-OH, D-COOH, and D-NH_2 on flattened mouse colonic tissue. Images are representative of $n \geq 3$ mice and 6 images per tissue. White scale bar indicates 300 µm. Data are calculated as means ± SEM. *$P < 0.05$ compared to D-COOH and **$P < 0.01$ compared to D-NH_2, Student's t-test.

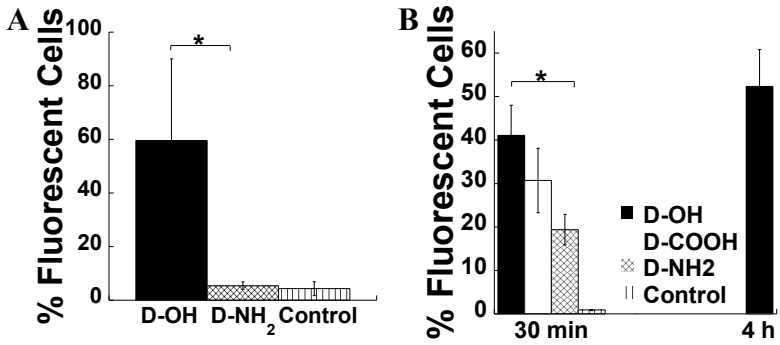

Figure II-3. Quantified cell uptake of PAMAM dendrimers after intrarectal administration to mice. (A) Uptake of D-OH, D-COOH, and D-NH_2 2 h after intrarectal administration to mice and extraction by tissue dissolution. (B) Uptake of PAMAM-OH, D-COOH, and D-NH_2 30 min and 4 h after intrarectal administration to mice and extraction by removing only the mucosa. Data are calculated as means ± SEM. *$P < 0.05$ compared to D-NH_2, Student's t-test.

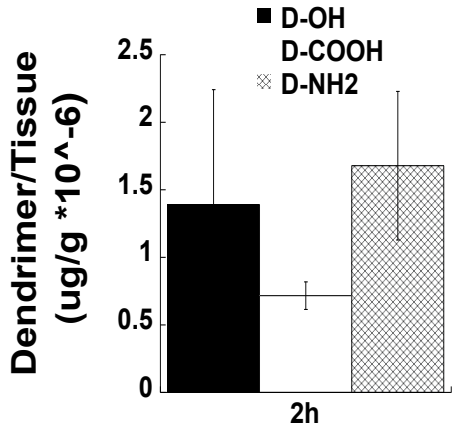

Figure II-4. Retention PAMAM dendrimers after intrarectal administration to mice. Data are representative of n≥3 mice and are calculated as average ± SEM. **P* < 0.05 compared to NH_2, Student's t-test.

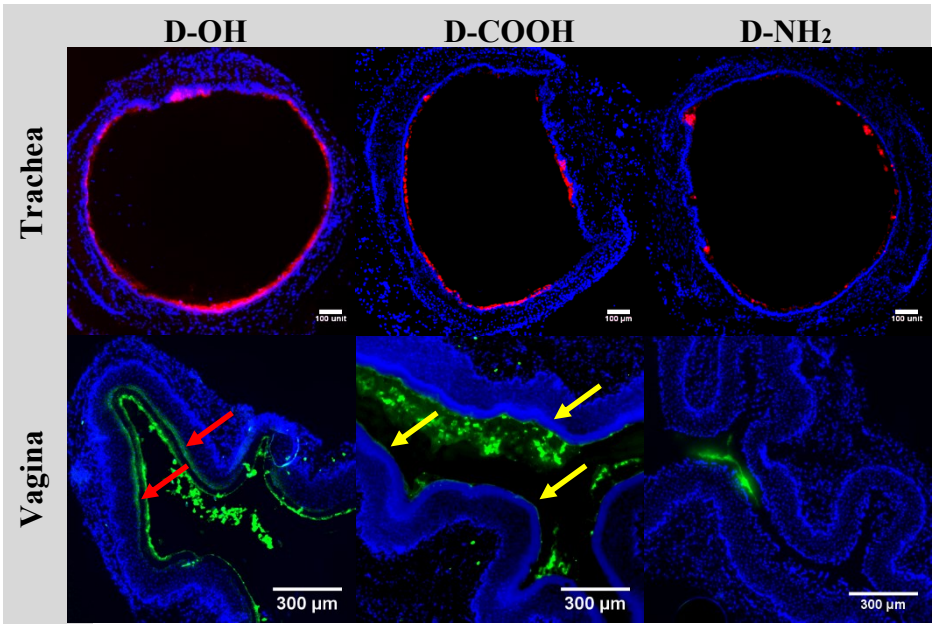

Figure II-5. Distribution of PAMAM dendrimers after vaginal and intranasal administration to mice. Distribution in transverse cryosections of the vagina and trachea of mice after hypotonic intravaginal or intranasal administration of D-OH, D-COOH, and D-NH_2. White scale bars represent 300 µm for vaginal sections and 100 µm for trachea sections. Cell nuclei are stained with DAPI. Images are representative of $n \geq 3$ mice.

REFERENCES

1. Cai, Z.; Wang, Y.; Zhu, L. J.; Liu, Z. Q. Nanocarriers: A General Strategy for Enhancement of Oral Bioavailability of Poorly Absorbed or Pre-Systemically Metabolized Drugs. *Curr Drug Metab* **2010**, 11, 197-207.

2. Roger, E.; Lagarce, F.; Garcion, E.; Benoit, J. P. Biopharmaceutical Parameters to Consider in Order to Alter the Fate of Nanocarriers after Oral Delivery. *Nanomedicine (Lond)* **2010**, 5, 287-306.

3. Gomez-Orellana, I. Strategies to Improve Oral Drug Bioavailability. *Expert Opin Drug Deliv* **2005**, 2, 419-33.

4. Ensign, L. M.; Cone, R.; Hanes, J. Oral Drug Delivery with Polymeric Nanoparticles: The Gastrointestinal Mucus Barriers. *Adv Drug Deliver Rev* **2012**, 64, 557-70.

5. Ensign, L. M.; Tang, B. C.; Wang, Y. Y.; Tse, T. A.; Hoen, T.; Cone, R.; Hanes, J. Mucus-Penetrating Nanoparticles for Vaginal Drug Delivery Protect against Herpes Simplex Virus. *Science translational medicine* **2012**, 4, 138ra79.

6. Schneider, C. Mucus-Penetrating Nanoparticles for Small Cell Lung Cancer Therapy. The Johns Hopkins University, Baltimore, MD, 2013.

7. Suk, J. S.; Kim, A. J.; Trehan, K.; Schneider, C. S.; Cebotaru, L.; Woodward, O. M.; Boylan, N. J.; Boyle, M. P.; Lai, S. K.; Guggino, W. B.; Hanes, J. Lung Gene Therapy with Highly Compacted DNA Nanoparticles That Overcome the Mucus Barrier. *J Control Release* **2014**, 178, 8-17.

8. Cone, R. A. Mucus. *Mucosal Immunology, 3rd Edition* **2005**, 49-72.

9. Cone, R. A. Barrier Properties of Mucus. *Adv Drug Deliv Rev* **2009**, 61, 75-85.

10. Krantz, K. E. The Gross and Microscopic Anatomy of the Human Vagina. *Ann N Y Acad Sci* **1959**, 83, 89-104.

11. Sigurdsson, H. H.; Kirch, J.; Lehr, C. M. Mucus as a Barrier to Lipophilic Drugs. *International Journal of Pharmaceutics* **2013**, 453, 56-64.

12. Macadam, A. The Effect of Gastrointestinal Mucus on Drug Absorption. *Adv Drug Deliv Rev* **1993**, 11, 201-220.

13. Matthes, I.; Nimmerfall, F.; Sucker, H. [Mucus Models for Investigation of Intestinal Absorption Mechanisms. 2. Mechanisms of Drug Interactions with Intestinal Mucus]. *Pharmazie* **1992**, 47, 609-13.

14. Matthes, I.; Nimmerfall, F.; Sucker, H. [Mucus Models for Investigation of Intestinal Absorption Mechanisms. 1. Validation and Optimization of the Model]. *Pharmazie* **1992**, 47, 505-15.

15. Lai, S. K.; O'Hanlon, D. E.; Harrold, S.; Man, S. T.; Wang, Y. Y.; Cone, R.; Hanes, J. Rapid Transport of Large Polymeric Nanoparticles in Fresh Undiluted Human Mucus. *Proc Natl Acad Sci U S A* **2007**, 104, 1482-7.

16. Khanvilkar, K.; Donovan, M. D.; Flanagan, D. R. Drug Transfer through Mucus. *Adv Drug Deliv Rev* **2001**, 48, 173-93.

17. Larhed, A. W.; Artursson, P.; Grasjo, J.; Bjork, E. Diffusion of Drugs in Native and Purified Gastrointestinal Mucus. *J Pharm Sci* **1997**, 86, 660-5.

18. Tlaskalova-Hogenova, H.; Stepankova, R.; Hudcovic, T.; Tuckova, L.; Cukrowska, B.; Lodinova-Zadnikova, R.; Kozakova, H.; Rossmann, P.; Bartova, J.; Sokol, D.; Funda, D. P.; Borovska, D.; Rehakova, Z.; Sinkora, J.; Hofman, J.; Drastich,

P.; Kokesova, A. Commensal Bacteria (Normal Microflora), Mucosal Immunity and Chronic Inflammatory and Autoimmune Diseases. *Immunology letters* **2004**, 93, 97-108.

19. Olmsted, S. S.; Padgett, J. L.; Yudin, A. I.; Whaley, K. J.; Moench, T. R.; Cone, R. A. Diffusion of Macromolecules and Virus-Like Particles in Human Cervical Mucus. *Biophysical journal* **2001**, 81, 1930-7.

20. Zeitlin, L.; Cone, R. A.; Whaley, K. J. Using Monoclonal Antibodies to Prevent Mucosal Transmission of Epidemic Infectious Diseases. *Emerging infectious diseases* **1999**, 5, 54-64.

21. Saltzman, W. M.; Radomsky, M. L.; Whaley, K. J.; Cone, R. A. Antibody Diffusion in Human Cervical Mucus. *Biophysical journal* **1994**, 66, 508-15.

22. Castle, P. E.; Whaley, K. J.; Hoen, T. E.; Moench, T. R.; Cone, R. A. Contraceptive Effect of Sperm-Agglutinating Monoclonal Antibodies in Rabbits. *Biology of reproduction* **1997**, 56, 153-9.

23. Zeitlin, L.; Cone, R. A.; Moench, T. R.; Whaley, K. J. Preventing Infectious Disease with Passive Immunization. *Microbes and infection / Institut Pasteur* **2000**, 2, 701-8.

24. Schade, C.; Flemstrom, G.; Holm, L. Hydrogen Ion Concentration in the Mucus Layer on Top of Acid-Stimulated and -Inhibited Rat Gastric Mucosa. *Gastroenterology* **1994**, 107, 180-8.

25. Bhaskar, K. R.; Garik, P.; Turner, B. S.; Bradley, J. D.; Bansil, R.; Stanley, H. E.; LaMont, J. T. Viscous Fingering of Hcl through Gastric Mucin. *Nature* **1992**, 360, 458-61.

26. Johansson, M.; Synnerstad, I.; Holm, L. Acid Transport through Channels in the Mucous Layer of Rat Stomach. *Gastroenterology* **2000**, 119, 1297-304.

27. Ho, S. B.; Takamura, K.; Anway, R.; Shekels, L. L.; Toribara, N. W.; Ota, H. The Adherent Gastric Mucous Layer Is Composed of Alternating Layers of Muc5ac and Muc6 Mucin Proteins. *Digestive diseases and sciences* **2004**, 49, 1598-606.

28. Lichtenberger, L. M. The Hydrophobic Barrier Properties of Gastrointestinal Mucus. *Annual review of physiology* **1995**, 57, 565-83.

29. Phillipson, M.; Johansson, M. E.; Henriksnas, J.; Petersson, J.; Gendler, S. J.; Sandler, S.; Persson, A. E.; Hansson, G. C.; Holm, L. The Gastric Mucus Layers: Constituents and Regulation of Accumulation. *Am J Physiol Gastrointest Liver Physiol* **2008**, 295, G806-12.

30. Wang, Y. Y.; Lai, S. K.; Ensign, L. M.; Zhong, W.; Cone, R.; Hanes, J. The Microstructure and Bulk Rheology of Human Cervicovaginal Mucus Are Remarkably Resistant to Changes in Ph. *Biomacromolecules* **2013**, 14, 4429-35.

31. Johansson, M. E.; Sjovall, H.; Hansson, G. C. The Gastrointestinal Mucus System in Health and Disease. *Nature reviews. Gastroenterology & hepatology* **2013**, 10, 352-61.

32. Rosenstiel, P.; Sina, C.; End, C.; Renner, M.; Lyer, S.; Till, A.; Hellmig, S.; Nikolaus, S.; Folsch, U. R.; Helmke, B.; Autschbach, F.; Schirmacher, P.; Kioschis, P.; Hafner, M.; Poustka, A.; Mollenhauer, J.; Schreiber, S. Regulation of Dmbt1 Via Nod2 and Tlr4 in Intestinal Epithelial Cells Modulates Bacterial Recognition and Invasion. *Journal of immunology* **2007**, 178, 8203-11.

33. Johansson, M. E.; Hansson, G. C. Microbiology. Keeping Bacteria at a Distance. *Science* **2011**, 334, 182-3.

34. Ouellette, A. J. Paneth Cells and Innate Mucosal Immunity. *Curr Opin Gastroenterol* **2010**, 26, 547-53.

35. Ambort, D.; Johansson, M. E.; Gustafsson, J. K.; Nilsson, H. E.; Ermund, A.; Johansson, B. R.; Koeck, P. J.; Hebert, H.; Hansson, G. C. Calcium and Ph-Dependent Packing and Release of the Gel-Forming Muc2 Mucin. *Proc Natl Acad Sci U S A* **2012**, 109, 5645-50.

36. Round, A. N.; Rigby, N. M.; Garcia de la Torre, A.; Macierzanka, A.; Mills, E. N.; Mackie, A. R. Lamellar Structures of Muc2-Rich Mucin: A Potential Role in Governing the Barrier and Lubricating Functions of Intestinal Mucus. *Biomacromolecules* **2012**, 13, 3253-61.

37. Johansson, M. E.; Phillipson, M.; Petersson, J.; Velcich, A.; Holm, L.; Hansson, G. C. The Inner of the Two Muc2 Mucin-Dependent Mucus Layers in Colon Is Devoid of Bacteria. *Proc Natl Acad Sci U S A* **2008**, 105, 15064-9.

38. Wong, J. M.; de Souza, R.; Kendall, C. W.; Emam, A.; Jenkins, D. J. Colonic Health: Fermentation and Short Chain Fatty Acids. *J Clin Gastroenterol* **2006**, 40, 235-43.

39. Ganong, W. *Review of Medical Physiology*. 5th ed.; Lange Medical Publications: Los Altos, California, 1971.

40. *Units of Measurement, Body Fluid, Composition of Body, and Nutrition*. 8 ed.; Ciba-Geigy: 1981; Vol. 1.

41. Barrett, K. E. Chapter 15. Carbohydrate, Protein, and Water-Soluble Vitamin Assimilation. In *Gastrointestinal Physiology, 2e*, The McGraw-Hill Companies: New York, NY, 2014.

42. Leung, P. S. The Gastrointestinal System Gastrointestinal, Nutritional and Hepatobiliary Physiology.

43. Hindle, W.; Code, C. F. Some Differences between Duodenal and Ileal Sorption. *Am J Physiol* **1962**, 203, 215-20.

44. Soergel, K. H.; Whalen, G. E.; Harris, J. A. Passive Movement of Water and Sodium across the Human Small Intestinal Mucosa. *J Appl Physiol* **1968**, 24, 40-8.

45. Powell, D. W.; Malawer, S. J. Relationship between Water and Solute Transport from Isosmotic Solutions by Rat Intestine in Vivo. *Am J Physiol* **1968**, 215, 49-55.

46. Worman, H. J.; Field, M. Osmotic Water Permeability of Small Intestinal Brush-Border Membranes. *J Membr Biol* **1985**, 87, 233-9.

47. van Heeswijk, M. P.; van Os, C. H. Osmotic Water Permeabilities of Brush Border and Basolateral Membrane Vesicles from Rat Renal Cortex and Small Intestine. *J Membr Biol* **1986**, 92, 183-93.

48. Laforenza, U. Water Channel Proteins in the Gastrointestinal Tract. *Mol Aspects Med* **2012**, 33, 642-50.

49. Masyuk, A. I.; Marinelli, R. A.; LaRusso, N. F. Water Transport by Epithelia of the Digestive Tract. *Gastroenterology* **2002**, 122, 545-62.

50. Rosenthal, R.; Milatz, S.; Krug, S. M.; Oelrich, B.; Schulzke, J. D.; Amasheh, S.; Gunzel, D.; Fromm, M. Claudin-2, a Component of the Tight Junction, Forms a Paracellular Water Channel. *J Cell Sci* **2010**, 123, 1913-21.

51. Fischbarg, J. Fluid Transport across Leaky Epithelia: Central Role of the Tight Junction and Supporting Role of Aquaporins. *Physiol Rev* **2010**, 90, 1271-90.

52. Tang, Y.; Clayburgh, D. R.; Mittal, N.; Goretsky, T.; Dirisina, R.; Zhang, Z.; Kron, M.; Ivancic, D.; Katzman, R. B.; Grimm, G.; Lee, G.; Fryer, J.; Nusrat, A.; Turner, J. R.; Barrett, T. A. Epithelial Nf-Kappab Enhances Transmucosal Fluid Movement by Altering Tight Junction Protein Composition after T Cell Activation. *Am J Pathol* **2010**, 176, 158-67.

53. Schultz, S. G. Epithelial Water Absorption: Osmosis or Cotransport? *Proc Natl Acad Sci U S A* **2001**, 98, 3628-30.

54. Zeuthen, T. Water-Transporting Proteins. *J Membr Biol* **2010**, 234, 57-73.

55. Ma, T.; Verkman, A. S. Aquaporin Water Channels in Gastrointestinal Physiology. *J Physiol* **1999**, 517 (Pt 2), 317-26.

56. Zeuthen, T.; Zeuthen, E.; Macaulay, N. Water Transport by Glut2 Expressed in Xenopus Laevis Oocytes. *J Physiol* **2007**, 579, 345-61.

57. Hamann, S.; Herrera-Perez, J. J.; Bundgaard, M.; Alvarez-Leefmans, F. J.; Zeuthen, T. Water Permeability of Na+-K+-2cl- Cotransporters in Mammalian Epithelial Cells. *J Physiol* **2005**, 568, 123-35.

58. Mansbach, C. M., 2nd; Cohen, R. S.; Leff, P. B. Isolation and Properties of the Mixed Lipid Micelles Present in Intestinal Content During Fat Digestion in Man. *J Clin Invest* **1975**, 56, 781-91.

59. Komiya, I.; Park, J. Y.; Kamani, A.; Ho, N. F. H.; Higuchi, W. I. Quantitative Mechanistic Studies in Simultaneous Fluid-Flow and Intestinal-Absorption Using Steroids as Model Solutes. *International Journal of Pharmaceutics* **1980**, 4, 249-262.

60. Macierzanka, A.; Rigby, N. M.; Corfield, A. P.; Wellner, N.; Bottger, F.; Mills, E. N. C.; Mackie, A. R. Adsorption of Bile Salts to Particles Allows Penetration of Intestinal Mucus. *Soft Matter* **2011**, 7, 8077-8084.

61. Ensign, L. M.; Hoen, T. E.; Maisel, K.; Cone, R. A.; Hanes, J. S. Enhanced Vaginal Drug Delivery through the Use of Hypotonic Formulations That Induce Fluid Uptake. *Biomaterials* **2013**, 34, 6922-9.

62. Kompella, U. B.; Lee, V. H. Delivery Systems for Penetration Enhancement of Peptide and Protein Drugs: Design Considerations. *Adv Drug Deliv Rev* **2001**, 46, 211-45.

63. Prego, C.; Torres, D.; Alonso, M. J. The Potential of Chitosan for the Oral Administration of Peptides. *Expert Opin Drug Deliv* **2005**, 2, 843-54.

64. Ensign, L. M.; Henning, A.; Schneider, C. S.; Maisel, K.; Wang, Y. Y.; Porosoff, M. D.; Cone, R.; Hanes, J. Ex Vivo Characterization of Particle Transport in Mucus Secretions Coating Freshly Excised Mucosal Tissues. *Molecular pharmaceutics* **2013**, 10, 2176-82.

65. Lai, S. K.; Suk, J. S.; Pace, A.; Wang, Y. Y.; Yang, M.; Mert, O.; Chen, J.; Kim, J.; Hanes, J. Drug Carrier Nanoparticles That Penetrate Human Chronic Rhinosinusitis Mucus. *Biomaterials* **2011**, 32, 6285-90.

66. Boylan, N. J.; Suk, J. S.; Lai, S. K.; Jelinek, R.; Boyle, M. P.; Cooper, M. J.; Hanes, J. Highly Compacted DNA Nanoparticles with Low Mw Peg Coatings: In Vitro, Ex Vivo and in Vivo Evaluation. *J Control Release* **2012**, 157, 72-9.

67. Schuster, B. S.; Suk, J. S.; Woodworth, G. F.; Hanes, J. Nanoparticle Diffusion in Respiratory Mucus from Humans without Lung Disease. *Biomaterials* **2013**, 34, 3439-46.

68. Suk, J. S.; Lai, S. K.; Wang, Y. Y.; Ensign, L. M.; Zeitlin, P. L.; Boyle, M. P.; Hanes, J. The Penetration of Fresh Undiluted Sputum Expectorated by Cystic Fibrosis Patients by Non-Adhesive Polymer Nanoparticles. *Biomaterials* **2009**, 30, 2591-7.

69. Ponchel, G.; Irache, J. Specific and Non-Specific Bioadhesive Particulate Systems for Oral Delivery to the Gastrointestinal Tract. *Adv Drug Deliv Rev* **1998**, 34, 191-219.

70. Boylan, N. J.; Suk, J. S.; Lai, S. K.; Jelinek, R.; Boyle, M. P.; Cooper, M. J.; Hanes, J. Highly Compacted DNA Nanoparticles with Low Mw Peg Coatings: In Vitro, Ex Vivo and in Vivo Evaluation. *Journal of Controlled Release* **2012**, 157, 72-79.

71. Peppas, N. A. Molecular Calculations of Poly(Ethyleneglycol) Transport across a Swollen Poly(Acrylic Acid) Mucin Interface. *J Biomat Sci-Polym E* **1998**, 9, 535-542.

72. Peppas, N. A.; Huang, Y. Nanoscale Technology of Mucoadhesive Interactions. *Adv Drug Deliv Rev* **2004**, 56, 1675-87.

73. Peppas, N. A.; Sahlin, J. J. Hydrogels as Mucoadhesive and Bioadhesive Materials: A Review. *Biomaterials* **1996**, 17, 1553-1561.

74. Peppas, N. A.; Thomas, J. B.; McGinty, J. Molecular Aspects of Mucoadhesive Carrier Development for Drug Delivery and Improved Absorption. *Journal of biomaterials science. Polymer edition* **2009**, 20, 1-20.

75. Wang, Y. Y.; Lai, S. K.; Suk, J. S.; Pace, A.; Cone, R.; Hanes, J. Addressing the Peg Mucoadhesivity Paradox to Engineer Nanoparticles That "Slip" through the Human Mucus Barrier. *Angew Chem Int Ed Engl* **2008**, 47, 9726-9.

76. Tang, B. C.; Dawson, M.; Lai, S. K.; Wang, Y. Y.; Suk, J. S.; Yang, M.; Zeitlin, P.; Boyle, M. P.; Fu, J.; Hanes, J. Biodegradable Polymer Nanoparticles That Rapidly Penetrate the Human Mucus Barrier. *Proc Natl Acad Sci U S A* **2009**, 106, 19268-73.

77. Yang, M.; Lai, S. K.; Wang, Y. Y.; Zhong, W.; Happe, C.; Zhang, M.; Fu, J.; Hanes, J. Biodegradable Nanoparticles Composed Entirely of Safe Materials That Rapidly Penetrate Human Mucus. *Angew Chem Int Ed Engl* **2011**, 50, 2597-600.

78. Xu, Q.; Boylan, N. J.; Cai, S.; Miao, B.; Patel, H.; Hanes, J. Scalable Method to Produce Biodegradable Nanoparticles That Rapidly Penetrate Human Mucus. *J Control Release* **2013**, 170, 279-86.

79. Maisel, K.; Ensign, L. M.; Reddy, M.; Cone, R. A.; Hanes, J. S. Effect of Surface Chemistry on Nanoparticle Interaction with Gastrointestinal Mucus and Distribution in the Gastrointestinal Tract Following Oral and Rectal Administration in the Mouse. *Journal of Controlled Release* **2014**.

80. Lai, S. K.; Wang, Y. Y.; Wirtz, D.; Hanes, J. Micro- and Macrorheology of Mucus. *Adv Drug Deliv Rev* **2009**, 61, 86-100.

81. Suh, J.; Dawson, M.; Hanes, J. Real-Time Multiple-Particle Tracking: Applications to Drug and Gene Delivery. *Adv Drug Deliv Rev* **2005**, 57, 63-78.

82. Ensign, L. M.; Schneider, C.; Suk, J. S.; Cone, R.; Hanes, J. Mucus Penetrating Nanoparticles: Biophysical Tool and Method of Drug and Gene Delivery. *Adv Mater* **2012**, 24, 3887-94.

83. Lai, S. K.; Wang, Y. Y.; Cone, R.; Wirtz, D.; Hanes, J. Altering Mucus Rheology to "Solidify" Human Mucus at the Nanoscale. *Plos One* **2009**, 4, e4294.

84. Mankertz, J.; Schulzke, J. D. Altered Permeability in Inflammatory Bowel Disease: Pathophysiology and Clinical Implications. *Curr Opin Gastroenterol* **2007**, 23, 379-83.

85. Podolsky, D. K. Inflammatory Bowel Disease. *N Engl J Med* **2002**, 347, 417-29.

86. Lakatos, P. L. Recent Trends in the Epidemiology of Inflammatory Bowel Diseases: Up or Down? *World J Gastroenterol* **2006**, 12, 6102-8.

87. Head, K. A.; Jurenka, J. S. Inflammatory Bowel Disease Part 1: Ulcerative Colitis--Pathophysiology and Conventional and Alternative Treatment Options. *Altern Med Rev* **2003**, 8, 247-83.

88. Khor, B.; Gardet, A.; Xavier, R. J. Genetics and Pathogenesis of Inflammatory Bowel Disease. *Nature* **2011**, 474, 307-17.

89. Fiocchi, C. Inflammatory Bowel Disease: Etiology and Pathogenesis. *Gastroenterology* **1998**, 115, 182-205.

90. Koutroubakis, I.; Manousos, O. N.; Meuwissen, S. G.; Pena, A. S. Environmental Risk Factors in Inflammatory Bowel Disease. *Hepatogastroenterology* **1996**, 43, 381-93.

91. Ogura, Y.; Inohara, N.; Benito, A.; Chen, F. F.; Yamaoka, S.; Nunez, G. Nod2, a Nod1/Apaf-1 Family Member That Is Restricted to Monocytes and Activates Nf-Kappab. *J Biol Chem* **2001**, 276, 4812-8.

92. Ogura, Y.; Bonen, D. K.; Inohara, N.; Nicolae, D. L.; Chen, F. F.; Ramos, R.; Britton, H.; Moran, T.; Karaliuskas, R.; Duerr, R. H.; Achkar, J. P.; Brant, S. R.; Bayless, T. M.; Kirschner, B. S.; Hanauer, S. B.; Nunez, G.; Cho, J. H. A Frameshift Mutation in Nod2 Associated with Susceptibility to Crohn's Disease. *Nature* **2001**, 411, 603-6.

93. Meissner, Y.; Lamprecht, A. Alternative Drug Delivery Approaches for the Therapy of Inflammatory Bowel Disease. *J Pharm Sci* **2008**, 97, 2878-91.

94. Gionchetti, P.; D'Arienzo, A.; Rizzello, F.; Manguso, F.; Maieron, R.; Lecis, P. E.; Valpiani, D.; Iaquinto, G.; Annese, V.; Balzano, A.; Varoli, G.; Campieri, M. Topical Treatment of Distal Active Ulcerative Colitis with Beclomethasone Dipropionate or

Mesalamine: A Single-Blind Randomized Controlled Trial. *J Clin Gastroenterol* **2005**, 39, 291-7.

95. Collnot, E. M.; Ali, H.; Lehr, C. M. Nano- and Microparticulate Drug Carriers for Targeting of the Inflamed Intestinal Mucosa. *Journal of Controlled Release* **2012**, 161, 235-246.

96. Cohen, R. D.; Woseth, D. M.; Thisted, R. A.; Hanauer, S. B. A Meta-Analysis and Overview of the Literature on Treatment Options for Left-Sided Ulcerative Colitis and Ulcerative Proctitis. *Am J Gastroenterol* **2000**, 95, 1263-76.

97. Mulder, C. J.; Tytgat, G. N. Review Article: Topical Corticosteroids in Inflammatory Bowel Disease. *Aliment Pharmacol Ther* **1993**, 7, 125-30.

98. Lautenschlager, C.; Schmidt, C.; Fischer, D.; Stallmach, A. Drug Delivery Strategies in the Therapy of Inflammatory Bowel Disease. *Adv Drug Deliv Rev* **2014**, 71, 58-76.

99. Wen, H.; Park, K. *Oral Controlled Release Formulation Design and Drug Delivery: Theory to Practice*. John Wiley & Sons, Inc.: Wiley, New Jersey, **2010**.

100. Wong, J. M.; Wei, S. C. Efficacy of Pentasa Tablets for the Treatment of Inflammatory Bowel Disease. *J Formos Med Assoc* **2003**, 102, 613-9.

101. Feagan, B. G.; Chande, N.; MacDonald, J. K. Are There Any Differences in the Efficacy and Safety of Different Formulations of Oral 5-Asa Used for Induction and Maintenance of Remission in Ulcerative Colitis? Evidence from Cochrane Reviews. *Inflamm Bowel Dis* **2013**, 19, 2031-40.

102. Klotz, U. Clinical Pharmacokinetics of Sulphasalazine, Its Metabolites and Other Prodrugs of 5-Aminosalicylic Acid. *Clin Pharmacokinet* **1985**, 10, 285-302.

103. Rafii, F.; Franklin, W.; Cerniglia, C. E. Azoreductase Activity of Anaerobic Bacteria Isolated from Human Intestinal Microflora. *Appl Environ Microbiol* **1990**, 56, 2146-51.

104. Doell, R. G.; Kretchmer, N. Studies of Small Intestine During Development. I. Distribution and Activity of Beta-Galactosidase. *Biochim Biophys Acta* **1962**, 62, 353-62.

105. Englyst, H. N.; Hay, S.; Macfarlane, G. T. Polysaccharide Breakdown by Mixed Populations of Human Fecal Bacteria. *Fems Microbiol Ecol* **1987**, 45, 163-171.

106. Goldin, B. R.; Swenson, L.; Dwyer, J.; Sexton, M.; Gorbach, S. L. Effect of Diet and Lactobacillus Acidophilus Supplements on Human Fecal Bacterial Enzymes. *J Natl Cancer Inst* **1980**, 64, 255-61.

107. Green, J. R.; Lobo, A. J.; Holdsworth, C. D.; Leicester, R. J.; Gibson, J. A.; Kerr, G. D.; Hodgson, H. J.; Parkins, K. J.; Taylor, M. D. Balsalazide Is More Effective and Better Tolerated Than Mesalamine in the Treatment of Acute Ulcerative Colitis. The Abacus Investigator Group. *Gastroenterology* **1998**, 114, 15-22.

108. Courtney, M. G.; Nunes, D. P.; Bergin, C. F.; O'Driscoll, M.; Trimble, V.; Keeling, P. W.; Weir, D. G. Randomised Comparison of Olsalazine and Mesalazine in Prevention of Relapses in Ulcerative Colitis. *Lancet* **1992**, 339, 1279-81.

109. Lamprecht, A.; Schafer, U.; Lehr, C. M. Size-Dependent Bioadhesion of Micro- and Nanoparticulate Carriers to the Inflamed Colonic Mucosa. *Pharm Res* **2001**, 18, 788-93.

110. Lautenschlager, C.; Schmidt, C.; Lehr, C. M.; Fischer, D.; Stallmach, A. Peg-Functionalized Microparticles Selectively Target Inflamed Mucosa in Inflammatory Bowel Disease. *Eur J Pharm Biopharm* **2013**, 85, 578-86.

111. Lamprecht, A.; Ubrich, N.; Yamamoto, H.; Schafer, U.; Takeuchi, H.; Maincent, P.; Kawashima, Y.; Lehr, C. M. Biodegradable Nanoparticles for Targeted Drug Delivery in Treatment of Inflammatory Bowel Disease. *J Pharmacol Exp Ther* **2001**, 299, 775-81.

112. Schmidt, C.; Lautenschlaeger, C.; Collnot, E. M.; Schumann, M.; Bojarski, C.; Schulzke, J. D.; Lehr, C. M.; Stallmach, A. Nano- and Microscaled Particles for Drug Targeting to Inflamed Intestinal Mucosa-a First in Vivo Study in Human Patients. *Journal of Controlled Release* **2013**, 165, 139-145.

113. Johansson, M. E. V.; Gustafsson, J. K.; Sjoberg, K. E.; Petersson, J.; Holm, L.; Sjovall, H.; Hansson, G. C. Bacteria Penetrate the Inner Mucus Layer before Inflammation in the Dextran Sulfate Colitis Model. *Plos One* **2010**, 5.

114. Petersson, J.; Schreiber, O.; Hansson, G. C.; Gendler, S. J.; Velcich, A.; Lundberg, J. O.; Roos, S.; Holm, L.; Phillipson, M. Importance and Regulation of the Colonic Mucus Barrier in a Mouse Model of Colitis. *Am J Physiol Gastrointest Liver Physiol* **2011**, 300, G327-33.

115. Johansson, M. E.; Gustafsson, J. K.; Holmen-Larsson, J.; Jabbar, K. S.; Xia, L.; Xu, H.; Ghishan, F. K.; Carvalho, F. A.; Gewirtz, A. T.; Sjovall, H.; Hansson, G. C. Bacteria Penetrate the Normally Impenetrable Inner Colon Mucus Layer in Both Murine Colitis Models and Patients with Ulcerative Colitis. *Gut* **2014**, 63, 281-91.

116. Dvorak, A. M.; Dickersin, G. R. Crohn's Disease: Transmission Electron Microscopic Studies. I. Barrier Function. Possible Changes Related to Alterations of Cell Coat, Mucous Coat, Epithelial Cells, and Paneth Cells. *Hum Pathol* **1980**, 11, 561-71.

117. UNAIDS. *Aidsinfo 2011*.

118. Patel, P.; Borkowf, C. B.; Brooks, J. T.; Lasry, A.; Lansky, A.; Mermin, J. Estimating Per-Act Hiv Transmission Risk: A Systematic Review. *AIDS* **2014**, 28, 1509-19.

119. Beyrer, C.; Baral, S. D.; van Griensven, F.; Goodreau, S. M.; Chariyalertsak, S.; Wirtz, A. L.; Brookmeyer, R. Global Epidemiology of Hiv Infection in Men Who Have Sex with Men. *Lancet* **2012**, 380, 367-77.

120. Beyrer, C.; Baral, S. D.; Walker, D.; Wirtz, A. L.; Johns, B.; Sifakis, F. The Expanding Epidemics of Hiv Type 1 among Men Who Have Sex with Men in Low- and Middle-Income Countries: Diversity and Consistency. *Epidemiol Rev* **2010**, 32, 137-51.

121. McGowan, I. The Development of Rectal Microbicides for Hiv Prevention. *Expert Opin Drug Deliv* **2014**, 11, 69-82.

122. Grant, R. M.; Lama, J. R.; Anderson, P. L.; McMahan, V.; Liu, A. Y.; Vargas, L.; Goicochea, P.; Casapia, M.; Guanira-Carranza, J. V.; Ramirez-Cardich, M. E.; Montoya-Herrera, O.; Fernandez, T.; Veloso, V. G.; Buchbinder, S. P.; Chariyalertsak, S.; Schechter, M.; Bekker, L. G.; Mayer, K. H.; Kallas, E. G.; Amico, K. R.; Mulligan, K.; Bushman, L. R.; Hance, R. J.; Ganoza, C.; Defechereux, P.; Postle, B.; Wang, F.; McConnell, J. J.; Zheng, J. H.; Lee, J.; Rooney, J. F.; Jaffe, H. S.; Martinez, A. I.; Burns, D. N.; Glidden, D. V. Preexposure Chemoprophylaxis for Hiv Prevention in Men Who Have Sex with Men. *N Engl J Med* **2010**, 363, 2587-99.

123. Tellalian, D.; Maznavi, K.; Bredeek, U. F.; Hardy, W. D. Pre-Exposure Prophylaxis (Prep) for Hiv Infection: Results of a Survey of Hiv Healthcare Providers Evaluating Their Knowledge, Attitudes, and Prescribing Practices. *AIDS Patient Care STDS* **2013**, 27, 553-9.

124. Tripathi, A.; Whiteside, Y. O.; Duffus, W. A. Perceptions and Attitudes About Preexposure Prophylaxis among Seronegative Partners and the Potential of Sexual Disinhibition. *South Med J* **2013**, 106, 558-64.

125. Carballo-Dieguez, A.; O'Sullivan, L. F.; Lin, P.; Dolezal, C.; Pollack, L.; Catania, J. Awareness and Attitudes Regarding Microbicides and Nonoxynol-9 Use in a Probability Sample of Gay Men. *AIDS and behavior* **2007**, 11, 271-6.

126. Anton, P. A.; Saunders, T.; Elliott, J.; Khanukhova, E.; Dennis, R.; Adler, A.; Cortina, G.; Tanner, K.; Boscardin, J.; Cumberland, W. G.; Zhou, Y.; Ventuneac, A.; Carballo-Dieguez, A.; Rabe, L.; McCormick, T.; Gabelnick, H.; Mauck, C.; McGowan, I. First Phase 1 Double-Blind, Placebo-Controlled, Randomized Rectal Microbicide Trial Using Uc781 Gel with a Novel Index of Ex Vivo Efficacy. *Plos One* **2011**, 6, e23243.

127. Anton, P. A.; Cranston, R. D.; Kashuba, A.; Hendrix, C. W.; Bumpus, N. N.; Richardson-Harman, N.; Elliott, J.; Janocko, L.; Khanukhova, E.; Dennis, R.; Cumberland, W. G.; Ju, C.; Carballo-Dieguez, A.; Mauck, C.; McGowan, I. Rmp-02/Mtn-006: A Phase 1 Rectal Safety, Acceptability, Pharmacokinetic, and Pharmacodynamic Study of Tenofovir 1% Gel Compared with Oral Tenofovir Disoproxil Fumarate. *AIDS Res Hum Retroviruses* **2012**, 28, 1412-21.

128. Rohan, L. C.; Moncla, B. J.; Kunjara Na Ayudhya, R. P.; Cost, M.; Huang, Y.; Gai, F.; Billitto, N.; Lynam, J. D.; Pryke, K.; Graebing, P.; Hopkins, N.; Rooney, J. F.; Friend, D.; Dezzutti, C. S. In Vitro and Ex Vivo Testing of Tenofovir Shows It Is Effective as an Hiv-1 Microbicide. *Plos One* **2010**, 5, e9310.

129. Dezzutti, C. S.; Brown, E. R.; Moncla, B.; Russo, J.; Cost, M.; Wang, L.; Uranker, K.; Kunjara Na Ayudhya, R. P.; Pryke, K.; Pickett, J.; Leblanc, M. A.; Rohan,

L. C. Is Wetter Better? An Evaluation of over-the-Counter Personal Lubricants for Safety and Anti-Hiv-1 Activity. *PLoS One* **2012**, 7, e48328.

130. McGowan, I.; Hoesley, C.; Cranston, R. D.; Andrew, P.; Janocko, L.; Dai, J. Y.; Carballo-Dieguez, A.; Ayudhya, R. K.; Piper, J.; Hladik, F.; Mayer, K. A Phase 1 Randomized, Double Blind, Placebo Controlled Rectal Safety and Acceptability Study of Tenofovir 1% Gel (Mtn-007). *PLoS One* **2013**, 8, e60147.

131. Carballo-Dieguez, A.; Bauermeister, J.; Ventuneac, A.; Dolezal, C.; Mayer, K. Why Rectal Douches May Be Acceptable Rectal-Microbicide Delivery Vehicles for Men Who Have Sex with Men. *Sexually transmitted diseases* **2010**, 37, 228-33.

132. Cao, Y. J.; Caffo, B. S.; Fuchs, E. J.; Lee, L. A.; Du, Y.; Li, L.; Bakshi, R. P.; Macura, K.; Khan, W. A.; Wahl, R. L.; Grohskopf, L. A.; Hendrix, C. W. Quantification of the Spatial Distribution of Rectally Applied Surrogates for Microbicide and Semen in Colon with Spect and Magnetic Resonance Imaging. *Br J Clin Pharmacol* **2012**, 74, 1013-22.

133. Leyva, F. J.; Bakshi, R. P.; Fuchs, E. J.; Li, L.; Caffo, B. S.; Goldsmith, A. J.; Ventuneac, A.; Carballo-Dieguez, A.; Du, Y.; Leal, J. P.; Lee, L. A.; Torbenson, M. S.; Hendrix, C. W. Isoosmolar Enemas Demonstrate Preferential Gastrointestinal Distribution, Safety, and Acceptability Compared with Hyperosmolar and Hypoosmolar Enemas as a Potential Delivery Vehicle for Rectal Microbicides. *AIDS Res Hum Retroviruses* **2013**, 29, 1487-95.

134. Louissaint, N. A.; Nimmagadda, S.; Fuchs, E. J.; Bakshi, R. P.; Cao, Y. J.; Lee, L. A.; Goldsmith, J.; Caffo, B. S.; Du, Y.; King, K. E.; Menendez, F. A.; Torbenson, M. S.; Hendrix, C. W. Distribution of Cell-Free and Cell-Associated Hiv Surrogates in the

Colon after Simulated Receptive Anal Intercourse in Men Who Have Sex with Men. *J Acquir Immune Defic Syndr* **2012**, 59, 10-7.

135. das Neves, J.; Amiji, M.; Bahia, M. F.; Sarmento, B. Assessing the Physical-Chemical Properties and Stability of Dapivirine-Loaded Polymeric Nanoparticles. *International Journal of Pharmaceutics* **2013**, 456, 307-14.

136. das Neves, J.; Araujo, F.; Andrade, F.; Amiji, M.; Bahia, M. F.; Sarmento, B. Biodistribution and Pharmacokinetics of Dapivirine-Loaded Nanoparticles after Vaginal Delivery in Mice. *Pharm Res* **2014**, 31, 1834-45.

137. das Neves, J.; Araujo, F.; Andrade, F.; Michiels, J.; Arien, K. K.; Vanham, G.; Amiji, M.; Bahia, M. F.; Sarmento, B. In Vitro and Ex Vivo Evaluation of Polymeric Nanoparticles for Vaginal and Rectal Delivery of the Anti-Hiv Drug Dapivirine. *Mol Pharm* **2013**, 10, 2793-807.

138. das Neves, J.; Sarmento, B.; Amiji, M.; Bahia, M. F. Development and Validation of a Hplc Method for the Assay of Dapivirine in Cell-Based and Tissue Permeability Experiments. *J Chromatogr B Analyt Technol Biomed Life Sci* **2012**, 911, 76-83.

139. Dezzutti, C. S.; James, V. N.; Ramos, A.; Sullivan, S. T.; Siddig, A.; Bush, T. J.; Grohskopf, L. A.; Paxton, L.; Subbarao, S.; Hart, C. E. In Vitro Comparison of Topical Microbicides for Prevention of Human Immunodeficiency Virus Type 1 Transmission. *Antimicrob Agents Chemother* **2004**, 48, 3834-44.

140. Abner, S. R.; Guenthner, P. C.; Guarner, J.; Hancock, K. A.; Cummins, J. E., Jr.; Fink, A.; Gilmore, G. T.; Staley, C.; Ward, A.; Ali, O.; Binderow, S.; Cohen, S.; Grohskopf, L. A.; Paxton, L.; Hart, C. E.; Dezzutti, C. S. A Human Colorectal Explant

Culture to Evaluate Topical Microbicides for the Prevention of Hiv Infection. *Journal of Infectious Diseases* **2005**, 192, 1545-56.

141. Patton, D. L.; Cosgrove Sweeney, Y. T.; McCarthy, T. D.; Hillier, S. L. Preclinical Safety and Efficacy Assessments of Dendrimer-Based (Spl7013) Microbicide Gel Formulations in a Nonhuman Primate Model. *Antimicrob Agents Chemother* **2006**, 50, 1696-700.

142. Gipson, I. K. Mucins of the Human Endocervix. *Frontiers in bioscience : a journal and virtual library* **2001**, 6, D1245-55.

143. Audie, J. P.; Tetaert, D.; Pigny, P.; Buisine, M. P.; Janin, A.; Aubert, J. P.; Porchet, N.; Boersma, A. Mucin Gene Expression in the Human Endocervix. *Human reproduction* **1995**, 10, 98-102.

144. Sherwood, J. K.; Zeitlin, L.; Chen, X.; Whaley, K. J.; Cone, R. A.; Saltzman, W. M. Residence Half-Life of Igg Administered Topically to the Mouse Vagina. *Biology of reproduction* **1996**, 54, 264-9.

145. Clunes, M. T.; Boucher, R. C. Cystic Fibrosis: The Mechanisms of Pathogenesis of an Inherited Lung Disorder. *Drug discovery today. Disease mechanisms* **2007**, 4, 63-72.

146. Matsui, H.; Grubb, B. R.; Tarran, R.; Randell, S. H.; Gatzy, J. T.; Davis, C. W.; Boucher, R. C. Evidence for Periciliary Liquid Layer Depletion, Not Abnormal Ion Composition, in the Pathogenesis of Cystic Fibrosis Airways Disease. *Cell* **1998**, 95, 1005-15.

147. Tarran, R.; Grubb, B. R.; Gatzy, J. T.; Davis, C. W.; Boucher, R. C. The Relative Roles of Passive Surface Forces and Active Ion Transport in the Modulation of Airway

Surface Liquid Volume and Composition. *The Journal of general physiology* **2001**, 118, 223-36.

148. Thornton, D. J.; Howard, M.; Khan, N.; Sheehan, J. K. Identification of Two Glycoforms of the Muc5b Mucin in Human Respiratory Mucus. Evidence for a Cysteine-Rich Sequence Repeated within the Molecule. *J Biol Chem* **1997**, 272, 9561-6.

149. Ali, M. S.; Pearson, J. P. Upper Airway Mucin Gene Expression: A Review. *The Laryngoscope* **2007**, 117, 932-8.

150. Verkman, A. S.; Song, Y.; Thiagarajah, J. R. Role of Airway Surface Liquid and Submucosal Glands in Cystic Fibrosis Lung Disease. *American journal of physiology. Cell physiology* **2003**, 284, C2-15.

151. King-Smith, P. E.; Fink, B. A.; Hill, R. M.; Koelling, K. W.; Tiffany, J. M. The Thickness of the Tear Film. *Current eye research* **2004**, 29, 357-68.

152. Gipson, I. K.; Inatomi, T. Mucin Genes Expressed by the Ocular Surface Epithelium. *Prog Retin Eye Res* **1997**, 16, 81-98.

153. Greaves, J. L.; Wilson, C. G. Treatment of Diseases of the Eye with Mucoadhesive Delivery Systems. *Adv Drug Deliver Rev* **1993**, 11, 349-383.

154. Holly, F. J.; Lemp, M. A. Tear Physiology and Dry Eyes. *Survey of ophthalmology* **1977**, 22, 69-87.

155. Prydal, J. I.; Artal, P.; Woon, H.; Campbell, F. W. Study of Human Precorneal Tear Film Thickness and Structure Using Laser Interferometry. *Investigative ophthalmology & visual science* **1992**, 33, 2006-11.

156. Crater, J. S.; Carrier, R. L. Barrier Properties of Gastrointestinal Mucus to Nanoparticle Transport. *Macromolecular bioscience* **2010**, 10, 1473-83.

157. Matsuo, K.; Ota, H.; Akamatsu, T.; Sugiyama, A.; Katsuyama, T. Histochemistry of the Surface Mucous Gel Layer of the Human Colon. *Gut* **1997**, 40, 782-9.

158. van der Waaij, L. A.; Harmsen, H. J.; Madjipour, M.; Kroese, F. G.; Zwiers, M.; van Dullemen, H. M.; de Boer, N. K.; Welling, G. W.; Jansen, P. L. Bacterial Population Analysis of Human Colon and Terminal Ileum Biopsies with 16s Rrna-Based Fluorescent Probes: Commensal Bacteria Live in Suspension and Have No Direct Contact with Epithelial Cells. *Inflamm Bowel Dis* **2005**, 11, 865-71.

159. Behrens, I.; Stenberg, P.; Artursson, P.; Kissel, T. Transport of Lipophilic Drug Molecules in a New Mucus-Secreting Cell Culture Model Based on Ht29-Mtx Cells. *Pharmaceutical research* **2001**, 18, 1138-45.

160. Copeman, M.; Matuz, J.; Leonard, A. J.; Pearson, J. P.; Dettmar, P. W.; Allen, A. The Gastroduodenal Mucus Barrier and Its Role in Protection against Luminal Pepsins: The Effect of 16,16 Dimethyl Prostaglandin E2, Carbopol-Polyacrylate, Sucralfate and Bismuth Subsalicylate. *Journal of gastroenterology and hepatology* **1994**, 9 Suppl 1, S55-9.

161. Pullan, R. D.; Thomas, G. A.; Rhodes, M.; Newcombe, R. G.; Williams, G. T.; Allen, A.; Rhodes, J. Thickness of Adherent Mucus Gel on Colonic Mucosa in Humans and Its Relevance to Colitis. *Gut* **1994**, 35, 353-9.

162. Chaumeil, J. C. Micronization: A Method of Improving the Bioavailability of Poorly Soluble Drugs. *Methods Find Exp Clin Pharmacol* **1998**, 20, 211-5.

163. McInnes, G. T.; Asbury, M. J.; Ramsay, L. E.; Shelton, J. R.; Harrison, I. R. Effect of Micronization on the Bioavailability and Pharmacologic Activity of Spironolactone. *J Clin Pharmacol* **1982**, 22, 410-7.

164. Farinha, A.; Bica, A.; Tavares, P. Improved Bioavailability of a Micronized Megestrol Acetate Tablet Formulation in Humans. *Drug Dev Ind Pharm* **2000**, 26, 567-70.

165. Hunter, A. C.; Elsom, J.; Wibroe, P. P.; Moghimi, S. M. Polymeric Particulate Technologies for Oral Drug Delivery and Targeting: A Pathophysiological Perspective. *Nanomedicine* **2012**, 8 Suppl 1, S5-20.

166. Thanou, M.; Verhoef, J. C.; Junginger, H. E. Oral Drug Absorption Enhancement by Chitosan and Its Derivatives. *Adv Drug Deliv Rev* **2001**, 52, 117-26.

167. Duran-Lobato, M.; Munoz-Rubio, I.; Holgado, M. A.; Alvarez-Fuentes, J.; Fernandez-Arevalo, M.; Martin-Banderas, L. Enhanced Cellular Uptake and Biodistribution of a Synthetic Cannabinoid Loaded in Surface-Modified Poly(Lactic-Co-Glycolic Acid) Nanoparticles. *J Biomed Nanotechnol* **2014**, 10, 1068-79.

168. Steffansen, B.; Nielsen, C. U.; Brodin, B.; Eriksson, A. H.; Andersen, R.; Frokjaer, S. Intestinal Solute Carriers: An Overview of Trends and Strategies for Improving Oral Drug Absorption. *European journal of pharmaceutical sciences : official journal of the European Federation for Pharmaceutical Sciences* **2004**, 21, 3-16.

169. Hamman, J. H.; Demana, P. H.; Olivier, E. I. Targeting Receptors, Transporters and Site of Absorption to Improve Oral Drug Delivery. *Drug target insights* **2007**, 2, 71-81.

170. Gupta, S.; Kesarla, R.; Omri, A. Formulation Strategies to Improve the Bioavailability of Poorly Absorbed Drugs with Special Emphasis on Self-Emulsifying Systems. *ISRN pharmaceutics* **2013**, 2013, 848043.

171. Thomas, V. H.; Bhattachar, S.; Hitchingham, L.; Zocharski, P.; Naath, M.; Surendran, N.; Stoner, C. L.; El-Kattan, A. The Road Map to Oral Bioavailability: An Industrial Perspective. *Expert opinion on drug metabolism & toxicology* **2006**, 2, 591-608.

172. Frei, P.; Biedermann, L.; Manser, C. N.; Wilk, M.; Manz, M.; Vavricka, S. R.; Rogler, G. Topical Therapies in Inflammatory Bowel Disease. *Digestion* **2012**, 86 Suppl 1, 36-44.

173. Li, J.; Chen, C.; Cao, X. N.; Wang, G. H.; Hu, J. B.; Wang, J. Efficacy of Topical Versus Oral 5-Aminosalicylate for Treatment of 2,4,6-Trinitrobenzene Sulfonic Acid-Induced Ulcerative Colitis in Rats. *J Huazhong Univ Sci Technolog Med Sci* **2014**, 34, 59-65.

174. Lohr, K.; Sardana, H.; Lee, S.; Wu, F.; Huso, D. L.; Hamad, A. R.; Chakravarti, S. Extracellular Matrix Protein Lumican Regulates Inflammation in a Mouse Model of Colitis. *Inflamm Bowel Dis* **2012**, 18, 143-51.

175. Yazbeck, R.; Howarth, G. S.; Butler, R. N.; Geier, M. S.; Abbott, C. A. Biochemical and Histological Changes in the Small Intestine of Mice with Dextran Sulfate Sodium Colitis. *J Cell Physiol* **2011**, 226, 3219-24.

176. Nance, E. A.; Woodworth, G. F.; Sailor, K. A.; Shih, T. Y.; Xu, Q.; Swaminathan, G.; Xiang, D.; Eberhart, C.; Hanes, J. A Dense Poly(Ethylene Glycol) Coating Improves Penetration of Large Polymeric Nanoparticles within Brain Tissue. *Science translational medicine* **2012**, 4, 149ra119.

177. Ensign, L. M.; Tang, B. C.; Wang, Y. Y.; Tse, T. A.; Hoen, T.; Cone, R.; Hanes, J. Mucus-Penetrating Nanoparticles for Vaginal Drug Delivery Protect against Herpes Simplex Virus. *Science Translational Medicine* **2012**, 4, 138ra79.

178. Lai, S. K.; Hanes, J. Real-Time Multiple Particle Tracking of Gene Nanocarriers in Complex Biological Environments. *Methods Mol Biol* **2008**, 434, 81-97.

179. Suh, J.; Wirtz, D.; Hanes, J. Real-Time Intracellular Transport of Gene Nanocarriers Studied by Multiple Particle Tracking. *Biotechnology progress* **2004**, 20, 598-602.

180. Dawson, M.; Krauland, E.; Wirtz, D.; Hanes, J. Transport of Polymeric Nanoparticle Gene Carriers in Gastric Mucus. *Biotechnology progress* **2004**, 20, 851-7.

181. Dawson, M.; Wirtz, D.; Hanes, J. Enhanced Viscoelasticity of Human Cystic Fibrotic Sputum Correlates with Increasing Microheterogeneity in Particle Transport. *J Biol Chem* **2003**, 278, 50393-401.

182. Kim, A. J.; Boylan, N. J.; Suk, J. S.; Hwangbo, M.; Yu, T.; Schuster, B. S.; Cebotaru, L.; Lesniak, W. G.; Oh, J. S.; Adstamongkonkul, P.; Choi, A. Y.; Kannan, R. M.; Hanes, J. Use of Single-Site-Functionalized Peg Dendrons to Prepare Gene Vectors That Penetrate Human Mucus Barriers. *Angew Chem Int Ed Engl* **2013**, 52, 3985-8.

183. Eyles, J.; Alpar, O.; Field, W. N.; Lewis, D. A.; Keswick, M. The Transfer of Polystyrene Microspheres from the Gastrointestinal Tract to the Circulation after Oral Administration in the Rat. *J Pharm Pharmacol* **1995**, 47, 561-5.

184. Coco, R.; Plapied, L.; Pourcelle, V.; Jerome, C.; Brayden, D. J.; Schneider, Y. J.; Preat, V. Drug Delivery to Inflamed Colon by Nanoparticles: Comparison of Different Strategies. *Int J Pharm* **2013**, 440, 3-12.

185. Bruewer, M.; Samarin, S.; Nusrat, A. Inflammatory Bowel Disease and the Apical Junctional Complex. *Ann N Y Acad Sci* **2006**, 1072, 242-52.

186. Lamprecht, A.; Yamamoto, H.; Takeuchi, H.; Kawashima, Y. Nanoparticles Enhance Therapeutic Efficiency by Selectively Increased Local Drug Dose in Experimental Colitis in Rats. *J Pharmacol Exp Ther* **2005**, 315, 196-202.

187. Lai, S. K.; Wang, Y. Y.; Hanes, J. Mucus-Penetrating Nanoparticles for Drug and Gene Delivery to Mucosal Tissues. *Adv Drug Deliv Rev* **2009**, 61, 158-71.

188. Yoncheva, K.; Gomez, S.; Campanero, M. A.; Gamazo, C.; Irache, J. M. Bioadhesive Properties of Pegylated Nanoparticles. *Expert Opin Drug Deliv* **2005**, 2, 205-18.

189. Serra, L.; Domenech, J.; Peppas, N. A. Engineering Design and Molecular Dynamics of Mucoadhesive Drug Delivery Systems as Targeting Agents. *European Journal of Pharmaceutics and Biopharmaceutics* **2009**, 71, 519-528.

190. Gupta, V.; Hwang, B. H.; Lee, J.; Anselmo, A. C.; Doshi, N.; Mitragotri, S. Mucoadhesive Intestinal Devices for Oral Delivery of Salmon Calcitonin. *J Control Release* **2013**, 172, 753-62.

191. Shen, Z.; Mitragotri, S. Intestinal Patches for Oral Drug Delivery. *Pharm Res* **2002**, 19, 391-5.

192. Uskokovic, V.; Lee, P. P.; Walsh, L. A.; Fischer, K. E.; Desai, T. A. Pegylated Silicon Nanowire Coated Silica Microparticles for Drug Delivery across Intestinal Epithelium. *Biomaterials* **2012**, 33, 1663-72.

193. Kararli, T. T. Comparison of the Gastrointestinal Anatomy, Physiology, and Biochemistry of Humans and Commonly Used Laboratory Animals. *Biopharmaceutics & drug disposition* **1995**, 16, 351-80.

194. Wang, Y.; Zhang, X.; Cheng, C.; Li, C. Mucoadhesive and Enzymatic Inhibitory Nanoparticles for Transnasal Insulin Delivery. *Nanomedicine (Lond)* **2014**, 9, 451-64.

195. Momoh, M. A.; Kenechukwu, F. C.; Nnamani, P. O.; Umetiti, J. C. Influence of Magnesium Stearate on the Physicochemical and Pharmacodynamic Characteristics of Insulin-Loaded Eudragit Entrapped Mucoadhesive Microspheres. *Drug Deliv* **2014**.

196. Bakhru, S. H.; Furtado, S.; Morello, A. P.; Mathiowitz, E. Oral Delivery of Proteins by Biodegradable Nanoparticles. *Adv Drug Deliver Rev* **2013**, 65, 811-21.

197. Furtado, S.; Abramson, D.; Burrill, R.; Olivier, G.; Gourd, C.; Bubbers, E.; Mathiowitz, E. Oral Delivery of Insulin Loaded Poly(Fumaric-Co-Sebacic) Anhydride Microspheres. *Int J Pharm* **2008**, 347, 149-55.

198. Carino, G. P.; Mathiowitz, E. Oral Insulin Delivery. *Adv Drug Deliv Rev* **1999**, 35, 249-257.

199. Takeuchi, H.; Sugihara, H. [Absorption of Calcitonin in Oral and Pulmonary Administration with Polymer-Coated Liposomes]. *Yakugaku Zasshi* **2010**, 130, 1135-42.

200. Makhlof, A.; Werle, M.; Tozuka, Y.; Takeuchi, H. A Mucoadhesive Nanoparticulate System for the Simultaneous Delivery of Macromolecules and Permeation Enhancers to the Intestinal Mucosa. *J Control Release* **2011**, 149, 81-8.

201. Sinsuebpol, C.; Chatchawalsaisin, J.; Kulvanich, P. Preparation and in Vivo Absorption Evaluation of Spray Dried Powders Containing Salmon Calcitonin Loaded Chitosan Nanoparticles for Pulmonary Delivery. *Drug Des Devel Ther* **2013**, 7, 861-73.

202. Chen, D.; Xia, D.; Li, X.; Zhu, Q.; Yu, H.; Zhu, C.; Gan, Y. Comparative Study of Pluronic((R)) F127-Modified Liposomes and Chitosan-Modified Liposomes for Mucus Penetration and Oral Absorption of Cyclosporine a in Rats. *Int J Pharm* **2013**, 449, 1-9.

203. Hussain, N.; Florence, A. T. Utilizing Bacterial Mechanisms of Epithelial Cell Entry: Invasin-Induced Oral Uptake of Latex Nanoparticles. *Pharmaceutical research* **1998**, 15, 153-156.

204. Behrens, I.; Pena, A. I.; Alonso, M. J.; Kissel, T. Comparative Uptake Studies of Bioadhesive and Non-Bioadhesive Nanoparticles in Human Intestinal Cell Lines and Rats: The Effect of Mucus on Particle Adsorption and Transport. *Pharm Res* **2002**, 19, 1185-93.

205. Reineke, J. J.; Cho, D. Y.; Dingle, Y. T.; Morello, A. P., 3rd; Jacob, J.; Thanos, C. G.; Mathiowitz, E. Unique Insights into the Intestinal Absorption, Transit, and Subsequent Biodistribution of Polymer-Derived Microspheres. *Proc Natl Acad Sci U S A* **2013**, 110, 13803-8.

206. Safdi, M.; DeMicco, M.; Sninsky, C.; Banks, P.; Wruble, L.; Deren, J.; Koval, G.; Nichols, T.; Targan, S.; Fleishman, C.; Wiita, B. A Double-Blind Comparison of Oral Versus Rectal Mesalamine Versus Combination Therapy in the Treatment of Distal Ulcerative Colitis. *Am J Gastroenterol* **1997**, 92, 1867-71.

207. Marteau, P.; Probert, C. S.; Lindgren, S.; Gassul, M.; Tan, T. G.; Dignass, A.; Befrits, R.; Midhagen, G.; Rademaker, J.; Foldager, M. Combined Oral and Enema Treatment with Pentasa (Mesalazine) Is Superior to Oral Therapy Alone in Patients with

Extensive Mild/Moderate Active Ulcerative Colitis: A Randomised, Double Blind, Placebo Controlled Study. *Gut* **2005**, 54, 960-5.

208. Andreoli, A.; Spinella, S.; Levenstein, S.; Prantera, C. 5-Asa Enema Versus Oral Sulphasalazine in Maintaining Remission in Ulcerative Colitis. *The Italian journal of gastroenterology* **1994**, 26, 121-5.

209. Ulbrich, W.; Lamprecht, A. Targeted Drug-Delivery Approaches by Nanoparticulate Carriers in the Therapy of Inflammatory Diseases. *J R Soc Interface* **2010**, 7 Suppl 1, S55-66.

210. Johansson, M. E. V.; Phillipson, M.; Petersson, J.; Velcich, A.; Holm, L.; Hansson, G. C. The Inner of the Two Muc2 Mucin-Dependent Mucus Layers in Colon Is Devoid of Bacteria. *Proceedings of the National Academy of Sciences of the United States of America* **2008**, 105, 15064-15069.

211. Schultsz, C.; van den Berg, F. M.; ten Kate, F. W.; Tytgat, G. N. J.; Dankert, J. The Intestinal Mucus Layer from Patients with Inflammatory Bowel Disease Harbors High Numbers of Bacteria Compared with Controls. *Gastroenterology* **1999**, 117, 1089-1097.

212. Lautenschlager, C.; Schmidt, C.; Lehr, C. M.; Fischer, D.; Stallmach, A. Peg-Functionalized Microparticles Selectively Target Inflamed Mucosa in Inflammatory Bowel Disease. *European Journal of Pharmaceutics and Biopharmaceutics* **2013**, 85, 578-86.

213. Baria, R.; Joshi, N.; Pandya, D. Clinical Efficacy of Panchamuladi Kaala Basti (Enema) in the Management of Amavata (Rheumatoid Arthritis). *Ayu* **2011**, 32, 90-4.

214. Szabo, S.; Deng, X.; Tolstanova, G.; Khomenko, T.; Paunovic, B.; Chen, L.; Jadus, M.; Sandor, Z. Angiogenic and Anti-Angiogenic Therapy for Gastrointestinal Ulcers: New Challenges for Rational Therapeutic Predictions and Drug Design. *Current pharmaceutical design* **2011**, 17, 1633-42.

215. Sugisaki, K.; Honma, F.; Iwadate, H.; Shio, K.; Shioya, Y.; Fukaya, E.; Sato, K.; Saito, H.; Sekine, H.; Kobayashi, H.; Orikasa, H.; Watanabe, H.; Sato, Y. Ulcerative Colitis Occurring in the Course of Rheumatoid Arthritis: A Case Successfully Treated with Mesalamine Enema. *Internal medicine* **2004**, 43, 1046-50.

216. Herrstedt, J.; Jorgensen, M.; Angelo, H. R.; Rassing, M. R.; Moller-Sonnergaard, J.; Dombernowsky, P. Bioavailability of the Antiemetic Metopimazine Given as a Microenema. *Br J Clin Pharmacol* **1996**, 41, 613-5.

217. Nance, E. A.; Woodworth, G. F.; Sailor, K. A.; Shih, T. Y.; Xu, Q.; Swaminathan, G.; Xiang, D.; Eberhart, C.; Hanes, J. A Dense Poly(Ethylene Glycol) Coating Improves Penetration of Large Polymeric Nanoparticles within Brain Tissue. *Science translational medicine* **2012**, 4, 149ra119.

218. McGowan, I.; Dezzutti, C. Rectal Microbicide Development. *Current topics in microbiology and immunology* **2013**.

219. Chang, W. W.; Nadler, N. J. Renewal of the Epithelium in the Descending Colon of the Mouse. Iv. Cell Population Kinetics of Vacuolated-Columnar and Mucous Cells. *Am J Anat* **1975**, 144, 39-56.

220. Chang, W. W.; Leblond, C. P. Renewal of the Epithelium in the Descending Colon of the Mouse. I. Presence of Three Cell Populations: Vacuolated-Columnar, Mucous and Argentaffin. *Am J Anat* **1971**, 131, 73-99.

221. Fuchs, E. J.; Lee, L. A.; Torbenson, M. S.; Parsons, T. L.; Bakshi, R. P.; Guidos, A. M.; Wahl, R. L.; Hendrix, C. W. Hyperosmolar Sexual Lubricant Causes Epithelial Damage in the Distal Colon: Potential Implication for Hiv Transmission. *J Infect Dis* **2007**, 195, 703-10.

222. Sandle, G. I. Salt and Water Absorption in the Human Colon: A Modern Appraisal. *Gut* **1998**, 43, 294-9.

223. Noach, A. B.; Sakai, M.; Blom-Roosemalen, M. C.; de Jonge, H. R.; de Boer, A. G.; Breimer, D. D. Effect of Anisotonic Conditions on the Transport of Hydrophilic Model Compounds across Monolayers of Human Colonic Cell Lines. *J Pharmacol Exp Ther* **1994**, 270, 1373-80.

224. Billich, C. O.; Levitan, R. Effects of Sodium Concentration and Osmolality on Water and Electrolyte Absorption Form the Intact Human Colon. *J Clin Invest* **1969**, 48, 1336-47.

225. Carballo-Dieguez, A.; Bauermeister, J. A.; Ventuneac, A.; Dolezal, C.; Balan, I.; Remien, R. H. The Use of Rectal Douches among Hiv-Uninfected and Infected Men Who Have Unprotected Receptive Anal Intercourse: Implications for Rectal Microbicides. *AIDS and behavior* **2008**, 12, 860-6.

226. Misegades, L.; Page-Shafer, K.; Halperin, D.; McFarland, W.; Survey, Y. W. S. S. I. G. Y. W. s. Anal Intercourse among Young Low-Income Women in California: An Overlooked Risk Factor for Hiv? *AIDS* **2001**, 15, 534-5.

227. Brody, S.; Potterat, J. J. Assessing the Role of Anal Intercourse in the Epidemiology of Aids in Africa. *International journal of STD & AIDS* **2003**, 14, 431-6.

228. Boily, M. C.; Baggaley, R. F.; Wang, L.; Masse, B.; White, R. G.; Hayes, R. J.; Alary, M. Heterosexual Risk of Hiv-1 Infection Per Sexual Act: Systematic Review and Meta-Analysis of Observational Studies. *The Lancet infectious diseases* **2009**, 9, 118-29.

229. Mosher, W. D.; Chandra, A.; Jones, J. *Sexual Behavior and Selected Health Measures: Men and Women 15–44 Years of Age, United States, 2002* Center for Disease Control: 2005; pp 1-56.

230. Dezzutti, C. S.; Rohan, L. C.; Wang, L.; Uranker, K.; Shetler, C.; Cost, M.; Lynam, J. D.; Friend, D. Reformulated Tenofovir Gel for Use as a Dual Compartment Microbicide. *The Journal of antimicrobial chemotherapy* **2012**, 67, 2139-42.

231. Moench, T. R.; Mumper, R. J.; Hoen, T. E.; Sun, M.; Cone, R. A. Microbicide Excipients Can Greatly Increase Susceptibility to Genital Herpes Transmission in the Mouse. *BMC infectious diseases* **2010**, 10, 331.

232. Pais, R.; Jha, R.; Omosun, Y.; He, Q.; Fujihashi, K.; Black, C.; Igietseme, J.; Eko, F. Rectal Immunization with an Rvcg Vaccine Protects against Genital Chlamydia Challenge (Vac7p.962). *The Journal of Immunology* **2014**, 192, 141.7.

233. Mayr, U. B.; Kudela, P.; Atrasheuskaya, A.; Bukin, E.; Ignatyev, G.; Lubitz, W. Rectal Single Dose Immunization of Mice with Escherichia Coli O157:H7 Bacterial Ghosts Induces Efficient Humoral and Cellular Immune Responses and Protects against the Lethal Heterologous Challenge. *Microbial biotechnology* **2012**, 5, 283-94.

234. Nardelli-Haefliger, D.; Kraehenbuhl, J. P.; Curtiss, R., 3rd; Schodel, F.; Potts, A.; Kelly, S.; De Grandi, P. Oral and Rectal Immunization of Adult Female Volunteers with a Recombinant Attenuated Salmonella Typhi Vaccine Strain. *Infection and immunity* **1996**, 64, 5219-24.

235. Hamajima, K.; Hoshino, Y.; Xin, K. Q.; Hayashi, F.; Tadokoro, K.; Okuda, K. Systemic and Mucosal Immune Responses in Mice after Rectal and Vaginal Immunization with Hiv-DNA Vaccine. *Clinical immunology* **2002**, 102, 12-8.

236. McMahon, J. M.; Myers, J. E.; Kurth, A. E.; Cohen, S. E.; Mannheimer, S. B.; Simmons, J.; Pouget, E. R.; Trabold, N.; Haberer, J. E. Oral Pre-Exposure Prophylaxis (Prep) for Prevention of Hiv in Serodiscordant Heterosexual Couples in the United States: Opportunities and Challenges. *AIDS Patient Care STDS* **2014**, 28, 462-74.

237. Maartens, G.; Celum, C.; Lewin, S. R. Hiv Infection: Epidemiology, Pathogenesis, Treatment, and Prevention. *Lancet* **2014**, 384, 258-71.

238. Shattock, R. J.; Warren, M.; McCormack, S.; Hankins, C. A. Aids. Turning the Tide against Hiv. *Science* **2011**, 333, 42-3.

239. Coutinho, B.; Prasad, R. Emtricitabine/Tenofovir (Truvada) for Hiv Prophylaxis. *American family physician* **2013**, 88, 535-40.

240. Pennings, P. S. Hiv Drug Resistance: Problems and Perspectives. *Infectious disease reports* **2013**, 5, e5.

241. Gupta, S. K.; Nutan. Clinical Use of Vaginal or Rectally Applied Microbicides in Patients Suffering from Hiv/Aids. *Hiv/Aids* **2013**, 5, 295-307.

242. D'Cruz, O. J.; Uckun, F. M. Vaginal Microbicides and Their Delivery Platforms. *Expert Opin Drug Deliv* **2014**, 11, 723-40.

243. Machado, R. M.; Palmeira-de-Oliveira, A.; Martinez-De-Oliveira, J.; Palmeira-de-Oliveira, R. Vaginal Films for Drug Delivery. *J Pharm Sci* **2013**, 102, 2069-81.

244. Adams, J. L.; Kashuba, A. D. Formulation, Pharmacokinetics and Pharmacodynamics of Topical Microbicides. *Best practice & research. Clinical obstetrics & gynaecology* **2012**, 26, 451-62.

245. das Neves, J.; Bahia, M. F. Gels as Vaginal Drug Delivery Systems. *Int J Pharm* **2006**, 318, 1-14.

246. Achilles, S. L.; Shete, P. B.; Whaley, K. J.; Moench, T. R.; Cone, R. A. Microbicide Efficacy and Toxicity Tests in a Mouse Model for Vaginal Transmission of Chlamydia Trachomatis. *Sexually transmitted diseases* **2002**, 29, 655-64.

247. Wang, L. L.; Zheng, W. S.; Chen, S. H.; Fang, X. Q. Development of in Situ Gelling and Bio Adhesive 5-Fluorouracil Enema. *PLoS One* **2013**, 8, e71037.

248. Dezzutti, C. S.; Russo, J.; Wang, L.; Abebe, K. Z.; Li, J.; Friend, D. R.; McGowan, I. M.; Rohan, L. C. Development of Hiv-1 Rectal-Specific Microbicides and Colonic Tissue Evaluation. *PLoS One* **2014**, 9, e102585.

249. Jeong, B.; Kim, S. W.; Bae, Y. H. Thermosensitive Sol-Gel Reversible Hydrogels. *Adv Drug Deliv Rev* **2002**, 54, 37-51.

250. Gilbert, J. C.; Richardson, J. L.; Davies, M. C.; Palin, K. J.; Hadgraft, J. The Effect of Solutes and Polymers on the Gelation Properties of Pluronic F-127 Solutions for Controlled Drug Delivery. *Journal of Controlled Release* **1987**, 5, 113-118.

251. das Neves, J.; Sarmento, B.; Amiji, M. M.; Bahia, M. F. Development and Validation of a Rapid Reversed-Phase Hplc Method for the Determination of the Non-Nucleoside Reverse Transcriptase Inhibitor Dapivirine from Polymeric Nanoparticles. *Journal of pharmaceutical and biomedical analysis* **2010**, 52, 167-72.

252. Das, K.; Lewi, P. J.; Hughes, S. H.; Arnold, E. Crystallography and the Design of Anti-Aids Drugs: Conformational Flexibility and Positional Adaptability Are Important in the Design of Non-Nucleoside Hiv-1 Reverse Transcriptase Inhibitors. *Progress in biophysics and molecular biology* **2005**, 88, 209-31.

253. Gorbach, P. M.; Weiss, R. E.; Fuchs, E.; Jeffries, R. A.; Hezerah, M.; Brown, S.; Voskanian, A.; Robbie, E.; Anton, P.; Cranston, R. D. The Slippery Slope: Lubricant Use and Rectal Sexually Transmitted Infections: A Newly Identified Risk. *Sexually transmitted diseases* **2012**, 39, 59-64.

254. Mogensen, T. H.; Melchjorsen, J.; Larsen, C. S.; Paludan, S. R. Innate Immune Recognition and Activation During Hiv Infection. *Retrovirology* **2010**, 7, 54.

255. Xu, H.; Wang, X.; Veazey, R. S. Mucosal Immunology of Hiv Infection. *Immunological reviews* **2013**, 254, 10-33.

256. Deascentiis, A.; Degrazia, J. L.; Bowman, C. N.; Colombo, P.; Peppas, N. A. Mucoadhesion of Poly(2-Hydroxyethyl Methacrylate) Is Improved When Linear Poly(Ethylene Oxide) Chains Are Added to the Polymer Network. *Journal of Controlled Release* **1995**, 33, 197-201.

257. Peppas, N. A. Molecular Calculations of Poly(Ethylene Glycol) Transport across a Swollen Poly(Acrylic Acid)/Mucin Interface. *Journal of biomaterials science. Polymer edition* **1998**, 9, 535-42.

258. Martini, L.; Attwood, D.; Collett, J. H.; Demanuele, A. The Bioadhesive Properties of a Triblock Copolymer of Epsilon-Caprolactone and Ethylene-Oxide. *International Journal of Pharmaceutics* **1995**, 113, 223-229.

259. Sahlin, J. J.; Peppas, N. A. Enhanced Hydrogel Adhesion by Polymer Interdiffusion: Use of Linear Poly(Ethylene Glycol) as an Adhesion Promoter. *Journal of biomaterials science. Polymer edition* **1997**, 8, 421-36.

260. Huang, Y.; Leobandung, W.; Foss, A.; Peppas, N. A. Molecular Aspects of Muco- and Bioadhesion: Tethered Structures and Site-Specific Surfaces. *J Control Release* **2000**, 65, 63-71.

261. Boylan, N. J.; Kim, A. J.; Suk, J. S.; Adstamongkonkul, P.; Simons, B. W.; Lai, S. K.; Cooper, M. J.; Hanes, J. Enhancement of Airway Gene Transfer by DNA Nanoparticles Using a Ph-Responsive Block Copolymer of Polyethylene Glycol and Poly-L-Lysine. *Biomaterials* **2012**, 33, 2361-71.

262. DeRouchey, J.; Walker, G. F.; Wagner, E.; Radler, J. O. Decorated Rods: A "Bottom-up" Self-Assembly of Monomolecular DNA Complexes. *The journal of physical chemistry. B* **2006**, 110, 4548-54.

263. Smart, J. D. The Basics and Underlying Mechanisms of Mucoadhesion. *Adv Drug Deliv Rev* **2005**, 57, 1556-68.

264. Serra, L.; Domenech, J.; Peppas, N. A. Design of Poly(Ethylene Glycol)-Tethered Copolymers as Novel Mucoadhesive Drug Delivery Systems. *Eur J Pharm Biopharm* **2006**, 63, 11-8.

265. He, X. H.; Shaw, P. C.; Tam, S. C. Reducing the Immunogenicity and Improving the in Vivo Activity of Trichosanthin by Site-Directed Pegylation. *Life sciences* **1999**, 65, 355-68.

266. Yang, M.; Yu, T.; Wang, Y. Y.; Lai, S. K.; Zeng, Q.; Miao, B.; Tang, B. C.; Simons, B. W.; Ensign, L. M.; Liu, G.; Chan, K. W.; Juang, C. Y.; Mert, O.; Wood, J.;

Fu, J.; McMahon, M. T.; Wu, T. C.; Hung, C. F.; Hanes, J. Vaginal Delivery of Paclitaxel Via Nanoparticles with Non-Mucoadhesive Surfaces Suppresses Cervical Tumor Growth. *Advanced healthcare materials* **2014**, 3, 1044-52.

267. da Silva, A. L.; Martini, S. V.; Abreu, S. C.; Samary Cdos, S.; Diaz, B. L.; Fernezlian, S.; de Sa, V. K.; Capelozzi, V. L.; Boylan, N. J.; Goya, R. G.; Suk, J. S.; Rocco, P. R.; Hanes, J.; Morales, M. M. DNA Nanoparticle-Mediated Thymulin Gene Therapy Prevents Airway Remodeling in Experimental Allergic Asthma. *J Control Release* **2014**, 180, 125-33.

268. Boskey, E. R.; Moench, T. R.; Hees, P. S.; Cone, R. A. A Self-Sampling Method to Obtain Large Volumes of Undiluted Cervicovaginal Secretions. *Sexually transmitted diseases* **2003**, 30, 107-9.

269. Champlin, A. K.; Dorr, D. L.; Gates, A. H. Determining the Stage of the Estrous Cycle in the Mouse by the Appearance of the Vagina. *Biology of reproduction* **1973**, 8, 491-4.

270. Asscher, A. W.; De Boer, C. H.; Turner, C. J. Cornification of the Human Vaginal Epithelium. *Journal of anatomy* **1956**, 90, 547-52.

271. Smith, B. G.; Brunner, E. K. The Structure of the Human Vaginal Mucosa in Relation to the Menstrual Cycle and to Pregnancy. *American Journal of Anatomy* **1934**, 54, 27-85.

272. Rosen, H.; Abribat, T. The Rise and Rise of Drug Delivery. *Nature reviews. Drug discovery* **2005**, 4, 381-5.

273. Shmulewitz, A.; Langer, R. The Ascendance of Combination Products. *Nature biotechnology* **2006**, 24, 277-80.

274. Langer, R. Drug Delivery. Drugs on Target. *Science* **2001**, 293, 58-9.

275. Yuan, F.; Leunig, M.; Huang, S. K.; Berk, D. A.; Papahadjopoulos, D.; Jain, R. K. Microvascular Permeability and Interstitial Penetration of Sterically Stabilized (Stealth) Liposomes in a Human Tumor Xenograft. *Cancer research* **1994**, 54, 3352-6.

276. Prego, C.; Garcia, M.; Torres, D.; Alonso, M. J. Transmucosal Macromolecular Drug Delivery. *Journal of controlled release : official journal of the Controlled Release Society* **2005**, 101, 151-62.

277. de la Fuente, M.; Csaba, N.; Garcia-Fuentes, M.; Alonso, M. J. Nanoparticles as Protein and Gene Carriers to Mucosal Surfaces. *Nanomedicine* **2008**, 3, 845-57.

278. Adjei, I. M.; Sharma, B.; Labhasetwar, V. Nanoparticles: Cellular Uptake and Cytotoxicity. *Advances in experimental medicine and biology* **2014**, 811, 73-91.

279. Allen, T. M.; Cullis, P. R. Drug Delivery Systems: Entering the Mainstream. *Science* **2004**, 303, 1818-22.

280. Sankar, V.; Hearnden, V.; Hull, K.; Juras, D. V.; Greenberg, M. S.; Kerr, A. R.; Lockhart, P. B.; Patton, L. L.; Porter, S.; Thornhill, M. Local Drug Delivery for Oral Mucosal Diseases: Challenges and Opportunities. *Oral Dis* **2011**, 17 Suppl 1, 73-84.

281. Kunert, K. S.; Tisdale, A. S.; Stern, M. E.; Smith, J. A.; Gipson, I. K. Analysis of Topical Cyclosporine Treatment of Patients with Dry Eye Syndrome: Effect on Conjunctival Lymphocytes. *Arch Ophthalmol* **2000**, 118, 1489-96.

282. Lambiase, A.; Rama, P.; Bonini, S.; Caprioglio, G.; Aloe, L. Topical Treatment with Nerve Growth Factor for Corneal Neurotrophic Ulcers. *N Engl J Med* **1998**, 338, 1174-80.

283. Yamada, H.; Kohno, S.; Koga, H.; Maesaki, S.; Kaku, M. Topical Treatment of Pulmonary Aspergilloma by Antifungals. Relationship between Duration of the Disease and Efficacy of Therapy. *Chest* **1993**, 103, 1421-5.

284. Sung, J. C.; Pulliam, B. L.; Edwards, D. A. Nanoparticles for Drug Delivery to the Lungs. *Trends Biotechnol* **2007**, 25, 563-70.

285. Sheikh, S.; Gupta, D.; Pallagatti, S.; Singla, I.; Gupta, R.; Goel, V. Role of Topical Drugs in Treatment of Oral Mucosal Diseases. A Literature Review. *N Y State Dent J* **2013**, 79, 58-64.

286. Fröhlich, E.; Roblegg, E. Mucus as Physiological Barrier to Intracellular Delivery. In *Intracellular Delivery Ii*, Aleš Prokop, Y. I., Atsushi Harada, Ed. Springer Netherlands: 2014; Vol. 2, pp 139-163.

287. Ensign, L. M.; Tang, B. C.; Wang, Y. Y.; Tse, T. A.; Hoen, T.; Cone, R.; Hanes, J. Mucus-Penetrating Nanoparticles for Vaginal Drug Delivery Protect against Herpes Simplex Virus. *Sci Transl Med* **2012**, 4.

288. Maisel, K.; Ensign, L.; Reddy, M.; Cone, R.; Hanes, J. Effect of Surface Chemistry on Nanoparticle Interaction with Gastrointestinal Mucus and Distribution in the Gastrointestinal Tract Following Oral and Rectal Administration in the Mouse. *Journal of Controlled Release* **2015**, 197, 48-57.

289. Yang, M.; Yu, T.; Wang, Y. Y.; Lai, S. K.; Zeng, Q.; Miao, B.; Tang, B. C.; Simons, B. W.; Ensign, L. M.; Liu, G.; Chan, K. W.; Juang, C. Y.; Mert, O.; Wood, J.; Fu, J.; McMahon, M. T.; Wu, T. C.; Hung, C. F.; Hanes, J. Vaginal Delivery of Paclitaxel Via Nanoparticles with Non-Mucoadhesive Surfaces Suppresses Cervical Tumor Growth. *Adv Healthc Mater* **2013**.

290. Kitchens, K. M.; Foraker, A. B.; Kolhatkar, R. B.; Swaan, P. W.; Ghandehari, H. Endocytosis and Interaction of Poly (Amidoamine) Dendrimers with Caco-2 Cells. *Pharm Res* **2007**, 24, 2138-45.

291. Kitchens, K. M.; Kolhatkar, R. B.; Swaan, P. W.; Eddington, N. D.; Ghandehari, H. Transport of Poly(Amidoamine) Dendrimers across Caco-2 Cell Monolayers: Influence of Size, Charge and Fluorescent Labeling. *Pharm Res* **2006**, 23, 2818-26.

292. Goldberg, D. S.; Ghandehari, H.; Swaan, P. W. Cellular Entry of G3.5 Poly (Amido Amine) Dendrimers by Clathrin- and Dynamin-Dependent Endocytosis Promotes Tight Junctional Opening in Intestinal Epithelia. *Pharm Res* **2010**, 27, 1547-57.

293. Kannan, R. M.; Nance, E.; Kannan, S.; Tomalia, D. A. Emerging Concepts in Dendrimer-Based Nanomedicine: From Design Principles to Clinical Applications. *J Intern Med* **2014**.

294. Olson, E. S.; Jiang, T.; Aguilera, T. A.; Nguyen, Q. T.; Ellies, L. G.; Scadeng, M.; Tsien, R. Y. Activatable Cell Penetrating Peptides Linked to Nanoparticles as Dual Probes for in Vivo Fluorescence and Mr Imaging of Proteases. *Proceedings of the National Academy of Sciences of the United States of America* **2010**, 107, 4311-6.

295. Thomas, T. P.; Goonewardena, S. N.; Majoros, I. J.; Kotlyar, A.; Cao, Z.; Leroueil, P. R.; Baker, J. R., Jr. Folate-Targeted Nanoparticles Show Efficacy in the Treatment of Inflammatory Arthritis. *Arthritis and rheumatism* **2011**, 63, 2671-80.

296. Gerard, H. C.; Mishra, M. K.; Mao, G.; Wang, S.; Hali, M.; Whittum-Hudson, J. A.; Kannan, R. M.; Hudson, A. P. Dendrimer-Enabled DNA Delivery and Transformation of Chlamydia Pneumoniae. *Nanomedicine* **2013**, 9, 996-1008.

297. Chauhan, A. S.; Diwan, P. V.; Jain, N. K.; Tomalia, D. A. Unexpected in Vivo Anti-Inflammatory Activity Observed for Simple, Surface Functionalized Poly(Amidoamine) Dendrimers. *Biomacromolecules* **2009**, 10, 1195-202.

298. Inapagolla, R.; Guru, B. R.; Kurtoglu, Y. E.; Gao, X.; Lieh-Lai, M.; Bassett, D. J.; Kannan, R. M. In Vivo Efficacy of Dendrimer-Methylprednisolone Conjugate Formulation for the Treatment of Lung Inflammation. *Int J Pharm* **2010**, 399, 140-7.

299. Malik, N.; Evagorou, E. G.; Duncan, R. Dendrimer-Platinate: A Novel Approach to Cancer Chemotherapy. *Anti-cancer drugs* **1999**, 10, 767-76.

300. Gajbhiye, V.; Jain, N. K. The Treatment of Glioblastoma Xenografts by Surfactant Conjugated Dendritic Nanoconjugates. *Biomaterials* **2011**, 32, 6213-25.

301. Vincent, L.; Varet, J.; Pille, J. Y.; Bompais, H.; Opolon, P.; Maksimenko, A.; Malvy, C.; Mirshahi, M.; Lu, H.; Vannier, J. P.; Soria, C.; Li, H. Efficacy of Dendrimer-Mediated Angiostatin and Timp-2 Gene Delivery on Inhibition of Tumor Growth and Angiogenesis: In Vitro and in Vivo Studies. *International journal of cancer. Journal international du cancer* **2003**, 105, 419-29.

302. Kannan, S.; Dai, H.; Navath, R. S.; Balakrishnan, B.; Jyoti, A.; Janisse, J.; Romero, R.; Kannan, R. M. Dendrimer-Based Postnatal Therapy for Neuroinflammation and Cerebral Palsy in a Rabbit Model. *Sci Transl Med* **2012**, 4, 130ra46.

303. Sadekar, S.; Thiagarajan, G.; Bartlett, K.; Hubbard, D.; Ray, A.; McGill, L. D.; Ghandehari, H. Poly(Amido Amine) Dendrimers as Absorption Enhancers for Oral Delivery of Camptothecin. *Int J Pharm* **2013**, 456, 175-85.

304. Sadekar, S.; Ghandehari, H. Transepithelial Transport and Toxicity of Pamam Dendrimers: Implications for Oral Drug Delivery. *Adv Drug Deliv Rev* **2012**, 64, 571-88.

305. Malik, N.; Wiwattanapatapee, R.; Klopsch, R.; Lorenz, K.; Frey, H.; Weener, J. W.; Meijer, E. W.; Paulus, W.; Duncan, R. Dendrimers: Relationship between Structure and Biocompatibility in Vitro, and Preliminary Studies on the Biodistribution of 125i-Labelled Polyamidoamine Dendrimers in Vivo. *Journal of controlled release : official journal of the Controlled Release Society* **2000**, 65, 133-48.

306. Perumal, O. P.; Inapagolla, R.; Kannan, S.; Kannan, R. M. The Effect of Surface Functionality on Cellular Trafficking of Dendrimers. *Biomaterials* **2008**, 29, 3469-76.

307. Hubbard, D.; Ghandehari, H.; Brayden, D. J. Transepithelial Transport of Pamam Dendrimers across Isolated Rat Jejunal Mucosae in Ussing Chambers. *Biomacromolecules* **2014**.

308. Bai, S.; Thomas, C.; Ahsan, F. Dendrimers as a Carrier for Pulmonary Delivery of Enoxaparin, a Low-Molecular Weight Heparin. *J Pharm Sci* **2007**, 96, 2090-106.

309. Dong, Z.; Hamid, K. A.; Gao, Y.; Lin, Y.; Katsumi, H.; Sakane, T.; Yamamoto, A. Polyamidoamine Dendrimers Can Improve the Pulmonary Absorption of Insulin and Calcitonin in Rats. *J Pharm Sci* **2011**, 100, 1866-78.

310. Li, C.; Liu, H.; Sun, Y.; Wang, H.; Guo, F.; Rao, S.; Deng, J.; Zhang, Y.; Miao, Y.; Guo, C.; Meng, J.; Chen, X.; Li, L.; Li, D.; Xu, H.; Li, B.; Jiang, C. Pamam Nanoparticles Promote Acute Lung Injury by Inducing Autophagic Cell Death through the Akt-Tsc2-Mtor Signaling Pathway. *J Mol Cell Biol* **2009**, 1, 37-45.

311. Conti, D. S.; Brewer, D.; Grashik, J.; Avasarala, S.; da Rocha, S. R. Poly(Amidoamine) Dendrimer Nanocarriers and Their Aerosol Formulations for Sirna Delivery to the Lung Epithelium. *Mol Pharm* **2014**, 11, 1808-22.

312. Lesniak, W. G.; Mishra, M. K.; Jyoti, A.; Balakrishnan, B.; Zhang, F.; Nance, E.; Romero, R.; Kannan, S.; Kannan, R. M. Biodistribution of Fluorescently Labeled Pamam Dendrimers in Neonatal Rabbits: Effect of Neuroinflammation. *Mol Pharm* **2013**, 10, 4560-71.

313. Kurtoglu, Y. E.; Mishra, M. K.; Kannan, S.; Kannan, R. M. Drug Release Characteristics of Pamam Dendrimer-Drug Conjugates with Different Linkers. *Int J Pharm* **2010**, 384, 189-94.

314. Booth, C.; O'Shea, J. A. Isolation and Culture of Intestinal Epithelial Cells. In *Culture of Epithelial Cells*, 2nd ed.; Freshney, I.; Freshney, M. G., Eds. John Wiley & Sons, Inc.: 2002; pp 304-335.

315. Bjerknes, M.; Cheng, H. Methods for the Isolation of Intact Epithelium from the Mouse Intestine. *Anat Rec* **1981**, 199, 565-74.

316. Qi, X.; Pan, Y.; Hu, Z.; Kang, W.; Willis, J. E.; Olowe, K.; Sivak, M. V., Jr.; Rollins, A. M. Automated Quantification of Colonic Crypt Morphology Using Integrated Microscopy and Optical Coherence Tomography. *Journal of biomedical optics* **2008**, 13, 054055.

317. Johansson, M. E.; Gustafsson, J. K.; Sjoberg, K. E.; Petersson, J.; Holm, L.; Sjovall, H.; Hansson, G. C. Bacteria Penetrate the Inner Mucus Layer before Inflammation in the Dextran Sulfate Colitis Model. *PloS one* **2010**, 5, e12238.

318. El-Sayed, M.; Ginski, M.; Rhodes, C.; Ghandehari, H. Transepithelial Transport of Poly(Amidoamine) Dendrimers across Caco-2 Cell Monolayers. *Journal of controlled release : official journal of the Controlled Release Society* **2002**, 81, 355-65.

319. El-Sayed, M.; Ginski, M.; Rhodes, C. A.; Ghandehari, H. Influence of Surface Chemistry of Poly(Amidoamine) Dendrimers on Caco-2 Cell Monolayers. *J Bioact Compat Pol* **2003**, 18, 7-22.

320. Bravo-Osuna, I.; Noiray, M.; Briand, E.; Woodward, A. M.; Argueso, P.; Molina Martinez, I. T.; Herrero-Vanrell, R.; Ponchel, G. Interfacial Interaction between Transmembrane Ocular Mucins and Adhesive Polymers and Dendrimers Analyzed by Surface Plasmon Resonance. *Pharm Res* **2012**, 29, 2329-40.

321. Price, C. F.; Tyssen, D.; Sonza, S.; Davie, A.; Evans, S.; Lewis, G. R.; Xia, S.; Spelman, T.; Hodsman, P.; Moench, T. R.; Humberstone, A.; Paull, J. R.; Tachedjian, G. Spl7013 Gel (Vivagel(R)) Retains Potent Hiv-1 and Hsv-2 Inhibitory Activity Following Vaginal Administration in Humans. *PloS one* **2011**, 6, e24095.

322. Wang, B.; Navath, R. S.; Menjoge, A. R.; Balakrishnan, B.; Bellair, R.; Dai, H.; Romero, R.; Kannan, S.; Kannan, R. M. Inhibition of Bacterial Growth and Intramniotic Infection in a Guinea Pig Model of Chorioamnionitis Using Pamam Dendrimers. *Int J Pharm* **2010**, 395, 298-308.

323. Landers, J. J.; Cao, Z.; Lee, I.; Piehler, L. T.; Myc, P. P.; Myc, A.; Hamouda, T.; Galecki, A. T.; Baker, J. R., Jr. Prevention of Influenza Pneumonitis by Sialic Acid-Conjugated Dendritic Polymers. *J Infect Dis* **2002**, 186, 1222-30.

324. Shcharbin, D.; Janaszewska, A.; Klajnert-Maculewicz, B.; Ziemba, B.; Dzmitruk, V.; Halets, I.; Loznikova, S.; Shcharbina, N.; Milowska, K.; Ionov, M.; Shakhbazau, A.; Bryszewska, M. How to Study Dendrimers and Dendriplexes Iii. Biodistribution, Pharmacokinetics and Toxicity in Vivo. *Journal of controlled release : official journal of the Controlled Release Society* **2014**, 181, 40-52.

CURRICULUM VITAE FOR Ph.D. CANDIDATES

The Johns Hopkins University School of Medicine

KATHARINA MAISEL **11/30/2014**

Educational History

PhD expected	2014	Program in Biomedical Engineering Mentors: Justin Hanes, PhD	Johns Hopkins School of Medicine
BSE	2010	Materials Science and Engineering	University of Michigan
IB	2006	International Baccalaureate	International Academy, Bloomfield Hills, MI

Other Professional Experience

Graduate Research	2010 – present	Lab of Dr. Justin Hanes, Johns Hopkins University
Undergraduate Research	2007 –2010	Lab of Dr. Jinsang Kim, University of Michigan
Undergraduate Research	2009	Lab of Dr. Eva Sinner, Max Planck Institute for Polymer Research
Undergraduate Research	2008	Lab of Dr. Kevin Yarema, Johns Hopkins University

Fellowships and Scholarships

2011 – 2014	Graduate Research Fellowship ($125,500)	National Science Foundation
2009 – 2010	Clarence A. Siebert Memorial Scholar	University of Michigan

2009 – 2010	Marian Sarah Parker Scholar	University of Michigan
2008 – 2009	Karl Schwartzwalder Memorial Scholar	University of Michigan
2006 – 2007	Regents Merit Scholar	University of Michigan

Honors and Awards

2014	Award for Research Excellence	Johns Hopkins Center for Nanomedicine
2008 – 2010	James B. Angell Scholar	University of Michigan
2006 – 2010	University Honors, Dean's List	University of Michigan
2007	Best Poster Award	ASM International Poster Competition
2007	Recognized as freshman poster presenter	9th Annual AVS symposium
2007	William J. Branstrom Freshman Prize	University of Michigan
2006	National Merit Scholarship Finalist	University of Michigan

Peer-Reviewed Publications

Maisel K, Ensign LM, Reddy M, Cone R, Hanes J. Effect of surface chemistry on nanoparticle interaction with gastrointestinal mucus and distribution in the gastrointestinal tract following oral and rectal administration in the mouse. *Journal of Controlled Release* (2015), 197: 48-57.

Ensign LM, Henning A, Schneider C, **Maisel K,** Wang YY, Porosoff M, Cone R, Hanes J. Ex vivo characterization of particle transport in mucus secretions coating freshly excised mucosal tissues. *Molecular Pharmaceutics* (2013), 10(6): 2176-82.

Ensign LM, Hoen T, **Maisel K,** Cone R, Hanes J. Enhanced vaginal drug delivery through the use of hypotonic formulations that induce fluid uptake. *Biomaterials* (2013), 34(28): 6922-9.

Lee K, **Maisel K,** Rouillard JM, Gulari E, Kim J. Sensitive and Selective Label-Free DNA Detection by Conjugated Polymer-Based Microarrays and Intercalating Dye. *Chemistry of Materials* (2008), 20(9): 2848-2850.

Campbell C, Aich U, Weier C, Wang J, Choi S, Wen M, **Maisel K,** Sampathkumar S, Yarema K. Targeting Pro-Invasive Oncogenes with Short Chain Fatty Acid-Hexosamine Analogues Inhibits the Mobility of Metastatic MDA-MB-231 Breast Cancer Cells. *Journal of Medicinal Chemistry* (2008) 51(24): 8135-8147.

To be submitted:

Maisel K, Chattopadhyay S, Moench T, Hendrix C, Cone R, Ensign LM, Hanes J. Optimizing local and systemic drug delivery via the colorectum: tuning enema formulations for systemic or local applications by varying ion composition. *In preparation*.

Maisel K, Reddy M, Xu Q, Ensign LM, Cone R, Hanes J. The mucoadhesivity paradox revisited: Nanoparticles densely coated with high molecular weight polyethylene glycol (PEG) are not mucoadhesive and rapidly penetrate human mucus. *In preparation*.

Maisel K, Chisholm J, Mishra M, Chattopadhyay S, Zhang F, Schneider C, Kannan R, Hanes J. Neutrally charged poly(amido amide) dendrimers evenly coat mucosal surfaces and have improved cellular uptake compared to anionic and cationic PAMAM dendrimers. *In preparation*.

Maisel K, Chattopadhyay S, Ensign LM, Cone R, Hanes J. A novel non-mucoadhesive nanocrystal formulation in a novel osmotic thermosensitive gel for improved vaginal and rectal pre-exposure prophylaxis. *In preparation*.

Posters and Abstracs

Maisel K, Moench T, Hendrix C, Cone R, Ensign LM, Hanes J. Enhanced colorectal drug delivery using hypotonic enema formulations. Poster presentation (presenter). *BMES 2014 Annual Meeting*.

Maisel K, Ensign LM, Reddy M, Cone R, Hanes J. Mucus Penetrating Nanoparticles Improve Drug and Gene Delivery to the Gastrointestinal Tract. Podium Presentation (presenter). *CRS 2014 Annual Meeting*.

Maisel K, Reddy M, Cone R, Hanes J, Ensign LM. Overcoming gastrointestinal barriers to nanoparticle delivery. Invited Presentation. *CRS 2014 Annual Meeting*.

Ensign LM, Hoen T, **Maisel K,** Cone R, Hanes J. Enhanced vaginal drug delivery using hypotonic vehicles. Podium Presentation (presenter), *BMES 2013 Annual Meeting*.

Lee K, Lee J, **Maisel K,** Jun H, Kim J. Signal-amplifying and Self-signaling Conjugated Polymer Biosensors and Sensor Arrays. Invited Presentation. *Korean-American Scientists and Engineers Association UKC 2010*.

Maisel K, Lee K, Rouillard JM, Gulari E, Kim J. Signal Amplifying DNA Microarray by Using Conjugated Polymer and Intercalating Dye for Sensitive Label-Free DNA Detection. Poster Presentation (presenter). *ASM International 2007 Annual Meeting*.

Lee K, **Maisel K,** Rouillard JM, Gulari E, Kim J. Signal-amplifying and label free DNA microarray

chips by combining conjugated polymer and intercalating dye. Poster Presentation *MRS National Meeting 2007*.

Patents

2014 "Method for Improved Distribution of In Situ Gelling Agents on Mucosal Epithelia". *Patent Pending*. JHU Reference #C12945.

2014 "Hypotonic enema formulation for safe and effective drug delivery to the colorectum". *Patent Pending*. JHU Reference #C13051.

2014 "At Home Testing Kit for Bacterial Vaginosis". *Patent Pending*. JHU reference #C13101.

Service and Leadership

2013 – present	Co-founder of the Graduate Women's Empowerment Network (GWEN)
2013 – present	Student Mentor, Joyce Ivy Foundation
2013	Instructor for Nanoparticles for Drug Delivery Applications in Medicine, Discover Hopkins program
2012 – present	Volunteer at Maryland Science Center Observatory
2012	Teaching Assistant, Cellular Engineering at the Johns Hopkins University Instructors: Professor Jordan Green and Professor Kevin Yarema
2012	Guest Scientist for MD Science Center Science Fair after school program
2008 – present	Science Fair Judge (Morgan State Science Fair, MD and Washtenaw Science Fair, MI)